POLITECNICO DI TORINO

Master's Degree in Mechatronic Engineering

Department of Control and Computer Engineering

Master's Degree Thesis

Development of alternative kinematic solutions for Cartesian control of a Series Elastic Actuated upper limb exoskeleton.

Supervisor:

Prof. Marcello CHIABERGE

Candidate:

Giulia BODO

Company supervisors:

Eng, Ph.D. Stefano BUCCELLI

Eng, Ph.D. Federico TESSARI

Eng. Anna BUCCHIERI

October 2021

Abstract

Robot-assisted rehabilitation is an arising approach used to help post-stroke patients to recover motor capacity. A stroke occurs when the carrying of oxygen and nutrients to the brain is interrupted and so part of the brain cannot get the blood it needs. The consequence is the death of brain cells in the region that controls a particular body function, as reflection a part of the body stops working as it is supposed to do.
Stroke causes in patients a loss of hand dexterity and motor impairment on the upper-limb movements, such as reaching and grasping, which are fundamental components of many of the Activities of Daily Living (ADLs). Therefore, these limitations drastically constrain the health-related quality of life of the subject.
Robotic mediated rehabilitation allows both to obtain a distributed interaction along the whole limb to be rehabilitated, and to perform movements with the same quality of the ones performed during the therapist mediated rehabilitation. The usage of sensors on the mechatronic structure allows to collect a relevant set of feedback data that can be used both to evaluate the performance of the exoskeleton from a robotic point of view, and to understand and improve the human-robot interaction.

The first part of the thesis focuses on the modelling, validation and driving of a torque sensitive actuator that can be employed to improve the human-robot interaction. A model of the motor has been developed inside a simulation environment (Simulink and Matlab), and then characterized with the data available in the datasheet of the mechanical components. The system is a Series Elastic Actuator (SEA) composed by a DC brushless motor, a harmonic drive, and a compliant element that provides a measure of the exerted torque. Different models of motors with different performances and different springs have been analyzed. The model developed has been validated by comparing the simulated data with the one collected at the test bench, demonstrating that the simulation can be used for testing purpose instead of the physical test bench to save time and avoid a damage in the mechanical components. All the tests have been performed on a real-time target machine.

During the second part of the thesis, it has been studied the kinematics of the shoulder joint complex of an upper limb active exoskeleton; after the study of the direct kinematics, an un-conventional method has been adopted to implement the inverse kinematics by employing a neuro-Fuzzy based technique. A first model has been deployed for off-line simulations, another model has been deployed to a

real-time target machine (Speedgoat), then the results have been compared. The exoskeleton can follow a desired trajectory defined inside the cartesian space by exploiting the position control employed by the drivers, and the on-line computed neuro-Fuzzy-Logic based inverse kinematics. It has also been developed an admittance control that exploits the potentiality of the SEA to make the system more compliant during the machine-human interaction.

Acknowledgements

*"Coming together is a beginning. Keeping together is progress.
Working together is success"*
Henry Ford

I would like to thank Prof. Marcello Chiaberge for his willingness in being my supervisor.

My sincere gratitude goes to Lorenzo De Michieli and Matteo Laffranchi that let me develop my thesis project at the Rehab Technology IIT-INAIL Lab of the Fondazione Istituto Italiano di Tecnologia.

My heartfelt thanks to my supervisors Stefano Buccelli, Federico Tessari and Anna Bucchieri, for believing in me, for teaching me to never give up even if facing unexpected problems and for transmitting me their passion for the research.

Special thanks to Gianluca Capitta, Luca De Guglielmo and Wellington De Souza Filho who supported and helped me at every stage of my thesis project.

Thanks to all my colleagues of the Float team, to Agnese Bruschi, Antonio Succi, Silvia Scarpetta, Riccardo Anfosso for their suggestions and for always answering all my questions.

Table of Contents

List of Tables

List of Figures

Acronyms

AAN
: Assistance-As-Needed

ADL
: Activities of Daily Living

ANFIS
: Adaptive Neuro-Fuzzy Inference System

ANN
: Artificial Neural Networks

BLDC
: BrushLess Direct Current (motor)

BMI
: Brain Machine Interface

CAD
: Computer Aided Design

CAN
: Controller Area Network

CSP
: Cyclic Synchronous Position

DC
: Direct Current

DH
: Denavit–Hartenberg convention

DOF
: Degree of Freedom

En
: Epoch number

FIS
: Fuzzy Inference System

GUI
: Graphic User Interface

HIL
: Hardware in the Loop

IIT
: Istituto Italiano di Tecnologia

Ik
: Inverse kinematics

INAIL
: Istituto Nazionale Assicurazione contro gli Infortuni sul Lavoro

mDH
: Modified Denavit–Hartenberg convention

Mf
: Membership functions

PID
: Proportional Integrative Derivative

PMSM
: Permanent Magnet Synchronous Motor

RCP

Rapid Control Prototyping

RMSE

Root Mean Square Error

RPY

Roll-Pitch-Yaw

SEA

Series Elastic Actuator

SPT1P

SPiral Titanium one Pin spring geometry

SPT2P

SPiral Titanium two Pins spring geometry

STA

STar Steel (A from Italian "acciaio") spring geometry

Chapter 1

State-of-the-art on Upper Limb Exoskeletons

1.1 Exoskeletons for rehabilitation

Robot-assisted rehabilitation is an arising approach used to help post-stroke patients to recover motor capacity.
Since 1990s the research on robotic devices and exoskeletons for rehabilitation has become of great interest, particularly by focusing on devices that can be used for neurorehabilitation of post stroke patients. Stroke is the main cause of acquired chronic disabilities in adults and the second leading cause of death in the world [1]. In Italy stroke is the second cause of death representing the 9-10% of the overall deaths. Every year about 90000 hospitalizations are due to cerebral stroke. Statistics reveal that the 20-30% of post stroke patients dies within a month and the 40-50% within the first year after the occurrence of the stroke. The 75% of the surviving patients is affected by disabilities that in half of the cases lets the patient unable to care of him/herself [2].
A stroke occurs when a blood vessel is blocked by a clot or bursts, in this condition the carrying of oxygen and nutrients to the brain is interrupted and when that happens, part of the brain cannot get the blood it needs. The consequence is the death of brain cells. Since in this condition blood flow can't reach the region of the brain that controls a particular body function, that part of the body will stop working as it is supposed to do [3].
Possible disabilities developed by post-stroke survivors are the loss of hand dexterity and motor impairment on the upper-limb movements such as reaching and grasping which are fundamentals components of many of the Activities of Daily Living (ADL). ADLs are strictly dependent on the arm functionality [4], in particular self-care activities such as feeding, dressing and grooming [5] cannot be autonomously

performed by the patient when the limb is impaired. These limitations drastically constraint the health-related quality of life of the subject [6]. Other post-stoke conditions are the decreasing of the muscle activation and the decreasing of the smoothness into performing movements, moreover the patient is also affected by dyscoordination between reach and grasp movements and weakness [7].
The purpose of the traditional rehabilitation therapy is the recovery of the muscle functionality after the stroke, in particular the therapy should reduce the muscle weakness and improve the quality of functional movements like grasp and release. Upper limb rehabilitation needs the cooperation between the patient and rehabilitation team in order to make the interventions efficient [5]. To succeed in the rehabilitation different techniques can be adopted by the therapist, moreover, therapy can be delivered through interventions of different intensity, frequency, and duration [8]. A commonly used approach is the bilateral arm training that consists in a coordinate identical movement of the healthy limb and of the impaired one. Another type of therapy is the Bobath [9] approach that tries to reduce the abnormal tone by facilitating the normal movement through a positioning while handling techniques. Also, repetitive task training [6] is a commonly used practice where the patient has to repeat with different intensity a specific functional task. Among the possible interventions there is also the usage of robotic devices that can deliver or enhance repetitive task training. Robotics devices can be used to support motor learning and to increase the motor control and strength [5]. The usage of multidegree-of-freedom robot allows both to obtain a distributed interaction along the whole limb to be rehabilitated, to perform movement with the same quality of the ones performed with the help of the therapist and to perform a selectable number of repetition according to the patient need [10]. Moreover the usage of sensors on the mechatronic structure allows to collect relevant set of feedback data that can be used both to evaluate the performance of the exoskeleton from a robotic point of view and to understand the human-robot interaction.
Even if robotic exoskeletons are of great interest, it is necessary to underline that it has not been noticed a qualitative benefit with respect to traditional therapist-led therapy [11] [12].
An effective rehabilitation is obtained when it is both intense and when the patient is actively involved, this last objective can be reached by employing technologies like gaming and virtual reality.
Dealing with exoskeletons it is possible to identify two important research fields: the mechatronic design and the control strategies development.

Mechatronic design

Mechatronic design is related to the components of the device and includes the study of the kinematic chain, the choice of the actuators and their components as well as the implementation of sensors [12].

From a mechatronic point of view, exoskeletons can be firstly categorized basing on the number of limbs that can be introduced inside the robot, in commerce it is possible to find unilateral or bilateral upper limb exoskeletons. Unilateral robots involve the movement of only one limb while bilateral require that during the movement both the limbs, the healthy and the impaired one, move similarly.
Another categorization is related to the portability of the device [13], the machine can be grounded if the structure is fixed to ground and cannot be shifted or moved, otherwise it is ungrounded [14].
The kinematic chain is characterized by the number of the degrees of freedom of the exoskeleton and during its study it is necessary to consider the joint alignment with the human anatomy [10] [15]. The anatomical structure of the human upper limb is complex and, in order to avoid uncomfortable condition for the patient, it is essential that the alignment between the human body and the exoskeleton is precise, if this condition is not satisfied tissue depression can occur and causing pain to the patient [16] [17]. Another issue is related to singularity configurations that occur when two joint axis are aligned to each other, this problem particularly arises for the shoulder internal/external rotation and for the forearm pronation/supination movements. In these configurations an infinity torque is required to move the exoskeleton away from the singularity position. Even though in rehabilitation protocols it might be rare for patients to reach such positions, the singularity is a problem that must be taken into consideration for the safety of the user. Exoskeletons can have different actuation types, the most common are the electrical, pneumatic and hydraulic ones [18]. Electrical actuation exploits the capability of electrical motors to produce high torques and realize very precise motion [10]. Pneumatically actuated robots have a higher power to weight ratio [19] with respect to ones actuated by electrical motor and their efficiency is related to the pressure loss due to friction and to air purity and compressibility [20]. The problem related to this type of actuation is that the bandwidth is low and so the rate at which they correctly respond to command signal is very limited. Hydraulic actuation provides high power to weight ratio, but the efficiency of the motion is negatively affected when a leak of fluid [6] or pressure loss occurs. This actuation also requires the design of systems able to reduce the noise. Independently from the adopted actuation, the requirement for the actuators employed in rehabilitation exoskeletons are low weight, high operating bandwidth, delivery of large amount of torque and precision during the perform of the movement.
A variable power transmission is required during the movement of the robot and this transmission must last for all the duration of the machine operation. The transmission can be implemented by cable or wire drop drives. Cable drivers allows to obtain low inertia, fast response time and a long range for the transmission of power and force. On the other hand, they are easily subject to stretch and slip thus resulting in a movement different from the target one [13]. Also gear

train transmission, pulley or harmonic drivers can be employed. Different research groups focused on harmonic drive design because this transmission method allows to avoid backslash and can be designed in a compact way, moreover it is a low weight solution and thanks to high gear ratios it allows to obtain the desired high torques.
Another important characteristic for exoskeletons is the joints decoupling that allows to avoid that the torque of a joint influences the others near joints. A good decoupling allows the robot to follow in the correct way the desired trajectory [13].

Control strategies
Control strategies can be considered the key characteristics that dictate the type of interaction between the robot and the patient. The implementation of different control methods is useful also in order to correctly follow the patient during the neurorehabilitation timeline (Figure 1.1).

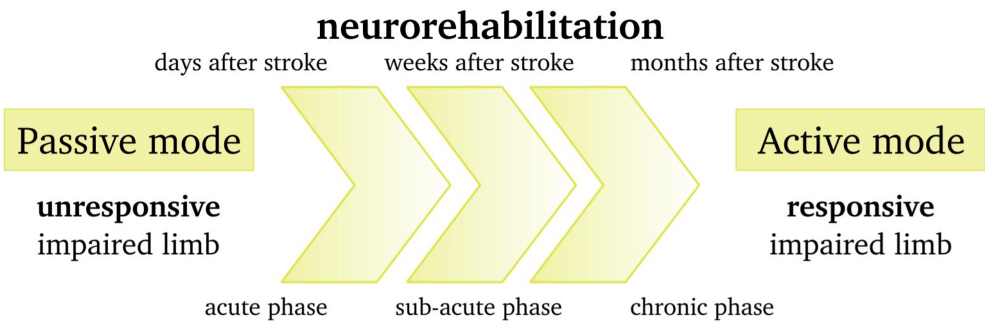

Figure 1.1: General neurorehabilitation timeline [11]. It is shown that it is needed to adapt the typology of assistance to the post-stroke phase, the nearest to the stroke occurrence the higher assistance is needed, the lower is the involvement of the patient. As time goes by a lower assistance is needed and an higher involvement of the patient is obtained.

Immediately after the stoke the patient is in the so called acute phase, a condition that typically lasts some days. During this first phase the impaired limb is quite completely unresponsive and a complete assistance is needed. As a consequence, a passive control mode should be employed, where the term “passive” indicates the involvement of the patient [6]. In this case the patient is not still able to collaborate during the rehabilitation sessions.
Once the acute phase is ended, in the weeks after the stroke the patient limb passes through a sub-acute phase till reaching, typically after some months, a chronic phase when the impaired limb is again responsive. In this last phase an active control mode can be adopted since the subject can be actively involved during the training.

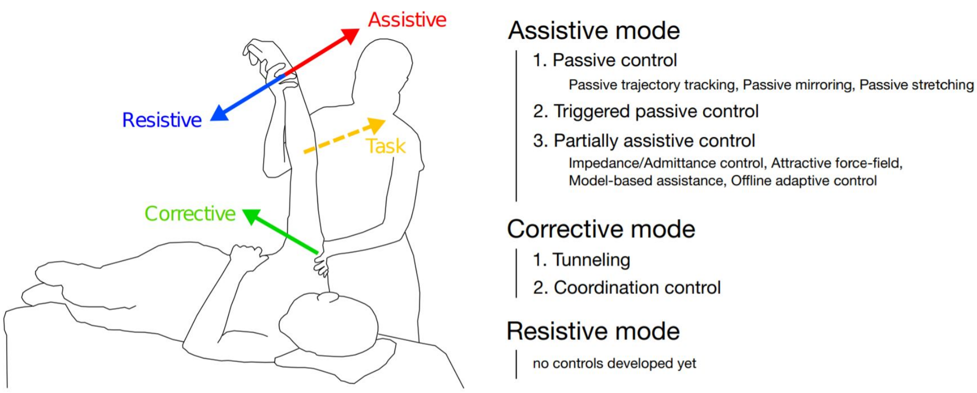

Figure 1.2: Global strategies implementable for robotic-mediated rehabilitation [11].

As stated by T. Proietti and colleagues [11] the exoskeletons mediated rehabilitation involves three main global control strategies, as show in *Figure 1.2* that are analysed below: assistance, correction and resistance.

Assistive modes

During the assistance the robot provides forces in order to complete the desired task, it also supports the weight of the impaired limb while the exercises are performed. Depending on the level of assistance, the task completion can be achieved even if any effort is produced by the patient. Three groups of assistance can be identified: passive, triggered passive, partially assistive control.

- *Passive control* is adopted especially in the first stages of the poststroke therapy [11] [21]. The motion is rigidly controlled in order to follow a precise trajectory, while doing the motion it is necessary that the exoskeleton shows a minimum of compliance to avoid hurting the subject in case of unexpected muscle contraction or other pathological synergies. Different techniques can be adopted, for example passive trajectory tracking allows to define and follow trajectories with a teach-and-replay method where in the teaching phase the movements performed by the patient under the control and guide of the physiotherapist are recorded and then the movement is reproduced on the patient without the assistance of the physiotherapist. Another technique to define trajectory is the record-and-replay that is similar to the already presented teach-and-replay but but, in this case, the trajectory is defined by using the healthy limb motion recorded within the exoskeleton. To follow the trajectory, it is often adopted a Proportional-Integrative-Derivative (PID) feedback control that can be applied either to the end effector or at the joint

level. It is also necessary to deal with uncertainty and tracking errors that must be minimised. A possible strategy is to use machine learning algorithms like the fuzzy logic technique that allows, for example, to estimate the human-robot system dynamical uncertainties.
Another passive control technique is the passive mirroring where the impaired limb motion follows and mimics the motion of the healthy limb, this control can be implemented by developing a master-slave configuration. In literature it is also present another technique called passive stretching [22] that works by stretching each single joint to identify its angle-resistance torque relationship that is the first step to then perform exercises that stretch multiple joints at the same time. This method is useful to reduce the cross-couple stiffness of the impaired limb.

- *Triggered passive control* allows to the user to trigger the assistance provided by the exoskeleton: following an on-set trigger, a passive controller computes the command inputs to the device such that the error between the desired trajectory and the actual one is minimum [11] [21]. For this control strategy different kind of triggers can be exploited, such as brain-machine interface (BMI) which detects the user motion intention.

- *Partially assistive control* is introduced because it is important that as soon as the patient has recovered a minimal motor capacity, he/she can take part to the control of the movement and realize a shared control with the robot [19]. This is because the pure passive motion can stimulate neuroplasticity [23] only in a limited way since the patient in this first part of the training is not able to provide effort to complete the tasks, so he is not involved. The so-called Assistance-As-Needed (AAN) strategies are developed which include all the control methods that allow the patient to move freely by controlling the motion and supporting the movement basing on some performance indexes [11] [21] [10], so if the patient can reach a certain point of the task he/she can do it on his/her own, then it is supported by the exoskeleton to complete the wanted movement. To develop such strategies, exoskeletons can rely on flexible control methods like admittance and impedance control that allow to obtain human like mechanical behaviour by using reduced corrective gains instead of high corrective gain used in industrial position feedback controllers. Admittance control is a position controller with a force or torque feedback. It is adopted especially in exoskeletons that lack back drivability where is useful to measure the forces at the machine-human interface to move the robot, taking into account inertial and dynamical effects. Impedance control is a model-based force controller [6] with position feedback that can be considered the dual of admittance control. it is employed especially for lightweight back drivable systems. Alternatively to admittance and impedance, control strategy like attractive force-field, model based assistance and offline adaptive control can be adopted. The first approach is a time-independent control that exploits attractive force fields to control the exoskeleton movement during the rehabilitation therapy [24]. The second one allows to maintain a desired pose by deriving and applying the necessary muscle force that is estimated thanks to a musculoskeletal model. The latter one groups iterative learning control and provides assistance using trial by trial adaptation that allows to modulate the robot contribution to the motion basing on performance indexes.

Corrective modes
Correction occurs when the patient is not performing the movement correctly, in this situation the robot works in order to force the impaired limb to recover a certain inter-joint coordination. Correction does not support the reaching of the task but helps to complete the exercise in a correct way. Corrective strategies are time independent. The controller is fed with desired path and allows to act only on the current position that can eventually be corrected. The domain of the corrective control is the application of forces in the orthogonal direction to the motion. Two principal approaches are the tunnelling and coordination control. Tunneling consist in creating an allowed range of motion around the desired trajectory and to correct the motion of the patient when the performed movement goes out of this channel [11]. This technique can be applied both to the end effector and at joints level. To avoid a stuck during the motion it is provided also a force along the direction of the channel that supports the movement [25]. This control can be also seen as an impedance control with a path-cantered non-action zone. Coordination control aim is to prevent negative compensatory strategies typical for post-stroke survivors by realizing a synergetic work of the joints. Particularly, the relative positions and velocities are controlled in order to realize the desired coordination during the movement.

Resistive modes
When resistance technique is adopted, the exoskeleton provides forces against the movement (Figure 1.2), this is done to make the task harder for the subject, to test the ability to adapt to external perturbations, and to complete the task also in these situations. These modes are still a work in progress in exoskeletons applications.

All the presented control strategies are strictly dependent on the quality of an important feature of the exoskeleton: the transparency. Transparency is a measure of the robot capability to not apply resistance during the motion. In other words, it is the characteristic of the exoskeleton that allows to the patient to don't feel the weight of the robot while wearing it and while performing free movements. Transparency can be considered a quality indicator for the mechanical properties structure like inertia, friction, and weight. It is also a good indicator to understand the quality of the actuation by evaluating back driveability and frictions, and to understand if the low-control level is compensating in an accurate way these perturbing phenomena. If a lack in transparency occurs, what might happen is that unwanted resistive forces are applied to the impaired limb during the motion, which is a completely unacceptable condition in rehabilitation purpose. This problem might also lead to the impossibility to develop pure corrective control strategies. For these reasons, it is important to be able to evaluate the transparency performance of the exoskeleton. A method to do this evaluation is the comparison between the range of motion, so the reachable space, of a healthy subject that moves with and without wearing the robot [11].

1.2 Float and FloatEVO exoskeletons

The device subject of the study and the tests presented in the following chapters is a prototype of FloatEVO an upper limb unilateral exoskeleton designed and realized by the Rehab Technology IIT-INAIL Lab of the Fondazione Istituto Italiano di Tecnologia. FloatEVO will be the evolution of the Float exoskeleton (Figure 1.3) designed to rehabilitate patients following traumas and surgeries involving the shoulder complex.

Figure 1.3: Float exoskeleton.

Float device is intended for professional use, therefore its use is confined to rehabilitation sessions under the strict supervision of trained healthcare personnel. The exoskeleton can move the patient's upper limb in different ways depending on the degree of motor deficit or the rehabilitation phase: the exoskeleton can both leave to the patient the possibility of free motion by providing assistance only when needed, or perform passive mobilization by completely driving the movement according to trajectories set by the therapist. The transmission of movement between the the exoskeleton structure and the patient occurs through three ergonomic interfaces at the level of the torso, arm and forearm.
Compared to Float, FloatEVO will have a new kinematic structure and torque sensors on all joints. Such additional sensors will allow the treatment of neurological patients (e.g. post-stroke) suffering spasticity.
It is expected that the device will be a valuable tool in the hands of physiotherapists by help in overcoming the limitations of the traditional therapist-assisted rehabilitation, that usually is difficult and tiring, with limitations in terms of duration and intensity of training exercises, and often influenced by the experience and sensitivity of the therapist that is the critical point in determine the reproducibility of the exercises. The exoskeletons should allow to intensify the motor training through repetitive and task-oriented exercises. The intensification of the training can result in an improvement of the general physical condition of the target patient, bringing benefits for circulation and tissue re-oxygenation and is also a good way of prevent muscle atrophy. Moreover, in neurological patients a more intensive training results in a stimulation of the patient's voluntary movement which allows to provide an assistance to the movement only when needed. The presented exoskeletons, Float and FloatEVO have been compared with three main competitors that are actually present on commerce, in *Table 1.1* have been analyzed the devices clinical features, while, in *Table 1.2* the technical features of the devices have been collected.

Figure 1.4: Commercial Exoskelethons: ALEx, ArmeoPower and HARMONY.

The reported information are taken from official sites [26] [27] [28], scientific papers [29] [30] and datasheet [31].
The commercial exoskeletons under observation were: ALEx, ArmeoPower and

HARMONY (Figure 1.4).

Devices Comparison					
	Float	**FloatEVO**	**ALEx**	**ArmeoPower**	**HARMONY**
Clinical features					
Intended use	• Rehabilitation after shoulder joint injuries. • Musculoskeletal rehabilitation.	• Neurological rehabilitation. • Musculoskeletal rehabilitation.	• Neurological rehabilitation. • Musculoskeletal rehabilitation.	• Neurological rehabilitation. • Musculoskeletal rehabilitation.	• Neurological rehabilitation. • Musculoskeletal rehabilitation. • Upper-limb prosthetic or transplant rehabilitation
Anthropometric requirements	Height range: 160÷185 cm Maximum weight: 95 kg			Maximum weight: 135 kg	
Target patients	Patients affected by orthopaedic, musculoskeletal disorders and disfunctions. Post-traumatic or post-surgical injuries patients.	Patients affected by neurological, orthopaedic, musculoskeletal disorders and disfunctions.	Patients affected by neurological, orthopaedic, musculoskeletal disorders and disfunctions.	Patients affected by neurological (central or peripheral nervous system, spinal cord injuries), orthopaedic, musculoskeletal disorders and disfunctions.	Patients affected by neurological, orthopaedic, musculoskeletal disorders and disfunctions.
Wearability	Three fabric interface braces: arm/forearm/corset	Wearable on right or left harm (tipper). Three wearable fabric interfaces: a corset for the torso, one brace for arm and forearm (each).	Wearable on right and left harm. Two wearable fabric interfaces: one brace for arm and forearm (each). One hand handles.	Three wearable fabric interfaces: one brace for arm and forearm (each) and a hand brace.	Wearable on right and left harm. Two wearable fabric interfaces: one brace for arm and forearm (each). One hand handles.
Involved joints	• Shoulder • Elbow	• Shoulder • Elbow • Wrist	• Shoulder • Elbow • Wrist	• Shoulder • Elbow • Wrist • Hand	• Shoulder • Elbow • Wrist
Component sizes	Link 1 From sagittal plane to shoulder centre: 157.55 ÷ 202.8 mm Link 2 From coronal plane to shoulder centre: 74.9 ÷ 129.9 mm Link 3 From the shoulder centre to elbow centre: 250.05 ÷ 300.05 mm		The exoskeleton can be adapted to different anthropometric measures.	Height adjustment Range 400mm Forearm lenghts Elbow to handgrip 310÷420mm Upper arm lenghts Shoulder to elbow 250÷340mm	Autosizing adjustment
Users	• Patient • Therapist	• Patient • Therapist	• Patient • Therapist	• Patient • Therapis	• Patient • Therapist

Table 1.1: Clinical features comparison between IIT-Rehab Technology devices and competitors.

Devices Comparison					
	Float	**FloatEVO**	**ALEx**	**ArmeoPower**	**HARMONY**
Technical features					
Exoskeleton weight	Overall: 230 kg Only robotic arm: 13 kg		Overall: 16.4 kg Robotic arm: 4.5 kg	Overall: 205 kg	(Excluding the frame) 31.20 Kg
Max. joint velocity	45 deg/s		500 deg/s		
Torque			Max. continuous joint torque: 40Nm Max. peak torque: 80Nm		Continuous joint torque: - 34.4 Nm at shoulder - 13 Nm at elbow - 1.25 Nm at wrist
Operating temperature and humidity	18° - 30° C 40 - 60 %			10°- 35° C 30% -75 % relative air humidity	
Conditions of use	Indoor premises dedicated for therapy, dry and flat surfaces.	Intended for professional use, in indoor environments dedicated for rehabilitation (hospitals, clinics).	Intended for professional use, in indoor environments dedicated for rehabilitation (hospitals, clinics).	Intended for professional use, in indoor environments dedicated for rehabilitation (hospitals, clinics).	Intended for professional use, in indoor environments dedicated for rehabilitation (hospitals, clinics).
Actuated joints	• Shoulder flexion-extension • Shoulder abd-adduction • Horizontal shoulder flexion-extension • Shoulder intra-extra rotation	• Shoulder flexion-extension • Shoulder abd-adduction • shoulder horizontal flexion-extension • Shoulder intra-extra rotation • Elbow flexion-extension	• Shoulder flexion-extension • Shoulder abd-adduction • Shoulder intra-extra rotation • Elbow flexion-extension	• Shoulder flexion-extension • Horizontal shoulder abduction • Shoulder intra-extra rotation • Elbow flexion-extension • Forearm pronation-supination • Wrist flexion-extension. Actuated hand ManovoPower (optional).	• Shoulder flexion-extension • Shoulder abduction-adduction • Shoulder intra-extra rotation • Elbow flexion • Forearm pronation-supination • Wrist flexion-extension
Passive joints	• Elbow flexion-extension	• Forearm pronation-supination	• Forearm pronation-supination • Wrist flexion-extension	• Sensorized hand grip	
Implemented ADL	Reaching. Exploring surrounding.		Self-care, dressing and eating needs.	Reach and grasp, explore and manipulate objects.	Drink from a glass. Reach and grasp, explore and manipulate objects.
Movement control	A user interface (display) is used to set the desired operating mode and the control parameters.		A user interface (display) is used to set the desired operating mode and the control parameters.	A user interface (display) is used to set the desired exercise workspace and difficulty level of the exercise.	
Range of motion	SHOULDER • Horizontal abduction from 0° to 100° • Abduction from 15° to 110° • Flexion: from 30° to 90 • From 55° intra rotation to -55° extra rotation		SHOULDER • Abduction/adduction from 0° to 110° • Rotation from -40° to 60° • Flexion/extension from 10° to 155° ELBOW • Flexion/extension from 0° to 160° FOREARM • Pronation/supination from -90° to 90° WRIST • Flexion/extension from -50° to 50°	SHOULDER • Flexion/extension from 40° to 120°. • Horizontal abduction from -169° to 50°. • Internal/external rotation from 0° to 90°. ELBOW • Flexion/extension from 0° to 100° FOREARM • Pronation/supination from -60° to 60° WRIST • Flexion/extension from -60° to 60°	SHOULDER (ROM) • Abduction 118° (170) • Adduction 60° • Forward flexion 160° • Extension 45° • External rotation 79°(62) • Internal rotation 80°(48) • Elbow flexion 150° (145) • Pro/supination 172°
Feedback for the user	No feedback is provided.		Visual feedback on monitor or through virtual reality.	Assessment tools for patient's performance. Display.	
Type of mobilization	• Passive • Active-assistive		• Passive • Active-assistive	• Passive • Active-assistive • Assist-as-needed	• Passive • Active-assistive • Assist-as-needed
Weight/friction compensation	Friction compensation		Friction compensation Weight compensation	Friction compensation Weight compensation	Friction compensation Weight compensation
Operating mode	Kinematic: passive mobilization of the limb according to elementary movement of the shoulder with the recording of the trajectory (position control). Transparency: patient/therapist free active mobilization of the limb, the trajectory is recorded. Replay trajectory: passive mobilization of the shoulder by following the trajectories defined with kinematic or transparency mode (position control).		Passive: the robot moves the arm by replay a pre-recorded trajectory. Assist-as-needed: the robot detects patient's small intention of movement and provides a variable level of assistance according to patient's needs.	Passive operation: the movement is entirely performed by the robot. Active operation: patient's hand is supported by the robotic arm but not operated by it. All the motion activity is performed by the patient. Partial activation: patient's hand is supported by the robotic arm and is assisted by it in performing the movement, the therapist sets the degree of assistance. Arm support adapts to patient's capabilities.	Pre-programmed exercises. Torque control: transparent, assistive, resistive, corrective, support. Assist-as-needed.
Unilateral/Bilateral	Unilateral	Unilateral	Bilateral (It is possible to set the control only on one limb while the other is still or mirrored)	Unilateral	Bilateral (it is possible to set the control only on one limb while the other is still or mirrored)

Table 1.2: Technical features comparison between IIT-Rehab Technology devices and competitors.

Chapter 2

Materials and methods

2.1 Theoretical control background

Siciliano B. et al. "Robotics modelling planning and control" book, is the main reference of the presented theoretical robotic background [32].

2.1.1 Direct kinematics

A robotic manipulator can be represented as a kinematic chain composed of rigid bodies, also called links, connected each other by joints that can be revolute or prismatic depending on the relative movement that they can perform. The chain typically starts from a constrained base that is identified as fixed reference frame and ends with an end-effector. The objective is to obtain equations able to describe the motion of the end-effector in the space with respect to the base. The study of the motion of the structure can be done by composing the elementary motion that each link performs with respect to the previous one. The direct kinematic study provides the mathematical relations, obtained with approaches based on linear algebra, necessary to express the end-effector position and orientation as function of the joint variables of the mechanical structure. All the computations are done with respect to a reference frame.

Pose of a rigid body

The pose of a rigid body describes the position and the orientation of an end-effector with respect to a reference frame. In this way it is possible to correctly identify the end-effector inside the Cartesian space. A homogeneous transformation matrix allows to refer the analyzed reference frame of a rigid body in the kinematic chain to the reference frame of the previous one, between the two frames the relation is expressed in terms of rotation around the x,y,z axes and translation along the axes. By post-multiplying, in order from the base to the end-effector, all the successive transformation matrices computed along the kinematic chain, the overall transformation between the end-effector and the base frame is obtained [32].

Coordinate transformations

Elementary rotations

Some frames can be simply obtained via elementary rotations of the base frame around one of the x,y,z axis. These rotations are defined positive if counter-clockwise or negative if clockwise. Considering a rotation by an angle γ around x axes, a rotation by an angle β around y axes and a rotation by an angle α around z axes, the matrices that describe the rotation around an arbitrary axis in the space are:

$$R_x(\gamma) = \begin{bmatrix} 1 & 0 & 0 \\ 0 & cos\gamma & -sin\gamma \\ 0 & sin\gamma & cos\gamma \end{bmatrix}$$

$$R_y(\beta) = \begin{bmatrix} cos\beta & 0 & sin\beta \\ 0 & 1 & 0 \\ -sin\beta & 0 & cos\beta \end{bmatrix}$$

$$R_z(\alpha) = \begin{bmatrix} cos\alpha & -sin\alpha & 0 \\ sin\alpha & cos\alpha & 0 \\ 0 & 0 & 1 \end{bmatrix}$$

When more elementary rotations are needed to relate a frame i to a frame i-1, the different elementary rotation matrices can be multiplied to obtain the overall rotation matrix R_i^{i-1}.

Elementary translations

When the origins of the considered reference frames do not coincide, it means that also translations occurs, the translations along the axes are collected in the vector:

$$t = \begin{bmatrix} t_x \\ t_y \\ t_z \end{bmatrix}$$

Homogeneous transformations

The overall transformation between two body frames is the result of both rotations and translations collected together in a unique matrix called homogeneous transformation matrix. This matrix describes the transformations containing the rotation matrix of frame *i* with respect to frame *i-1* and the translation vector from the origin of frame *i-1* to the origin of frame *i*.

$$A_i^{i-1} = \begin{bmatrix} R_i^{i-1} & t_i^{i-1} \\ 0^T & 1 \end{bmatrix}$$

Orientation

As already anticipated, the pose is the combination of the position and the orientations. The position can be described by the homogeneous transformation matrix but, since the rotations are described by nine elements that are not independent, this description results to be redundant. To describe in an unique way the orientation of a rigid body are sufficient three parameters.
A minimal representation of the orientation is provided by a set composed of three angles $\Phi = \begin{bmatrix}\phi & \theta & \psi\end{bmatrix}^T$. By considering that the rotation matrix expresses the elementary rotation around one axis as function of only one angle, then it is possible to obtain a generic rotation matrix exploiting the composition of a suitable sequence of three elementary rotations. During the composition of the rotations it is necessary to keep into account that it must be avoided that two successive rotations are around parallel axes. In this way are defined the allowed sets of angles, these triplets are also called Euler angles.
One of the possible set of Euler angles is known as the ZYX angles set, also called Roll–Pitch–Yaw angles.

RPY Angles

Roll–Pitch–Yaw angles have their origin in the aeronautical field where are widely used to describe the changes of attitude of the aircraft, in this application the angles $\Phi = \begin{bmatrix}\phi & \theta & \psi\end{bmatrix}^T$ describe rotations that are defined with respect to a fixed frame located in the centre of mass of the aircraft [32].
The resulting rotations from Roll–Pitch–Yaw angles are obtained as described:

- *Yaw*
  The reference frame is rotated by the angle ψ around x axis. The rotation is described by $R_x(\psi)$.

- *Pitch*
  The reference frame is rotated by the angle θ around y axis. The rotation is described by $R_y(\theta)$.

- *Roll*
  The reference frame is rotated by the angle ϕ around z axis. The rotation is described by $R_z(\phi)$.

Defined:

$$R_x(\psi) = \begin{bmatrix} 1 & 0 & 0 \\ 0 & cos\psi & -sin\psi \\ 0 & sin\psi & cos\psi \end{bmatrix}$$

$$R_y(\theta) = \begin{bmatrix} cos\theta & 0 & sin\theta \\ 0 & 1 & 0 \\ -sin\theta & 0 & cos\theta \end{bmatrix}$$

$$R_z(\phi) = \begin{bmatrix} cos\phi & -sin\phi & 0 \\ sin\phi & cos\phi & 0 \\ 0 & 0 & 1 \end{bmatrix}$$

The frame orientation can be computed by composing the rotations with respect to the reference frame, so by pre-multiplying the matrices of elementary rotation. The obtained frame orientation can be obtained as:

$$R(\Phi) = R_z(\phi)\, R_y(\theta)\, R_x(\psi)$$

$$R(\Phi) = \begin{bmatrix} c_\phi c_\theta & c_\phi s_\theta s_\psi - s_\phi c_\psi & c_\phi s_\theta c_\psi + s_\phi s_\psi \\ s_\phi c_\theta & s_\phi s_\theta s_\psi + c_\phi c_\psi & s_\phi s_\theta c_\psi - c_\phi s_\psi \\ -s_\theta & c_\theta s_\psi & c_\theta c_\psi \end{bmatrix}$$

To compute the inverse solution and obtain the ZYX angles it is possible to compare with the matrix $R(\Phi)$, explicated above, the given rotation matrix in the form

$$R = \begin{bmatrix} r_{11} & r_{12} & r_{13} \\ r_{21} & r_{22} & r_{23} \\ r_{31} & r_{32} & r_{33} \end{bmatrix}$$

Considering θ in the range (-$\pi/2$),$\pi/2$) the solution is expressed as:

$$\phi = \arctan(r_{21}, r_{11})$$

$$\theta = \arctan\left(-r_{31}, \sqrt{r_{32}^2 + r_{33}^2}\right)$$

$$\psi = \arctan(r_{32}, r_{33})$$

Notice that when $c_\theta = 0$ the solution degenerates, if this condition occurs it is possible to determine only the sum or the difference of ϕ and ψ [32].

Denavit–Hartenberg Convention

The purpose of the direct kinematic is to compute the pose of the end-effector as function of the joints variables. A manipulator is made of rigid bodies, called links connected each other by means of joints (revolute or prismatic). Each joint provides a single DOF to the system. Those manipulator composed by a sequence of links that connect the extremity of the chain fixed to a constrained base with the other extremity, the end-effector, without forming loops are defined kinematic open chain. Considering an open chain manipulator that is composed by *n+1* links connected by n joints to obtain the overall description of the kinematic of the system, it is reasonable to consider successive transformation between consecutive links and then compute for recursion the overall description of the manipulator. If at each link is associated a coordinate frame, the coordinate transformation that describes the pose of the frame n, with respect to the frame 0, is given by:

$$T_n^0(q) = A_1^0(q_1)\, A_2^1(q_2) \ldots A_n^{n-1}(q_n)$$

Defined T_0^b and T_e^n the constant homogeneous transformations that respectively describe the pose of frame 0 with respect to the fixed base frame, and the pose of end-effector frame with respect to frame n, the coordinate transformation that describes the pose of the end-effector frame with respect to the base frame is defined as

$$T_e^b(q) = T_0^b T_n^0(q)\, T_e^n$$

The reported equation exploits the recursive form of T_n^0, to obtain the direct kinematics expressed with that recursive expression it has been defined a systematic general method in order to make it easier the computation of the relative position and orientation of two consecutive links.
This method is the so-called Denavit–Hartenberg convention (DH) [32]. and it defines some rules to be applied while defining the link frames.

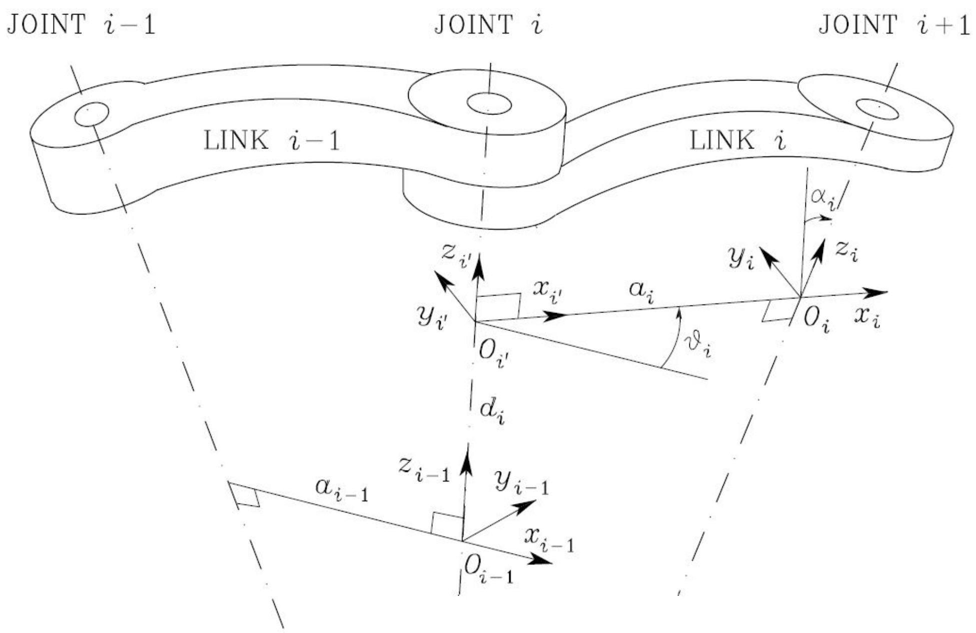

Figure 2.1: Kinematic parameters defined by DH convention [32].

By denoting the *Axis i* as the axis of the joint connecting *Link i-1* to *Link i*, the link *Frame i* is defined as follow [32]:

- Axis z_i is placed along the *Joint i+1* axis.
- The origin O_i is placed at the intersection between axis z_i and the common normal to axes z_{i-1} and z_i.
- The origin $O_{i'}$ is placed at the intersection between the common normal with axis z_{i-1}.
- Axis x_i is placed along the common normal to axes z_{i-1} and z_i following the direction form *Joint i* to *Joint i+1.*
- Axis y_i is chosen to complete a right-handed frame.

Once defined the link frames, the following parameters are used to identify the pose of *Frame i* with respect to *Frame i-1*, these parameters, also shown in *Figure 2.1*, are defined as follow:

- a_i is the distance between O_i and $O_{i'}$.
- d_i is the coordinate of $O_{i'}$ along the z_{i-1} axis.
- α_i is the angle between axes z_{i-1} and z_i around axis x_i. It is defined positive when for a counter-clockwise rotation.
- θ_i is the angle between axes x_{i-1} and x_i around axis z_{i-1} It is defined positive when for a counter-clockwise rotation.

Only one of these parameters is variable, and it characterize the joint. The variable parameter is θ_i for a revolute joint, while for a prismatic joint the variable parameter is d_i The revolute and prismatic joints representations can be seen in *Figure 2.2.*

If the reference frames have been placed like suggested by the DH convention, the coordinate transformation between one frame and the successive can be computed as [32]:

$$T_i^{i-1}(q_i) = \begin{bmatrix} c_{\theta_i} & -s_{\theta_i}c_{\alpha_i} & s_{\theta_i}s_{\alpha_i} & a_i c_{\theta_i} \\ s_{\theta_i} & c_{\theta_i}c_{\alpha_i} & -c\theta_i s_{\alpha_i} & a_i s_{\theta_i} \\ 0 & s_{\alpha_i} & c_{\alpha_i} & d_i \\ 0 & 0 & 0 & 1 \end{bmatrix}$$

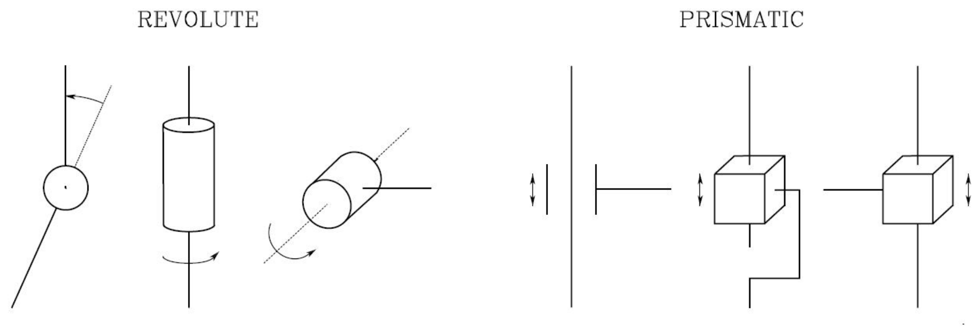

Figure 2.2: Revolute and prismatic joints conventional representation [32].

Modified Denavit–Hartenberg Convention

Alternatively, to the classical DH, a modified convention can be used. This convection defines that the link frames are named by number according to the link to which they are rigidly attached, so *Frame i* will be rigidly attached to *Link i* [33]. The identification of the frames is done by following the reported rules:

- Place the origin O_i where the common normal between z_i and z_{i+1} intersects the z_i axis.
- z_i axis is placed pointing along the the axis of the i^{th} joint.
- x_i axis is placed pointing along the common normal between z_i and z_{i+1} following the direction from z_i to z_{i+1}.
- Axis y_i is chosen to complete a right-handed frame.

The modified convention stands that the parameters which identify the pose of a frame with respect to the adjacent one are:

- a_{i-1} is the distance from axis z_{i-1} to z_i measured along x_{i-1}
- d_i is the distance from axis x_{i-1} to x_i measured along z_i
- α_{i-1} is the angle between axes z_{i-1} and z_i around axis x_{i-1}. It is defined positive when for a counter-clockwise rotation.
- θ_i is the angle between axes x_{i-1} and x_i around axis z_i It is defined positive when for a counter-clockwise rotation.

If the reference frames have been placed like suggested by the modified DH convention, the coordinate transformation between one frame and the successive can be computed as [33]:

$$T_i^{i-1}(q_i) = \begin{bmatrix} c_{\theta_i} & -s_{\theta_i} & 0 & a_{i-1} \\ s_{\theta_i}c_{\alpha_{i-1}} & c_{\theta_i}c_{\alpha_{i-1}} & -s_{\alpha_{i-1}} & -d_i s_{\alpha_{i-1}} \\ s_{\theta_i}s_{\alpha_{i-1}} & c_{\theta_i}s_{\alpha_{i-1}} & c_{\alpha_{i-1}} & d_i c_{\alpha_{i-1}} \\ 0 & 0 & 0 & 1 \end{bmatrix}$$

2.1.2 Inverse kinematics

Inverse kinematics allows to compute the joints variables that are needed to place the end-effector in a desired position, and with a desired orientation, inside the Cartesian space. Inverse kinematics problem can have or not a solution, in some cases an infinite number of solutions exists. In other cases even if the solution exists it cannot be reached because of internal collisions due to the mechanical construction of the manipulator [32][34]. The set of possible reachable points inside the three dimensional space is the robot work-space, the solutions must maintain the robot inside this space. In order to solve the inverse kinematics, depending on the complexity of the kinematic chain, different methods can be adopted.

Geometric and analytic based solutions

For industrial robot arms the analytic approach is widely used. This solution can be applied only under specific conditions such as the intersection of elbow joints and the absence of redundancy. A non-redundant manipulator is characterized by a structure with less then six DOFs. For these manipulators a pose inside the space can be reached with only one configuration of the joints, so the inverse kinematics has a unique solution [34][35]. A closed-form solution can be obtained either with algebraic computation or geometric intuition.
Algebraic computation aim is to obtain mathematical equations that contains as unknown variables the joint variables.
Another approach can be the geometric one, the purpose is to find interesting geometrical relations between points of the structure and to express, with respect to them, the variables relative to position and orientation as function of a reduced set of unknowns variables [32].
Sometimes it is possible to use the geometric approach also for redundant manipulators by decoupling the inverse kinematic problem and analyzing sub-systems of the chain instead of consider the entire structure [34].

Differential kinematics

The execution of a given task requires a certain number of DOFs but it is typical that manipulators possess more than the necessary DOFs to perform that task.

Any robotic arm with a structure composed by more than six DOFs is redundant. Since there is more than one way to reach the desired collocation of the end-effector inside the Cartesian space, the number of solutions for redundant manipulators grown to infinity.
For these manipulators a possible technique to solve the inverse kinematics is the implementation of the differential kinematics.
Differential kinematics requires the study of the Geometric Jacobian matrix a mathematical tool that allows to map the joint velocities into the Cartesian space and angular velocities of the end-effector.
Defined $\dot{p_e}$ the end-effector linear velocity, ω_e the end-effector angular velocity and $\dot{q}$ the joint velocities. It is possible to express the following relations:

$$\dot{p_e} = J_P\left(q\right)\dot{q}$$

$$\omega_e = J_O\left(q\right)\dot{q}$$

J_P and J_O are $(3 \times n)$ matrices that are used to relate the quantities. In compact form it is possible to write the expression of the geometric Jacobian as:

$$J = \begin{bmatrix} J_P \\ J_O \end{bmatrix}$$

Thus, the differential kinematics equation that describes the manipulator is:

$$v_e = \begin{bmatrix} \dot{p_e} \\ \omega_e \end{bmatrix} = J\left(q\right)\dot{q}$$

Depending on the joint i type the following relations hold:

- Prismatic joint

$$J_{P_i} = z_{i-1}$$

$$J_{O_i} = 0$$

- Revolute joint

$$J_{P_i} = z_{i-1} \times \left(p_e - p_{i-1}\right)$$

$$J_{O_i} = z_{i-1}$$

Thus basing on the direct kinematics relations, the Jacobian can be computed as:

$$\begin{bmatrix} J_{P_i} \\ J_{O_i} \end{bmatrix} = \begin{cases} \begin{bmatrix} z_{i-1} \\ 0 \end{bmatrix} & \text{for a prismatic joint} \\ \begin{bmatrix} z_{i-1} \times \left(p_e - p_{i-1}\right) \\ z_{i-1} \end{bmatrix} & \text{for a revolute joint} \end{cases}$$

Notice that vectors z_{i-1}, p_e and p_{i-1} are function of the joint variables [32].

- z_{i-1} is expressed by the third column of the rotation matrix R_{i-1}^{0}
- p_e is expressed by the first three elements of the fourth column of the transformation matrix T_e^0
- p_{i-1} is expressed by the first three elements of the fourth column of the transformation matrix T_{i-1}^{0}

Moreover, are defined the vectors $z_0 = \begin{bmatrix} 0 & 0 & 1 \end{bmatrix}^T$ and $p_0 = \begin{bmatrix} 0 & 0 & 0 & 1 \end{bmatrix}^T$. Finally by exploiting the inverse of the Jacobian the inverse kinematic problem for the time sample *k+1* can be solved by applying the recursive formula:

$$q\left(t_{k+1}\right) = q\left(t_k\right) + J^{-1}\left(q\left(t_k\right)\right) v_e\left(t_k\right) \Delta t$$

Some considerations can be done on this method: notice that the Jacobian matrix is strictly dependent on the frame where the end-effector velocity is expressed [32]. This numerical iterative method presents some disadvantages, the first is that the obtained solutions are only locally linearized approximations of the inverse kinematic problem [35].
Moreover, the computation of the inverse of the Jacobian is often a hard task, it is computationally heavy and needs high computational time. Additionally singularities represent the main problem of this kind of computation.

Artificial Neural Networks based solutions

Because of the limitations of the above described methods, new approaches based on machine learning are particularly interesting. Machine learning based solutions do not suffer from the highly non linearity and complexity of the inverse kinematic equations [35]. Moreover, singularities does not represent a problem anymore [35]. A class of adopted algorithms are the Artificial Neural Networks (ANN), the performances of these methods are dependent on the parameters to be tuned and on the network structure. ANN methods and others strategies based on ANN approach can be easily applied to solve the inverse kinematics problem since regression models can be locally obtained [35].

2.1.3 Introduction to Artificial Neural Networks and Fuzzy Logic

Introduction to ANN

ANN can be used to analyse the parameters of different systems; such networks are inspired to the human biological nervous system [36] and try to mimic the human reasoning. Human's brain is able to recognize and elaborate data in an easy way that, even if requires a small effort, make it possible to classify objects by analysing, for example, the amount of visual information available. The human brain performs task by exploiting the potentiality of nerve cells called neurons that works together by communicating and exchanging information. The aim of the artificial network is to resemble this kind of structure so to make it easier to automate processes that involves difficult tasks like pattern recognition and that requires the implementation of an intelligence [36].
ANN structure is organized in multiple layers, each layer is composed by processing units called neurons. The neurons are the core of the information-processing learning algorithm, they collect the input data and provide the computed output. The networks can have different characteristics that can be set thanks to some parameters, the type of functions used to evaluate the performances, the rules applied, the type of computation are different aspects of the mathematical model of an ANN [36]. The network also needs a training phase that is done by using known input-output data pairs, after the training the ANN can be used to estimate and evaluate unknown parameters.

Introduction to Fuzzy logic

Thanks to their ability ANNs are able to learn in an automatic way from the training data set, are able to find a good approximation to relate a given input with a predicted output [37].
An adoptable intelligent decision making technique is the Fuzzy Inference System (FIS). Fuzzy Logic is a particular method of reasoning that tries to mimic the human ability of assign a level of truth to the assertions. Thanks to its concise form, fuzzy logic makes it possible to capture the imprecise modes of thinking that are typical of the humans, fuzzy logic proposes to take decisions in an environment of uncertainty and imprecision [38].
Fuzzy logic establishes the input-output relation by making use of if-then rules. This logic allows to assign a linguistic value to the assertion to be evaluated, different levels of truth that ranges from the linguistic value "yes" to the linguistic value "no" can be explored, for example linguistic levels such as "possibly yes", "cannot say" or "possibly no" can be associated to a preposition. In this way it is possible to explore all the range of possibilities between the traditional Boolean

values 0 and 1.
If-then rules are the FIS core, they can be of different type, here it is reported an example of Takagi and Sugeno's if-then rule:

$$\text{"}\textit{If the velocity is high, then the force is } F = k\,(v)^2\text{"}$$

In the first part of the statement the word "high" is a linguistic label and it is associated with a membership function [38]. A membership function is a graph used to define how to map a point of the input space to a membership value that is included between the logic values 0 and 1.
The second part of the statement the output is obtained as a non-fuzzy function of the input. Inside a FIS the output of each Takagi and Sugeno's if-then rule is obtained as linear combination of the input variables with the addiction of a constant term [38]. The FIS structure is composed of different blocks, a schematic is reported (Figure 2.3) to show how the input is elaborated to obtain the final output, each block of the FIS is dedicated to a particular purpose:

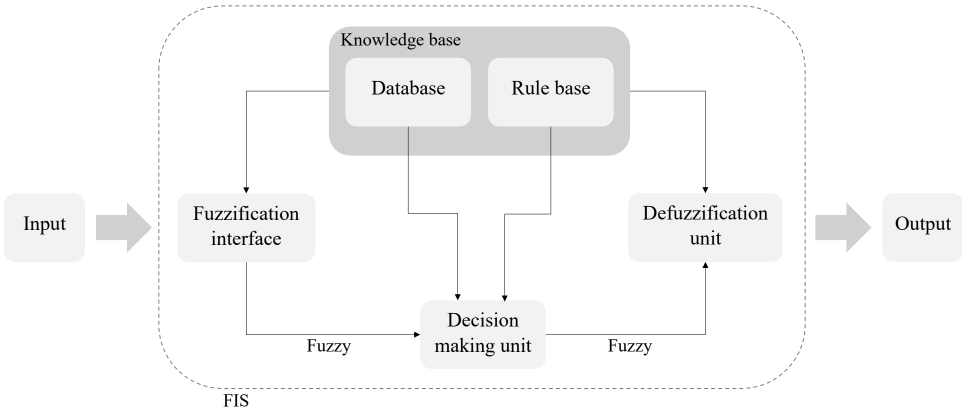

Figure 2.3: Fuzzy inference system block diagram [38].

- The database identifies the membership functions to be used in the fuzzy rules.
- The rule base contains a certain number of fuzzy if-then rules.
- The decision-making unit performs the operations of inference on the rules.
- The fuzzification interface computes the degrees of match between the crisp inputs and linguistic values.
- The defuzzification interface elaborates and aggregates the qualified consequents of the inference fuzzy results to obtain the crisp output.

The type of the FIS is determined by the way of reasoning adopted and the type of if-then rules. For example, if Takagi and Sugeno's if-then rules have been adopted, the final output of the system will be the weighted average of all the rules output.

Adaptive-Network-Based Fuzzy Inference System

Adaptive neuro-fuzzy inference systems (ANFIS) are obtained by combining ANN and FIS strategies and taking advantages of both of them. ANFIS can be described as a multilayer feedforward network [38], all the nodes of the network perform different actions on the received input. Nodes can belong to two different categories: square nodes and circles nodes, the difference between the two is that square nodes have parameters associated to them, these parameters describe the adaptability of the node. On the other hand, circle nodes do not have assigned parameters, they are also called fixed nodes.
The parameters corresponding to the adaptive nodes are updated depending on the training data set, in this way it is possible to obtain the correct input-output mapping. ANFIS makes use of fuzzy if-then rules, implemented inside a neural network-like structure, and of learning algorithm to predict the output with the minimal possible error. The learning algorithm employed by the ANFIS can be described in two steps: the first step is typically called off-line learning and it is a mechanism, this phase is a forward pass with evaluation of least square error, then the second step is a gradient descent algorithm that exploits mathematical strategies like the back propagation [37][39].
A fuzzy based procedure is used to acquire information on the data set [40]. The neuro-adaptive learning techniques allow to identify the best parameters for the membership functions to obtain the optimal FIS tracking for the given input-output data. The obtained input-output map can be interpreted through a network structure like the ANN [40].
As stated above, ANFIS is a multi-layer network (Figure 2.4), each layer provides a different function: *Layer 1* is responsible for the fuzzification operation, *Layer 2* applies the defined rules, *Layer 3* operates a normalization, *Layer 4* actuates the defuzzification, finally *Layer 5* is the output layer and provides the system output [41][42].
As shown in*Figure 2.4*, that represents a Takagi Sugeno Fuzzy inference system implemented by the ANFIS different inputs can be provided to the system, while a single output is computed. A description of each layers is provided:

- *Layer 1*: the nodes of this layer are of square type, so they are adaptive. The node i of layer 1 can by described by the node function $O_i^1 = \mu_{A_i}(x)$, x is the node input, μ is a bell-shaped function, typically with maximum equal to 1 and minimum equal to 0 and A_i is the linguistic value that is associated with the node function [38]. The described node function O_i^1 represents the

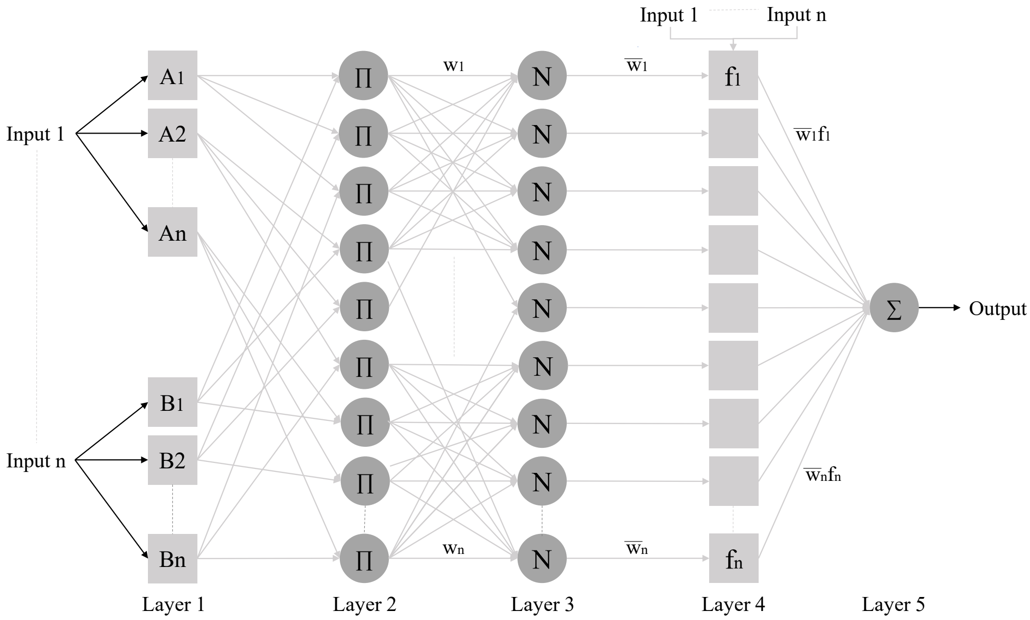

Figure 2.4: Multilayer ANFIS network structure [38].

membership function of A_i and quantify the degree of match between the given input x and the quantifier A_i [43][38]. There are different possible expressions for the function $\mu_{A_i}(x)$, here are reported two possible formulations:

$$\mu_{A_i}(x) = \frac{1}{1 + \left[\left(\frac{x-c_i}{a_i}\right)^2\right]^{b_i}}$$

$$\mu_{A_i}(x) = \exp - \left(\frac{x-c_i}{a_i}\right)^2$$

The reported equations depend on the set of premise parameters a_i, b_i, c_i, by varying these parameters it is possible to obtain different bell-shaped functions, thus different membership functions [43][38].

- *Layer 2*: the nodes of this layer are of circle type, so they implement a fixed function that is a generalized fuzzy AND logic. The node multiplies all the incoming signals, it implements the firing strength of a certain rule. For the structure proposed, the rules are if-then rules of Takagi and Sugeno's type [43][38]. For instance the equation will be of the form:

$$\omega_i = \mu_{A_i}(x_1) \times ... \times \mu_{B_i}(x_2), i = 1,2, ...n$$

Layer 3: the nodes of this layer are circle type, it is computed the ratio between the i^{th} rule's firing strength and the sum of all the others rule's firing strengths [38]. Thus,the so called normalized firing strengths can be computed as:

$$\bar{\omega_i} = \frac{\omega_i}{\sum_{i=1}^{n} \omega_i}, i = 1,2,...n$$

Layer 4: the nodes are of square type, the input to this nodes are the output of *Layer 3*. Once defined the set of the consequent parameters $[p_i, q_i, r_i]$ [38], the node function can be expressed as:

$$O_i^4 = \bar{\omega_i} f_i = \bar{\omega_i} \left(p_i x + q_i y + r_i \right)$$

Layer 5: it is composed by a single circle node that computes the overall sum of all the incoming signals [38], the equation of this node is:

$$O_i^5 = overalloutput = \sum_{i=1}^{n} \bar{\omega_i} f_i$$

The described layered structure, after a proper training, is able to map the inputs provided to the system to the corresponding predicted outputs. This predictive system can be used for several applications (control systems, image processing, decision making), it is of our interest to apply these networks for the solution of the inverse kinematic problem.

ANFIS application for inverse kinematic

ANFIS can be applied to robotic kinematic chains study to generate the necessary joints configuration to obtain a desired behaviour of the manipulator [44]. Neural networks can be implemented to overcome the main limitations of the analytic and geometric solutions in terms of high amount of required calculation [45]. The predictive methods can be used to find an approximation mapping function able to correlate the pose of the end-effector with the joints configuration, an opportune training is needed to obtain an accurate and repeatable estimated solution [46]. During the training phase the parameters related to membership functions and weights have to be adjusted in order to satisfy the minimum error requirement [47]. Using this modelling technique the direct kinematic study is employed to create the data set for the training of the networks [44] , then the trained ANFIS are used to generate the servomotors correct positions for the actuation of the manipulator [44].

The application of this unconventional approach, in solving the inverse kinematic problem, results in a simple algorithm with fast learning and competitive performance with respect to the traditional computational method in terms of precision in the estimated measurement [45].

2.1.4 Admittance control

Human robot interaction is a fundamental aspect to be analysed when dealing with robotic systems used for rehabilitative purposes. Different control techniques can be adopted, the admittance control is one of the possible choices. Admittance control can be implemented to handle the exchange of generalized forces (forces or torques) between the human user and the robotic structure [48]. Thanks to the implemented control, the system becomes compliant when a force or a torque is sensed [49], in this way the position of the end-effector is modulated according to the force applied by the human and, since the admittance control is used in combination with a position controlled plant [50], the joint configurations will be dependent on the output of the admittance control [51]. The resulting control signal is a combination of the target position and of a term due to the application of a user torque (force), the system during the application of the torque (force) behaves in a compliant way allowing a deviation from the target position.

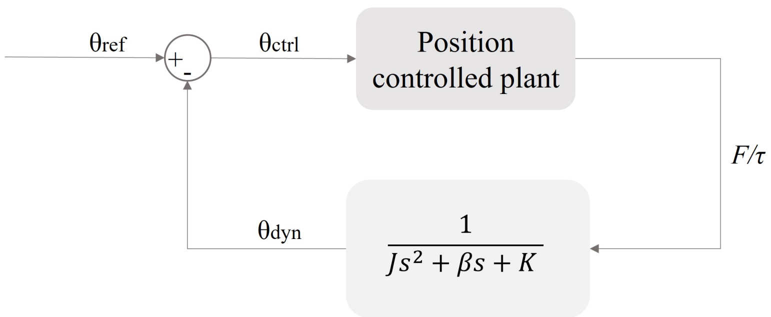

Figure 2.5: Admittance control scheme: the position controlled plant represents the actuator that allows the joint movement, it is controlled by a position control that receives as input a signal θ_{ctrl} that considers both the target position θ_{ref} and the dynamic deviation θ_{dyn} contributes. θ_{dyn} is computed considering the effect of the external force or torque that is sensed from the controlled plant.

A deviation from the desired trajectory is computed depending on the applied external torque (force): the definition of this relationship is the fundamental aspect of the implementation of the admittance control [50].
Admittance control mathematics description can be done by studying a mass, spring, damper system: to obtain a desired effect of the controller, a proper value for the inertia, the damping coefficient and the spring stiffness have to been set [52].

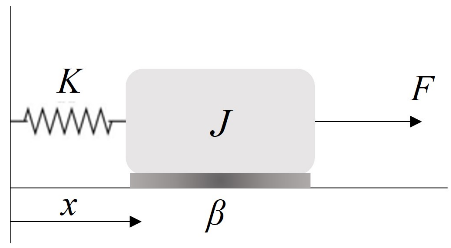

Figure 2.6: Mass, spring, damper system used to describe the admittance control dynamics equation.

The described system can be described with a second order equation that relates the joint position with the sensed torques by means of a dedicated transfer function [53]. Considering the system in *Figure 2.6*, the dynamics of the system can be described as

$$\frac{d}{dt}\left[J\dot{x}\left(t\right)\right] = F\left(t\right) - \beta\dot{x}\left(t\right) - Kx\left(t\right)$$

$$F\left(t\right) = J\ddot{x}\left(t\right) + \beta\dot{x}\left(t\right) + Kx\left(t\right)$$

Thus, the transfer function of the system, in Laplace transform domain, is described as

$$G\left(s\right) = \frac{X\left(s\right)}{F\left(s\right)} = \frac{1}{Js^2 + \beta s + K}$$

The contribute in position term given by the admittance control is given by

$$X\left(s\right) = F\left(s\right)\frac{1}{Js^2 + \beta s + K}$$

Where $F\left(s\right)$ is a generalized force (force or torque).

2.1.5 Metrics for results evaluation

In order to evaluate the performance of test, simulations and acquisitions, the collected data results can be compared with the theoretical expected ones. For this purpose some mathematics indicators can be used.

Absolute Error
It is a measure of how far is the measured data, the one obtained for example during testing and simulation, from the theoretically expected one. It is an algebraic measure, its value can be positive or negative, expressed in the same unit of the acquired data. Defined:
i = *index of the sample*
d_i = *experimentally measured value*

f_i = *theoretically computed value*

$$AbsoluteError = \left(d_i - f_i\right)$$

Root Mean Square Error
The Root Mean Square Error (RMSE) is the standard deviation of the residuals and is a measure of how the residuals are spread out. The residuals gave information about how far the obtained data points are from the regression line. RMSE gave an indication of how concentrated are the collected data with respect to the line of the best fit. It is an absolute error measurement where the deviations, differences between the measured value and the expected one, are squared in order to avoid that positive and negative values cancel out each other when summing all of them. The mean is computed on N data points. It is expressed in the same unit of the measured data. Defined:
N = *number of samples*
i = *index of the sample*
d_i = *experimentally measured value*
f_i = *theoretically computed value*

$$RMSE = \sqrt{\frac{1}{N}\sum_{i=1}^{N}\left(d_i - f_i\right)^2}$$

2.1.6 Vicon Nexus motion capture system

Nexus is a powerful modeling and processing tool that is intended to be used for movement analysis [54]. In Vicon Nexus it is possible to capture and analyze the movement of both live subjects, such as human beings, and of inanimate objects, such as experimental set up and test bench. It provides precise, repeatable and clinically validated data. The applications of this system are several, for example gait analysis, rehabilitation evaluation, bio-mechanics study and motor control.
The acquisitions can be done for different purposes that require motion capture applications. The motion data can be streamed real time or also captured, saved and post processed offline.
The acquired data can be processed in different modeling environment by using scripts created in Vicon BodyBuilder, Python, MATLAB or Vicon ProCalc.

The system works by acquiring and recording the motion of the markers, pearl hard marker on plastic base that are fixed on point of interest and recognized by the system of cameras. The movement of those markers is referred to a reference frame chosen and allocated inside the space during the calibration phase.

Figure 2.7: Vicon Nexus components: Vero camera and markers [55].

The typical workflow of the operation to be performed to acquire the motion are [54]:

- *Settings of the Vicon system*
  The system for the motion capture has to be configured, Vicon Cameras, Vicon connectivity units and any other supported devices have to be set up.

- *Calibration of the Vicon system*
  It must be done before the beginning of the motion capture in order to ensure that possible changes in the system, like movement of the cameras or of other equipment from the precedent acquisition will not affect the new acquisition.

- *Preparation of the subject*
  When a new subject is under test it is necessary to define a labeling skelethon for the acquisition and to calibrate this skelethon. The markers are applied on the points of interest on the subject and labeled in order to make it possible to recognize them on the displayed 3D reconstruction.

- *Capture movement trials*
  Acquisition of the data. The movements of the markers, referred to the chosen reference, are recorded by the cameras.

- *Review trials and fill gaps*
  Process used to fill gaps in the data after the capture, the reconstruction and the labeling of the recorded movement.

- *Export of trial data*
  Final stage of the motion capture, data are imported and then elaborated on an host device with a desired software.

2.2 Software

2.2.1 MATLAB

MATLAB is a programming platform designed by MathWorks and it is intended to be used for systems design and analysis.
It is based on a matrix-based language that allows to write mathematics computation in an easy understandable form. It can be used for data analysis, algorithms development and creation of model and applications. Thanks to the different available tools it found application for robotics and machine learning too [56].

2.2.2 Simulink: Simscape and Simscape Multibody

Inside MATLAB different design environment can be found. For the purpose of the developed project Simulink, Simscape and Simscape Multibody have been used.

Simulink

Simulink allows to create graphical models through the combination of different blocks. Multi-domain modeling and simulations can be performed to evaluate how different parts of a system interact each other. The modeling is done by using predefined blocks where parameters can be set [57]. It is possible to use Simulink also to develop real time applications and to configure communication protocols when the developed application is intended for control a system that exchanges data with other devices.

Simscape

Simscape is a tool that allows to develop models of physical components inside the Simulink Environment. Several libraries are available to make it possible to design for example mechanical, hydraulics and electrical systems [58]. The physical components can be characterized by setting different parameters, in this way their behaviour will be as similar as possible to the one of reals components. Once all the components of the system are characterized and the interaction between them defined it is possible to run simulation that allows to understand the behaviour of the simulated system, that will correspond to the behaviour of the physical one. This method allows to avoid all the time consuming testing operation that are typically done with real test bench, it also allows to reduce the testing costs and to understand the performances and the limits of the analysed system.

Simscape Multibody

Simscape Multibody provides a simulation environment for mechanical 3D systems like robots. Blocks are available to represent bodies, joints, constraints, force sources and sensors. The software is able to compute and solve the motion equations and it provides 3D simulations where the dynamics of the system can be appreciated [59]. It is possible to import inside the body blocks geometry designed with CAD software with all the characteristics related to the mass, inertia, constraints and joints defined into the 3D design phase. One of the CAD software that can export a file importable in Simscape Multibody is Creo Parametric.

2.2.3 App Designer

Inside MATLAB it can be found the tool App Designer, an intuitive software that allows to develop professional applications [60]. Specifically, it allows to design graphic user interfaces (GUI) that are graphical applications that make it possible, for example, to modify parameters in a Simulink model during real time simulations, in fact, it is possible to set parameters in the Simulink blocks used to build the model components. To obtain the GUI two design phases are needed: the graphical definition of the components (buttons, switches, light indicators and so on) that is done inside the Designer section of the App Designer software and the definition of a MATLAB code that links the action performed on the GUI with the components of the controlled model defining the behaviour of the app and the corresponding response of the model itself, this second phase is done in the Editor section of App Designer.

2.2.4 Creo Parametric

Creo Parametric is a 3D modeling software used in different field like model based definition, generative design and additive manufacturing, augmented reality. Inside this virtual environment the digital prototype of the product can be designed and explored in detail. With this software it is possible to design and assemble mechanical components by defining the physical characteristics of the objects (dimension, mass, inertia, materials and so on) and also manipulate them [61].It is possible to drag the components to understand how they are assembled and how they interact each other, they can, for example, rotate or translate one respect to the other inside specific mechanical stops. There is the possibility to make precise measurements of the distances between parts of interest and of the sizes of the components. It is also possible to automatically compute the kinematic relations between different parts of the same assembled project: once reference frames have been defined for the points of interest the relation between them is provided in form of homogeneous transformation matrix.

2.3 Hardware

2.3.1 Series Elastic Actuators: an introduction

Robotic mediated rehabilitation must guarantee a safe human-robot interaction, for this purpose the actuation system has to be carefully designed, the objective is to implement a compliant actuation able to assist the human body during the desired dynamic motions [62], and able to follow the patient movements by minimizing the interaction forces [63]. Systems that allows the presence of a human in the control loop can be employed: the force-controlled Series Elastic Actuators (SEAs) are a widely used solution [64]. SEAs are compact size components characterized by the presence of an elastic element that is used to increase force accuracy by converting the traditional force control problem into a position control problem [65]. In fact, if the elastic characteristic of the spring is known, the deformation can then be traduced in a data relative to the transmitted force [66]. SEAs high reliability and response speed make this actuation system adoptable during the different rehabilitation stages [67]. SEAs allow to realize both position and torque control, the first control method is mostly used during the acute phase after the stroke occurrence while the torque control can be used to implement an assistance-as-needed during the second phase of the rehabilitation [68]. The human-robot interaction during the rehabilitation phase that sees the patient actively involved, can be made less stiff thanks to SEA implementation. Moreover, in case during the rehabilitation exercises sudden spastic contractions occur, thanks to the presence of the elastic element, the patient does not perceive the stiffness of the motor but experiences a compliance interaction thanks to the spring [68]. From a mechanical point of view, SEAs are composed of an electro-mechanical motor, a gear reducer and a spring placed after the gear stage (to make the output stage sensitive to the series elasticity) [66]. The stiffness of the compliant element can be chosen by evaluating different requirements such as shock resistance, safety and bandwidth [66]. Thus, SEAs show to have advantages over the traditional actuators that even if can be lighter, more compact and show to have a better behaviour in following trajectory control, have a worse time response and a worse dynamic bandwidth, with respect to SEAs, due to the limitations imposed by the control and by the electric properties of the actuator [62].

2.3.2 Series Elastic Actuators: components description

Series Elastic actuator system is composed of three components below analyzed: the motor, the gear reducer and the compliant element.

DC brush-less motor

The motors implemented inside the analyzed SEAs are:

- Maxon EC 45 flat Φ43.5 mm, brushless, 80 Watt
- Maxon EC 90 flat Φ90 mm, brushless, 90 Watt

The mechanical, thermal and electrical characteristics of *Maxon flat motors* are reported in *Table 2.1.*

Motor Data	**EC 90 flat BLDC**	**EC 45 flat BLDC**
Values at nominal voltage		
Nominal voltage [V]	24	24
No load speed [rpm]	3190	5600
No load current [mA]	544	270
Nominal speed [rpm]	2590	4560
Nominal torque (max. continuous torque) [mNm]	444	167
Nominal current (max. continuous current) [A]	6.06	3.96
Stall torque [mNm]	4940	1690
Stall current [A]	70	42
Max. efficiency [%]	84	84.9
Characteristics		
Terminal resistance phase to phase [W]	0.343	0.573
Terminal inductance phase to phase [mH]	0.264	0.301
Torque constant [mNm/A]	70.5	40.4
Speed constant [rpm/V]	135	236
Speed/torque gradient [rpm/mNm]	0.659	3.350
Mechanical time constant [ms]	21.1	6.350
Rotor inertia [gcm^3]	3060	181

Table 2.1: EC90 and EC45 Maxon flat BLDC motors mechanical, thermal and electrical characteristics.

Encoders

AksIM-2 off-axis rotary absolute encoder is a high performance device, it works conctactless and thanks to the reduced dimensions it can be easily integrated in systems where there is not lot of space available. The system is composed of two elements: a magnetised ring and a readhead. The encoders allow the transmission of data through different communication protocols, UART, SPI PWM and SSI are allowed. The binary resolution of the readings varies in a range up to 20 bits per revolution. The AksIM-2 system is able to self monitor its functionality and to report errors or warning condition. For this purpose some bits of the sent message are reserved to identify if the system is working correctly, if there is a warning or an error, these conditions are also provided by an on-board LED. The light of the led can assume three colors: green (correct), orange (warning) and red (error) according to the result of the self-monitoring.

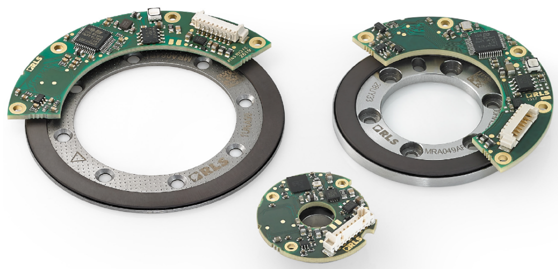

Figure 2.8: AksIM-2, RLS Off-Axis Rotary Absolute Magnetic Encoder

Wrap operation

AksIM-2 encoders provide measurements in a digital discrete unit: ticks unit is adopted. Once the data have been acquired it is necessary to elaborate them by performing the so called *wrap operation*. Wrap is a mathematical operation that allows to modulate measurement in the linear domain $[-\infty, +\infty]$ to measurement in the circular domain $[-\pi, +\pi]$ or $[-180{,}180]$ depending on the unit adopted, radians or degrees.

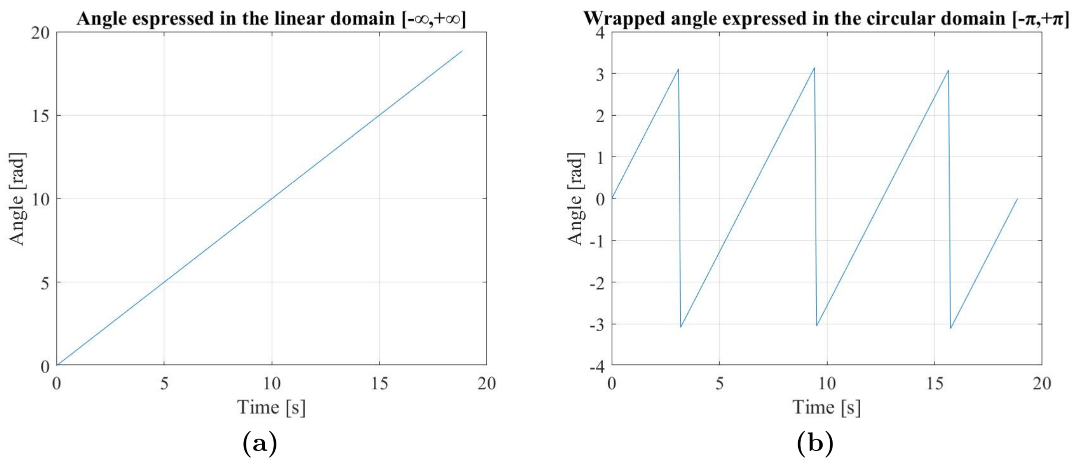

Figure 2.9: Example of the effect of the wrapping operation. a) Angle expressed in the linear domain b) Wrapped angle, the domain range is restricted to $[-\pi, +\pi]$ thus the angle is expressed inside this interval.

Harmonic drive

The CSD-17-2A-100 harmonic drive is made of three components: an elliptic steel disc, a flexspline and a cylindrical outer ring [69]. The first element is connected to the motor shaft, the second element outer circumference is sourronded by teeth that are in conctant with the teeth of inner circumference of the last components. The main features are the numbers of the flexspline and of the circular spline [69]. The gear reduction ratio depends on these quantities. The number of teeth present on the outer toothing of the flexspline is lower than the number of teeth on the inner toothing of the circular spline. The reduction ratio is obtained as:

$$\text{Reduction ratio} = \frac{\text{Flex spline teeth-Circular spline teeth}}{\text{Flex spline teeth}}$$

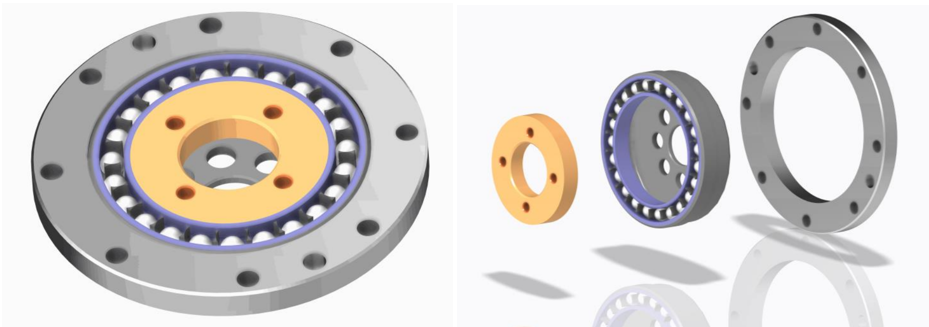

Figure 2.10: CSD-17-2A-100 Harmonic Drive CAD model. System assembled and single components view.

The advantages provided by the Harmonic drive are the small size and low weight that makes this device usable for compact systems, moreover the backslash does not augment during the lifetime of the components. The harmonic drive works play-free and guarantees for the whole torque range high level of torsional rigidity [69].

Compliant element

The compliant element mounted inside the SEA is a custom made torsional spring. All the analyzed components have been designed by IIT-Rehab technologies laboratory. Different geometries solutions have been adopted and different materials used to build the components. The springs mounted inside the analyzed actuators are:

- Titanium SPiral spring with two Pins (SPT2P)

- Steel STar spring (STA)
- Titanium SPiral spring with single Pins (SPT1P)

Analysing the State of the Art, it has been found that the provided torques at joint must worth about *35 Nm* for the spherical joint and about *60 Nm* for the scapular joint. In order to obtain the SEA desired performances in terms of maximum provided torque and maximum deformation, the materials and geometry for the design of the compliant element have been chosen. The opportune trade off between an high structural stiffness and a good sensibility of the measure is tried to be reached by analysing the different combinations of materials and geometries. It is known that an higher deformation, obtained under the same torque load, guarantees an higher quality of the measure, the problem arises from the control point of view: a less stiff structure can be more difficult to be controlled. The requirement for a valuable compliant element, considering torque and displacement measurements are: linear behaviour, low hysteresis and absence of death-band. The hysteresis is a loss of energy caused by frictions and sliding between components, it is of interest because a low hysteresis is an indicator of high sensor precision. The hysteresis is the measure of the maximum difference between the there and back measurements during a calibration cycle of the sensor. It is expressed as a percent of the full-scale. The effect of the presence of the hysteresis is that at the same input are associated more outputs (it depends from the input state at the measurement time, the input can be in the increasing phase or in the decreasing phase), and the wider is the hysteresis the higher is the output number and so the less precise is the sensor.

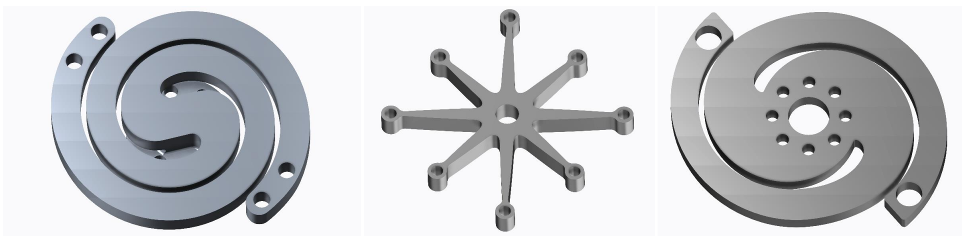

Figure 2.11: Custom made compliant elements designed by IIT-Rehab technologies laboratory. Different geometries are adopted, the first is a titanium spiral spring with two pins, the second a steel star spring and the last a titanium spiral spring with single pins.

Springs material
The high performances required to the designed SEA can be obtained by using materials able to correctly behave under elastic strain and that are characterized by high fatigue limits. The mostly implemented materials are the ones with high resilience, for this reason titanium alloys and steel alloys can be used to build the compliant element.

Springs geometry
The different geometries have been evaluated on the base of technical features (Table 2.2) to understand the preferable one for the desired application. The star and spring geometries have been studied to analyze the critical aspects of both the design: what resulted is that the spiral geometry is favorable because it better fit the available space. The spiral design allows to obtain higher deformation than the star geometry if evaluated under the same torque load. Also evaluating the hysteresis, the spiral spring resulted to be more performing than the star spring as shown in results *Section 3.1.2* in *Figure 3.11*.

	Rechable stifness	Maximum defomration or maximu rotation	Axial encumbrance	Uniform distribution of tensions	Compatibility with available space	Scalabilty
Star geometry (STA)	High	Low	Low	High	Low	Medium
Spiral geometry (SPT)	Low	High	Medium	Low	High	High
	Good		Fair		Bad	

Table 2.2: Qualitative evaluation of the main technical features of the analysed compliant element geometries. Star and Spiral geometries have been evaluated.

The geometry design must take into account different factors, it must guarantee an easy assembly, it must be compact to be integrated in the available space, a low weight is also required. Also the production cost and the necessary production methods must be evaluated to understand if the geometry can be reproduced and produced in several copies.

2.3.3 Actuators under test: system components

EC90 motor SPT2P compliant element

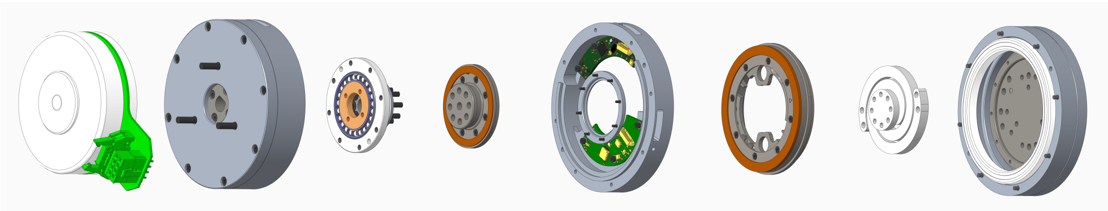

Figure 2.12: Components view of EC90 motor with SPT2P compliant element. The principal components are: EC90 BLDC motor, Harmonic drive, encoders and the titanium spiral compliant element.

The first SEA under test is composed as follows:

- Brushless DC motor: EC90 flat, $\Phi 90mm$
- Transmission element: Harmonic Drive, CSD-17-2A-100
- Encoders: AksIM-2 off-axis rotary absolute encoder 18-bit resolution. The two encoders are mounted one parallel to the other, the first located upstream of the compliant element, the other downstream of the compliant element. The measure of the displacement is provided by the difference between the readings of the two encoders.
- Compliant element: custom made torsional spring, titanium spiral with two pins (SPT2P)

EC90 motor STA compliant element

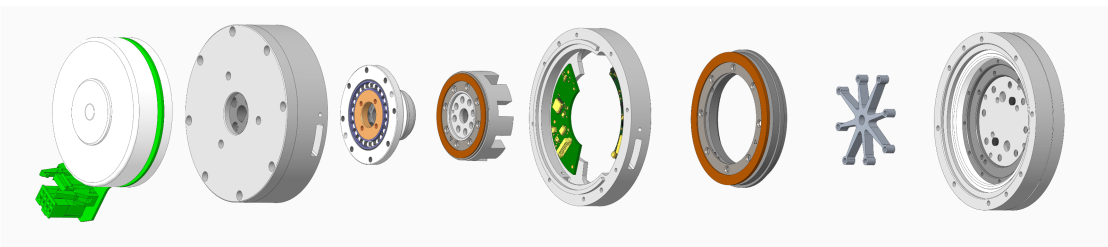

Figure 2.13: Components view of EC90 motor with SPT2P compliant element. The principal components are: EC90 BLDC motor, Harmonic drive, encoders and the steel star compliant element.

The second SEA under test is composed as follows:

- Brushless DC motor: EC90 flat, $\Phi 90mm$
- Transmission element: Harmonic Drive, CSD-17-2A-100
- Encoders: AksIM-2 off-axis rotary absolute encoder 18-bit resolution. The two encoders are mounted one parallel to the other, the first located upstream of the compliant element, the other downstream of the compliant element. The measure of the displacement is provided by the difference between the readings of the two encoders.
- Compliant element: custom made torsional spring, steel star (STA)

EC45 motor SPT1P compliant element

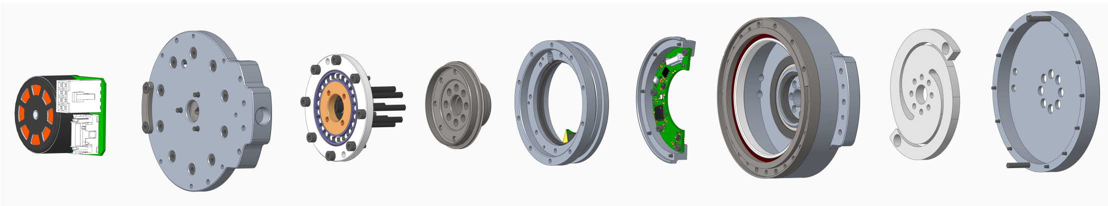

Figure 2.14: Components view of EC45 motor with SPT1P compliant element. The principal components are: EC45 BLDC motor, Harmonic drive, encoders and the spiral compliant element.

The last SEA under test is composed as follows:

- Brushless DC motor: EC45 flat, $\Phi 43.5mm$
- Transmission element: Harmonic Drive, CSD-17-2A-100
- Encoders: AksIM-2 off-axis rotary absolute encoder 20-bit resolution. The two encoders are mounted specularly one to the other, the first located upstream of the compliant element, the other downstream of the compliant element. The measure of the displacement is provided by the sum between the readings of the two encoders.
- Compliant element: custom made torsional spring, titanium spiral with single pin (SPT1P)

2.3.4 Real time target machine: SpeedGoat

In order to perform real time simulation, it has been employed a real time target machine. The one used for all the performed test is Speedgoat.

Figure 2.15: Performance real-time target machine.

This machine is intended to be used together with Simulink and Simulink Real-Time tools provided by MathWorks and allows to run real time applications created on MATLAB Simulink environment. By using the Speedgoat Simulink driver blocks inside the model, it is possible to automatically generate the application in real time, then it is download and run on the machine.
Speedgoat offers a wide range of multi-core with high performances and multi-CPU target computers. It can be adopted in different areas like rapid control prototyping (RCP) and Hardware-in-the-Loop (HIL) systems. In the figure below it is reported the so-called V-shape workflow used to design a real time application.

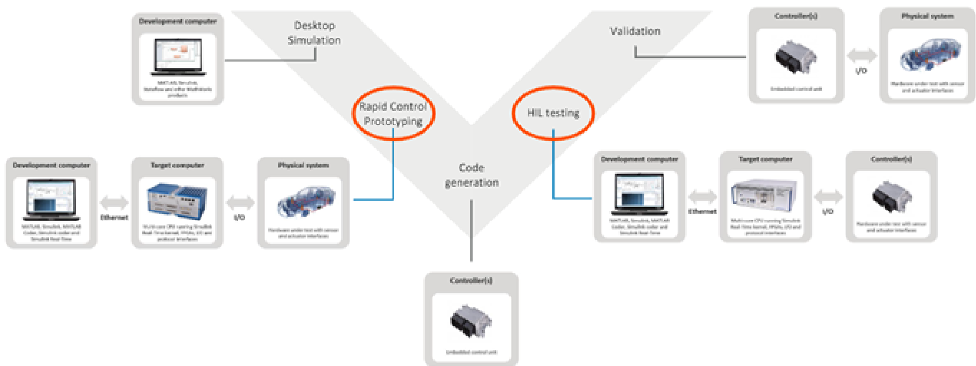

Figure 2.16: V-shape workflow for real time application develop process

Speedgoat is a powerful hardware that allows to interface, with several communication protocols, devices like prosthesis and exoskeletons and also, like motors and encoders. The rapid prototyping is an innovative solution useful to be able to test both controllers and the kinematic or dynamic during a real time simulation.

Onboard communication ports
The target machine has integrated communication ports that enable the device to interact with the outside world.
To interact with the device it is necessary to correctly set up the communication between the real time machine and the host device (user personal computer), this is done by configuring the Internet Protocol IPv4 with the necessary address and sub-net mask.
In order to visualize real time the data of interest, it can be connected to a target screen, particularly useful during testing phases. On the display here are shown all the data that inside the Simulink model of the application are addressed to a target scope. The target scope is a Simulink block that belongs to Simulink Real-Time displays and logging library.

Figure 2.17: Speedgoat typical connection configuration.

The real-time Scope block is used to acquire data from the real-time application that is executing on the target computer and display these data on the target computer screen connected to the system.
As already explained, Speedgoat can communicate with other devices trough external ports, for the purpose of the experiments also the CAN ports have been used. CAN protocol has been used by employing IO614 reading and writing modules on Speedgoat Performance Machine.
In Simulink can be found the configuration ports that allow to configure the port and the module used during the communication. It is also necessary to set the correct headers to receive, unpack and send the messages, for these operations it is possible to find the necessary blocks inside the CAN Communication library. The "CAN Read" block reads messages from one port of the IO61X input queue. A

message is read every execution step along with the indication of the presence or absence of other messages. A CAN message is sent to the IO61X output buffer at each execution of the "CAN Write" block. If multiple instances of the block are used, it is possible to send messages at multiple rates.

2.3.5 Commercial motor drivers

ESCON

To control the joint under test for the 1dof setup the ESCON 70/10 servo controller has been used. The Maxon device is a compact and powerful 4-quadrant PWM servo controller. It is adopted for its efficiency in controlling brushed DC motors activated by permanent magnet.
ESCON can operate in different modes: speed control in open or closed loop and current control. The current control mode has been adopted to test the 1dof system as described in *Section 2.5*. The featured operating modes – speed control (closed loop), speed control (open loop), and current control – meet the highest requirements. The ESCON 70/10 is designed being commanded by an analog set value and features extensive analog and digital I/O functionality.

EPOS

The motor controller EPOS4 Compact 50/8 CAN produced by Maxon motor is a compact, full digital, control unit used to perform positioning control of actuators. Thanks to the high power density the device can be used for brushed DC motors. The controller allows to set different feedback options: Hall sensors, incremental encoders or absolute sensors can be used.
The communication protocol to be used to work with EPOS4 is the CANopen protocol. Inside the CANopen network the EPOS4 controllers are controlled and commanded as slave nodes.

Position control
Cyclic Synchronous Position (CSP) mode allows to control the motor with a position control. In order to correctly exploit the EPOS4 position control, the driving signals have to be traduced in increments (ticks) unit. Depending on the motor controlled (EC45 or EC90) the number of increments for a revolution at slow axis, that corresponds to a full rotation of the motor, can be computed as the product between the number of pulses for revolution (npr), the number of received positions for each pulse (npp) and the reduction ratio of the harmonic drive (rr).
For the analysed motors:

EC45: npr=2048, npp=4, rr=100

$$Inc_{EC45} = 2048 * 4 * 100 = 819200 \frac{increments}{revolution}$$

EC90: npr=6400, npp=4, rr=100

$$Inc_{EC90} = 6400 * 4 * 100 = 2560000 \frac{increments}{revolution}$$

2.4 Test benches setup for real time simulations

2.4.1 Single motor testing setup

Infinite inertial load setup

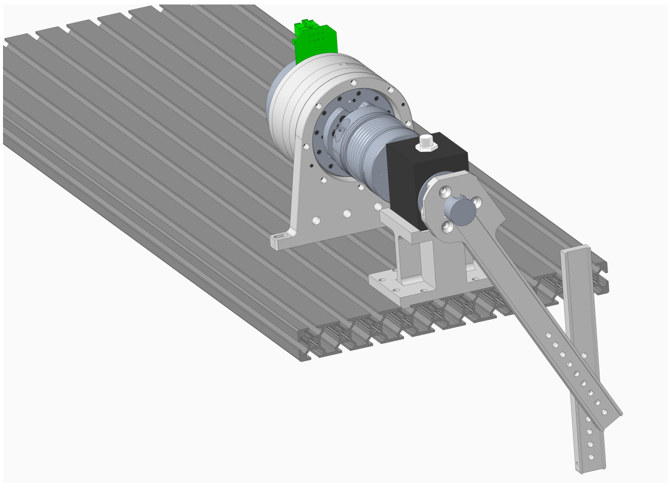

Figure 2.18: Single motor testing setup, infinite inertial load setup: the test bench is composed of the actuator (EC45-SPT1P or EC90-STA or EC90-SPT2P), a bellows used to guarantee the correct alignment of the elements, an industrial torsiometer and two steel bars used to fix the system to the bench.

The experimental set up used to analyze the frequency characteristic of the actuator is composed of the SEA that is fixed to the wall in order to provide to the system an infinite inertial load. It has been used an industrial torsiometer (2CA, RT2A 100 Nm (+/-10V)) to acquire a measure of the torque provided at the slow axis of the actuator, this measure is then compared with the torque computed through the Hooke's Law with the encoders data. The actuator is driven by the ESCON servo controller. The system is connected to the real time target machine Speedgoat that by running the developed model (Section 2.5.1) provides the input to the system and allows to collect the output information. The collected data can be downloaded from the target machine and then elaborated.

Finite inertial load setup

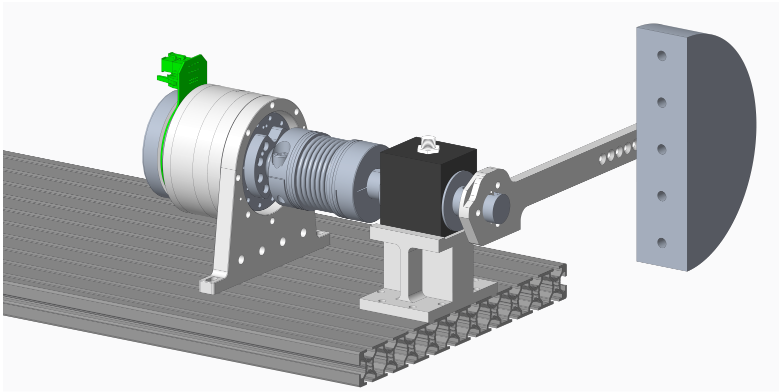

Figure 2.19: Single motor testing setup, finite inertial load setup: the test bench is composed of the actuator (EC45-SPT1P or EC90-STA or EC90-SPT2P), a bellows used to guarantee the correct alignment of the elements, an industrial torsiometer and a steel bar used to connect the desired load.

The experimental set up is used to analyze the actuator behaviour when a load is applied to the system. The load is a *3 Kg* mass attached to the actuator through a steel rod that is *0.6 m* long. The mass generates a resistive torque at the slow axis of the actuator so the system is subjected to a finite load and is free to rotate. Also for this setup the system is connected to the real time target machine Speedgoat.

2.4.2 Two degrees of freedom setup

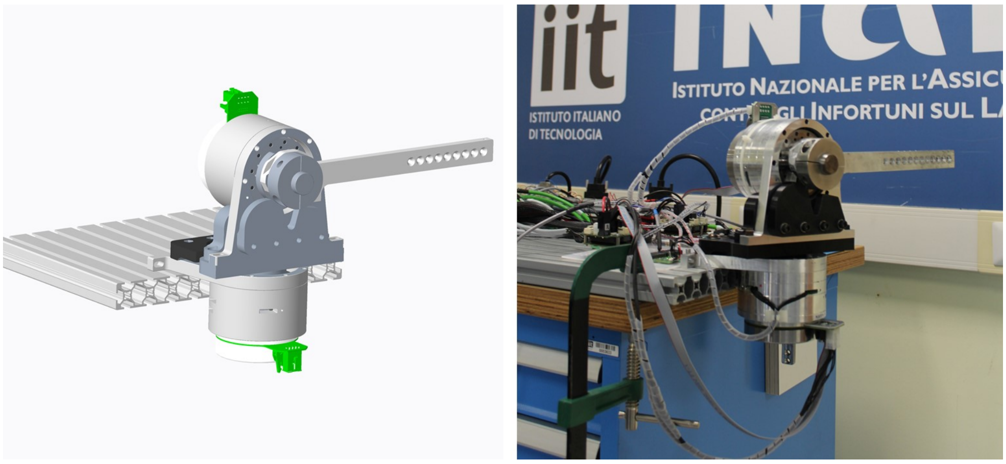

Figure 2.20: Two degrees of freedom experimental setup, CAD model and laboratory test bench: EC90 STA and EC90 SPT2P actuators mounted together.

The test bench is composed of two SEA mounted as shown in *Figure 2.20*. Both the SEA are actuated by an EC90 motor. The SEA compliant elements are the STA for one joint and SPT2P for the other one (the compliant element study is reported in *Section 3.1.2*). A steel bar is attached to the upper actuator and the extremity of this component is considered the end-effector of the system.

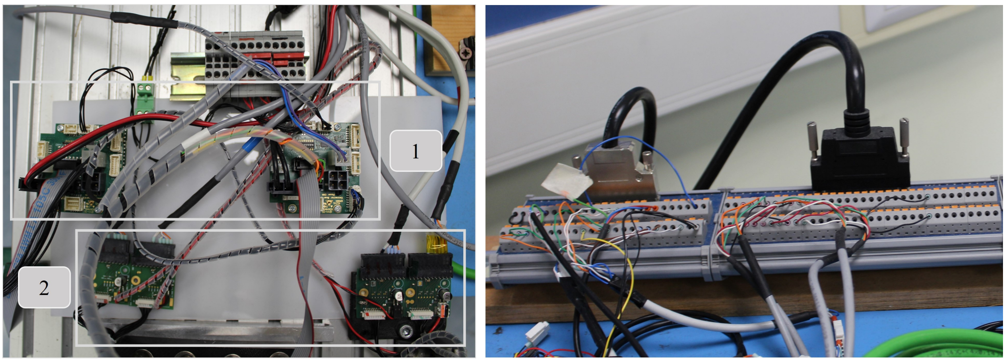

Figure 2.21: Electronic setup for 2dof system: on the left 1. EPOS boards used to drive the actuators 2.AksIM boards used to connect, by serial communication, the encoders to Speedgoat. On the right the breakout box for the AksIM-Speedgoat cabling set up communication.

The electronic setup is made of two EPOS boards that are used to control the motors rotations. EPOS is connected both to the motors and to Speedgoat by means of

CAN bus cable to allow the bidirectional communication between Speedgoat (and so with the GUI developed) and the boards. The encoders are connected in an analog wiring configuration that allows the exchange of data through serial communication to the Speedgoat real time target machine. A mushroom push button switch has been integrated to allow the power interruption in case of emergency.

2.4.3 Three degrees of freedom setup

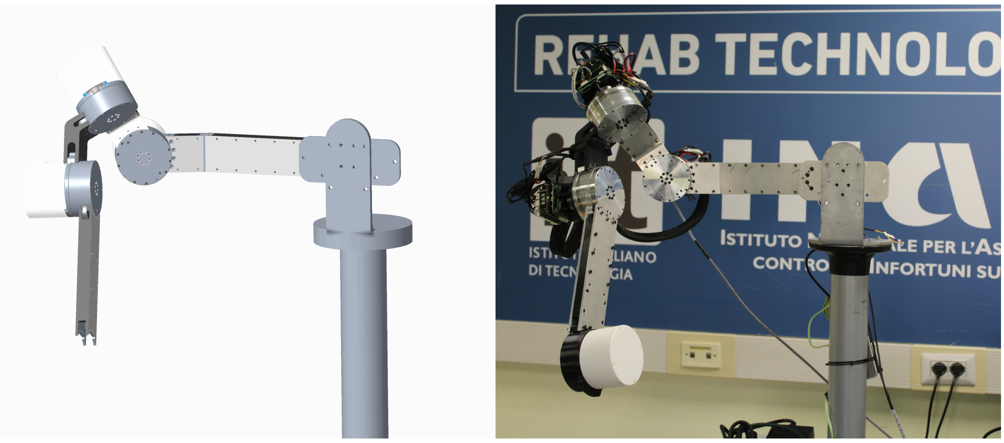

Figure 2.22: Three degrees of freedom set up, CAD and laboratory test bench. The three joints are FSJ45A01, FSJ45A02 and FSJ45A03 actuators. EC45 motors have been used and SPT1P springs mounted inside as compliant elements.

The test bench is composed by a column base mounted on a movable cart. The mechatronic structure represents the spherical joint, the structure purpose is the rehabilitation of the glenohumeral joint. Three SEA compose the structure and are connected each other by means of links made of folded aluminum sheets with ultem in the middle. The SEA all have EC45 motors and SPT1P compliant element mounted inside, referring to the characterization reported in *Section 3.1.2* the joints that compose the system are: FSJ45A01, FSJ45A02 and FSJ45A03.

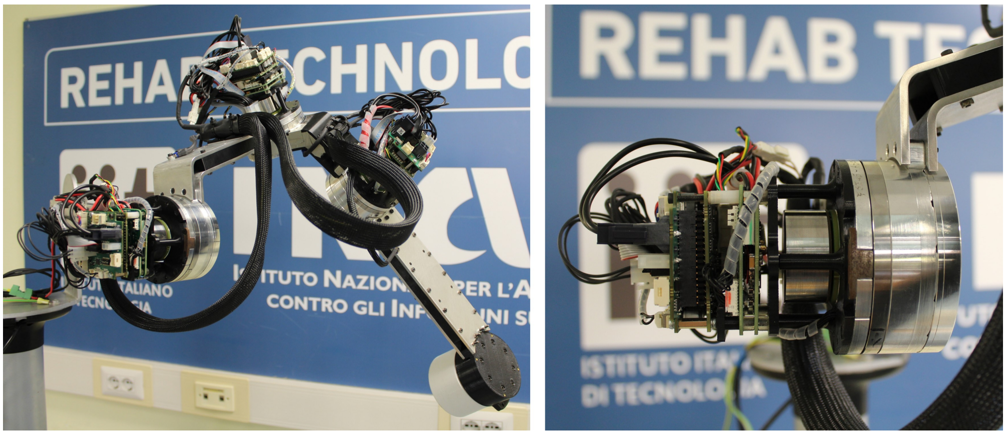

Figure 2.23: Electronic setup for the 3dof system: EPOS boards mounted on the joints, the wires for the CANopen and CAN communication are collected inside the cable sheaths.

SEAs are controlled by three EPOS boards mounted on the joints (Figure 2.23), a custom wiring system has been designed to allow the CANopen communication between EPOS and Speedgoat, also a CAN bus is used to stream data from all the AksIMs to the Speedgoat. A mushroom push button switch has been integrated to allow the power interruption in case of emergency.

Vicon motion capture room set up

Vicon motion capture instrumentation has been used to acquire the Certesian position of the end-effector, and of others points of interest, during the movement of the three degrees of freedom manipulator. The purpose of the test was to experimentally verify the set of reachable points for the end-effector. The experimental set-up is composed of the 3dof structure mounted on the movable base, Speedgoat instrumentation used to set up the encoders data acquisition, the calibration instrument for Vicon set up, the Vicon cameras and a set of markers. The manipulator has been placed in the middle of the equipped room (Figure 2.25), the markers have been fixed on points of interest. The room has been calibrated with the reference placed on the ground, in a location chosen to ensure that all the markers were visible to the cameras. The most relevant markers are the first and the last of the chain, one represents the base the other the end-effector (Figure 2.24) . The acquired data have been elaborated on Vicon Nexus 2.8.2 software in order to correctly label the markers and to avoid to consider valid the data due to light artifacts. Then a reconstruction of the acquisition has been performed, the data exported in Matlab and elaborated to refer the end-effector data to the base ones.

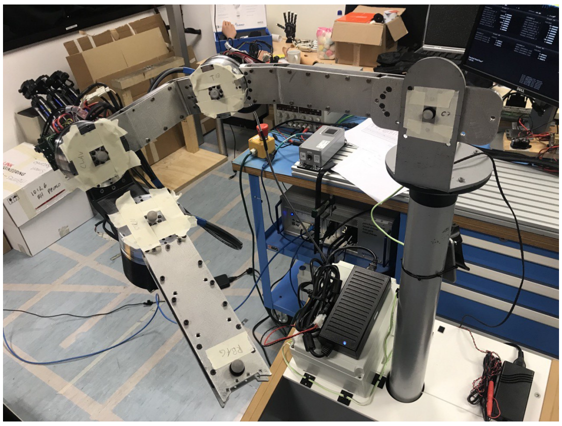

Figure 2.24: Set up of the three degrees of freedom system for Vicon motion capture acquisitions. The markers are located at points of interest to acquire their positions in the Cartesian space. To avoid light reflects, that can cause artifacts in the acquisitions, the surface around the markers has been covered.

Figure 2.25: Vicon motion capture room set up. The manipulator is placed in the middle of the equipped room, some of the Vicon Cameras are highlighted.

2.5 1 dof system study: Simulink and Simscape developed model for real-time test and simulations

2.5.1 Simulink model for real time SEA testing

In order to test real-time the actuators, it has been developed a Simulink model uploadable on the real time target machine Speedgoat.

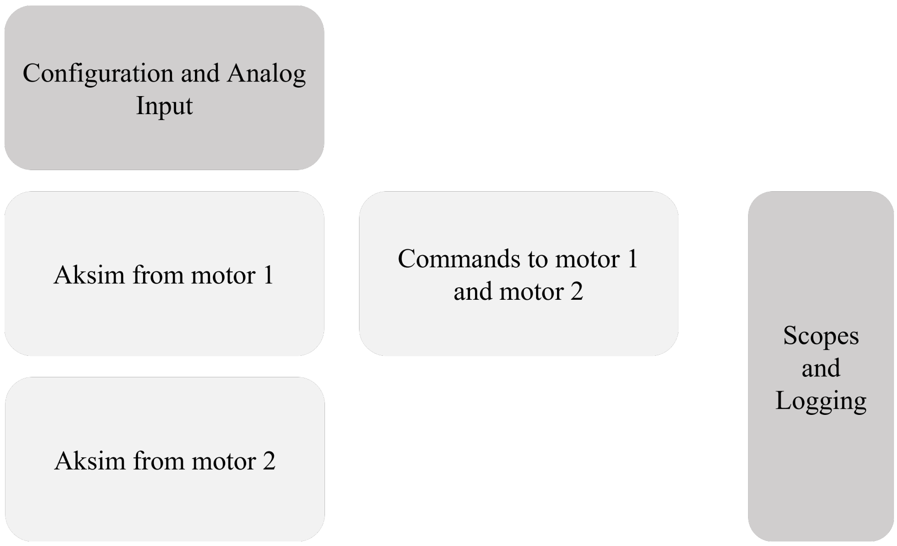

Figure 2.26: Schematic representation of the Simulink model developed to testing real time the SEAs on Speedgoat target machine. Blocks are used to setup the configurations of the analog devices, to communicate with ESCON servo motor controllers and to read data from AksIM encoders. Also scopes blocks to display and store signals have been configurated.

The aim of this model is to provide desired input to the actuator under test, the input is communicated to ESCON servo controller that drives the motor accordingly. The model also allows to identify the desired data to be saved and imported: AksIM encoders reading and industial torsiometer measure. The model is controlled by a graphic user interface, from the GUI it is possible to start and stop the simulation, to choose the AksIM resolution and to set the desired input current and the stiffness of the spring that has to be considered to compute the torque as $\tau = k_t \Delta\theta$. The input current signals provided are:

- Chirp current signal: it is a sinusoidal signal characterized by a constant amplitude and time dependent varying frequency. This signal can be adopted to obtain a frequency characterization of the behaviour of the actuator under test since a chirp signal allows to explore a wide range of working frequency. The chirp signal has been provided for the test performed with the infinite inertial load test bench configuration.

- Ramp current signal: a variable amplitude ramp signal is obtained by smoothing a variable step signal and provided to the system. The system cannot have a simple step as input because the variation of amplitude in this case is instantaneous, to test the actuator it is better to adjust the signal with a slope that makes the variation of the current gradual. The ramp signal has been provided for the test performed with the finite inertial load test bench configuration.

The model is composed of: a configuration block used to configure both the communication with Speedgoat and the analog devices ports used to connect and exchange data with the encoders. Thanks to this model it is possible to collect and import the data read by the AksIM encoders, the AksIM blocks are used for this purpose: the data are collected with a certain bit resolution and then elaborated to obtain measurement in the desired unit, degrees or radians, data are then wrapped to the $[-\pi, +\pi]$ range. Commands are sent to ESCON servomotor controllers from the dedicated block in order to set the working mode. Also the input signal is provided, different possibilities are allowed and set from the GUI.

2.5.2 SEA modelling on Simulink and Simscape

A model of the SEA has been realized in MATLAB Simulink environment, each physical component of the actuator has been modelized with different blocks available in the Simscape library and characterized with the parameters specified in the technical datasheet. The system is composed by a brushless DC motor, a transmission component, and a compliant element as shown in *Figure 2.27*.

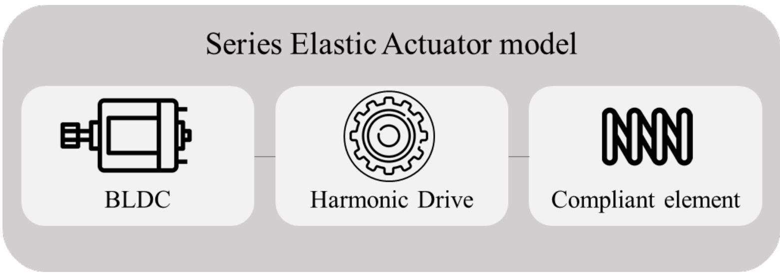

Figure 2.27: Series Elastic Actuator schematic model of the components: the system is build up by assembling a motor (BLDC), a gear reducer and a compliant element (torsional spring).

- BLDC motor: two different models have been analysed, EC 90 flat $\Phi 90mm$, 90 Watt and EC 45 flat $\Phi 43.5mm$, 80 Watt

- Transmission element: harmonic drive CSD-17-2A-100;

- Compliant element: torsional springs with different geometries

  – Springs for EC90: STA and SPT2P;

  – Springs for EC45: SPT1P

Depending on the analysed motor, from a developed MATLAB script it possible to correctly set the parameters inside the blocks. For each component the different properties must be carefully set, in this way the results of the simulation performed offline are comparable with the data collected during the test at the test bench. The objective is to obtain a Simulink model of the actuator able to behave like the physical actuator, after the validation of the model it can be used to perform test instead of the real actuator, the described offline testing procedure is useful to save time and to avoid a damage in the mechanical components.
From the components datasheets have been extracted the data to characterize the Simsape blocks.

Brushless DC motor modelling

The Simulink block used to simulate the BLDC motor requires specific technical data to reproduce the behaviour of the real actuator. The useful data are shown in *Table 2.3* for the BLDC EC90 motor and in *Table 2.4* for BLDC EC45 motor; the reported information are taken from the datasheet.

EC 90 flat BLDC			
Motor and driver overall efficiency	Speed at which efficiency is measured	Torque at which efficiency is measured	Constant voltage
84%	2590 rpm	444 mN*m	24 V
Torque control time constant	Supply series resistance	Rotor inertia	Torque constant
21.1 ms	0.343 Ω	3060 g*cm^2	70.5 mNm/A
Slow axis inertia		Fast axis inertia	
619.2 kgmm^2		3.46 kgmm^2	

Table 2.3: EC 90 flat BLDC datasheet mechanical and electrical data used to characterize the Simulink-Simscape *Simplified PMSM drive* motor block.

EC 45 flat BLDC			
Motor and driver overall efficiency	Speed at which efficiency is measured	Torque at which efficiency is measured	Constant voltage
84.9 %	4560 rpm	167 mNm	24 V
Torque control time constant	Supply series resistance	Rotor inertia	Torque constant
6.35 ms	0.573 Ω	181 gcm^2	40.4 mNm/A
Slow axis inertia		Fast axis inertia	
1001 kgmm^2		1.48 kgmm^2	

Table 2.4: EC 45 flat BLDC datasheet mechanical and electrical data used to characterize the Simulink-Simscape *Simplified PMSM drive* motor block.

The continuous operation maximum torque envelope, expressed in $[mNm]$, and the corresponding rotational speed, expressed in $[rpm]$, are other parameters that have been used to characterize the BLDC, these curves have been extracted from the datasheet and imported in MATLAB thanks to the tool WebPlotDigitizer tool, the resulting curves have been imported inside the corresponding Simulink block parameters.

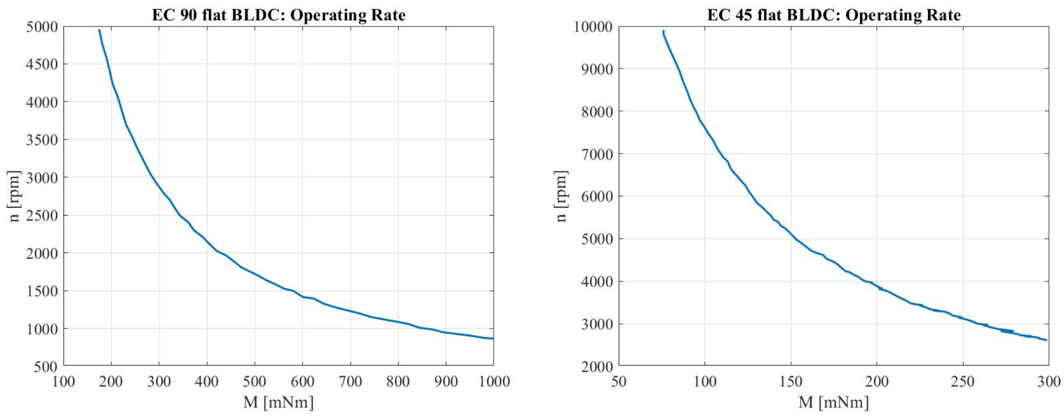

(a) Data for BLDC EC90 **(b)** Data for BLDC EC45

Figure 2.28: Operating rate of the analyzed actuators.

Harmonic drive modelling

The harmonic drive parameters have been computed by elaborating the information present inside the datasheet, in particular a focus is done about the efficiency and the torque in particular working conditions. From the datasheet graph that relates the efficiency to the temperature and to the motor speed (Figure 2.29a), considering a working temperature of 25°C, is obtained a speed efficiency curve (Figure 2.29b).

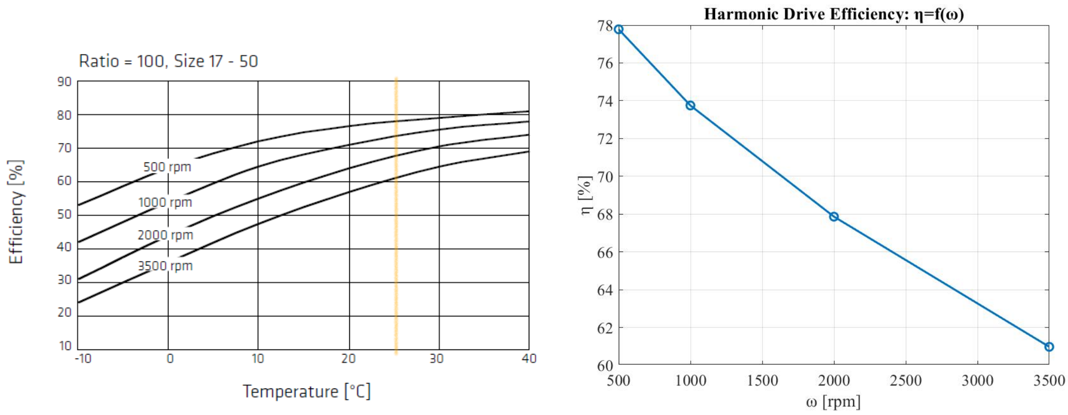

(a) (b)

Figure 2.29: a) Efficiency of the Harmonc Drive expressed as function of the working temperature, focus (yellow line) on $T = 25°C$, at this temperature it is studied the efficiency in function of the rotational speed.
b) Efficiency of the Harmonc Drive expressed as function of the rotational speed, computed at a working temperature of $T = 25°C$.

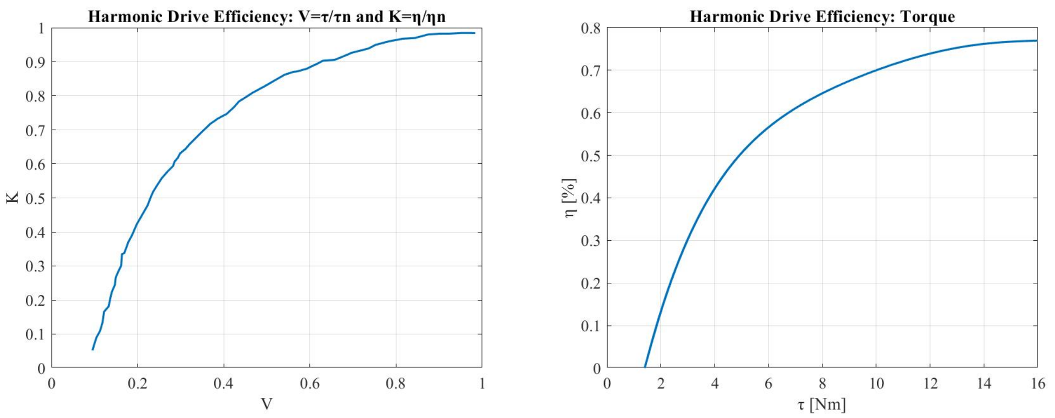

(a) (b)

Figure 2.30: a) Normalized K-V factors relation. b) Efficiency of the Harmonc Drive expressed as function of the torque. The points of this curve have been used to characterize the Simulink-Simscape block *Harmonic Drive* efficiency.

The datasheet normalized graph that relates K and V factors has been imported in MATLAB (Figure 2.30a). From the datasheet it is known that:

$$K = \frac{\eta}{\eta_{nom}}, V = \frac{\tau}{\tau_{nom}}$$

Thus, by inverting the formulas a η,τ normalized graph has been obtained for the exerted torque (Figure 2.30b). From the graph showed in *Figure 2.30b*, it is possible to derive the parameters for the characterization of the harmonic drive efficiency in Simulink. Data of particular interest were the input shaft torque at no load and the nominal output torque. The first measure is the torque at the lower efficiency, notice that the measure read in the graph (Figure 2.30b) needs to be divided for the reduction factor of the harmonic drive, while the second is obtained at the maximum efficiency, data are reported in *Table 2.5.*

Harmonic Drive CSD-17-2A-100		
Number of teeth on elliptical gear	Number of teeth on circular gear	Reduction Ratio
100	101	100
Input shaft torque at no load	Nominal output torque	Efficiency at nominal output torque
0.0140 [Nm]	15.997 [Nm]	0.77

Table 2.5: Harmonic Drive CSD-17-2A-100 datasheet characteristics and efficiency related information used to characterize the Simulink-Simscape block *Harmonic Drive.*

Compliant element modelling

For the compliant element the characterizing parameter is the torsional stiffness, these data have been obtained from the test described in *Section 3.1.2* and *Section 3.1.2* and are reported in *Table 2.6.*

Torsional Stiffness		
STA	SPT2P	SPT1P
1073 Nm/rad	385 Nm/rad	988 Nm/rad

Table 2.6: Compliant elements torsional stiffness used to characterize the Simulink-Simscape block *Rotational spring.*

The principal objective of all the developed models that exploits the SEA model already explained is to verify that the measured sensed torque at the slow axis is the same for the test at the test bench and for the simulations. From the comparison of the data it is possible to understand if the model of the SEA is appropriate to reproduce the real behaviour of the actuator, also other measurement are useful for this evaluation, in fact also data relative to the motor speed and the motor current have been collected. Regarding the torque, four measurements have been compared: torque measured by the industrial torsiometer at the test bench, torque measured with the Hooke's law from the encoders displacement readings, torque obtained with simulations and red with a torque sensor after the compliant element (to simulate the industrial torsiometer) and the torque obtained during the simulation with the Hooke's law from the ideal rotational motion sensors displacement measure. The comparison between the first two cited torques is also useful to verify that the SEA can effectively be used as a reliable torque sensor.

Behaviour analysis of the SEA model

In order to test the designed model of the actuator, it has been realized a Simulink model where the system is working under different load conditions.

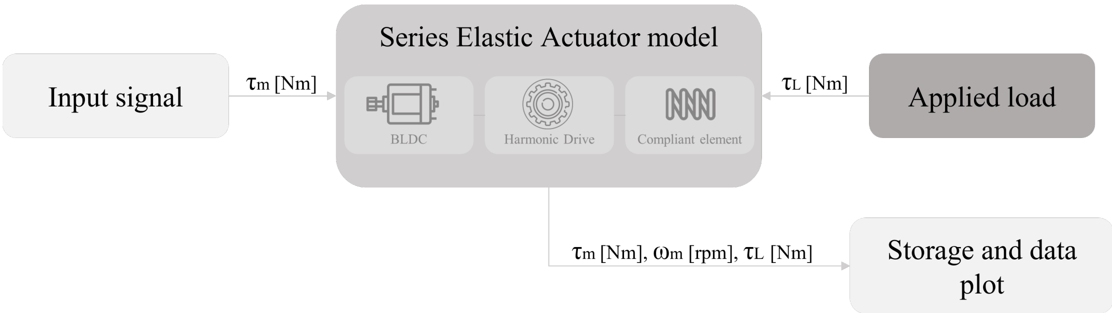

Figure 2.31: Schematic of the Simulink model implemented to test the SEA model behaviour, the realized Simscape SEAs system is tested under different load condition. The data relative to the motor torque, motor speed and load applied torque are stored.

The motor exerts a certain motor torque at one side of the compliant element, on the other side of the spring is applied a resistive torque. The objective of the simulation is to verify that the system behaves like expected in the different analysed conditions. The conditions analysed are:

- Free run system: any load is applied.
- No motion system: the system is blocked, it has null speed and null movement.
- Motor drags load: the power is transmitted from the motor to the load.
- Load drags motor: the power is transmitted from the load to the motor.

The applied torques during the test are reported in table. Notice that the torques required to the motor are successively affected by a factor 100 due to the harmonic drive, the harmonic drive is in fact used to obtain higher torques and lower speeds with respect to the ones provided by the motor itself.

2.5.3 Simulink model for infinite inertial load simulation

This model has been developed to reproduce the behaviour of the SEA mounted with one extremity blocked to wall.

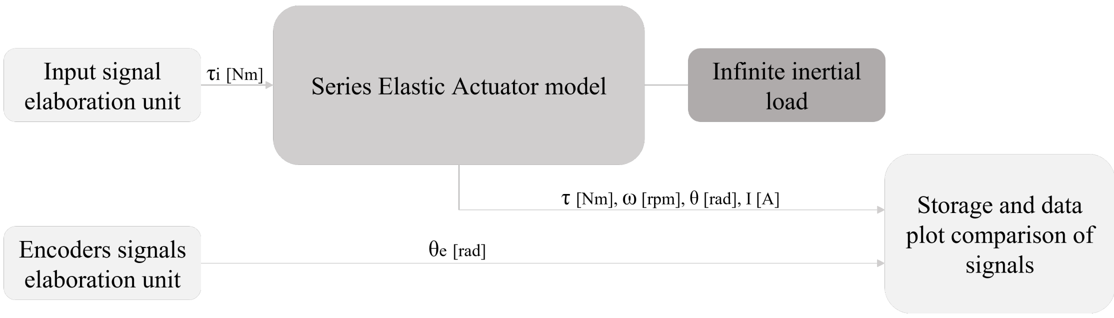

Figure 2.32: Schematic of the Simulink model implemented to simulate inside Simulink environment the SEA model. To the system is provided a chirp current signal, equal to the one used to test the SEA at the test bench, the behaviour of the system, when it is fixed to a wall (infinite inertial load), is simulated and then compared with the data collected during real-time test bench test.

In the described condition an infinite inertial load is applied. The model of the SEA has already been described in *Section 2.5.2*. The BLDC receive as input a current signal, this signal is the same chirp current signal used to perform the simulation at the test bench. After the compliant element the system is attached to a mechanical rotational reference block that allows to fix one side of the system. It is possible to modify the parameters of the system components from a MATLAB script, thus the model can be used to simulate the behaviour of EC90 actuator with SPT2P or STA springs and of EC45 actuator with SPT1P spring. Thanks to different sensing blocks the measurement relative to spring displacement, motor rotational speed and motor torque can be acquired. The acquired data are then compared with the ones collected experimentally.

2.5.4 Simulink model for finite inertial load simulation

This model has been developed to reproduce the behaviour of the SEA in a not blocked configuration and with a load applied at the slow axis of the actuator. It is possible to set the parameters from a MATLAB script to choose the SEA to be simulated. The signal provided to the model of the BLDC is a current signal. To validate the model the same signal provided to the system mounted at the test bench has been choosen: a variable amplitude ramp signal.

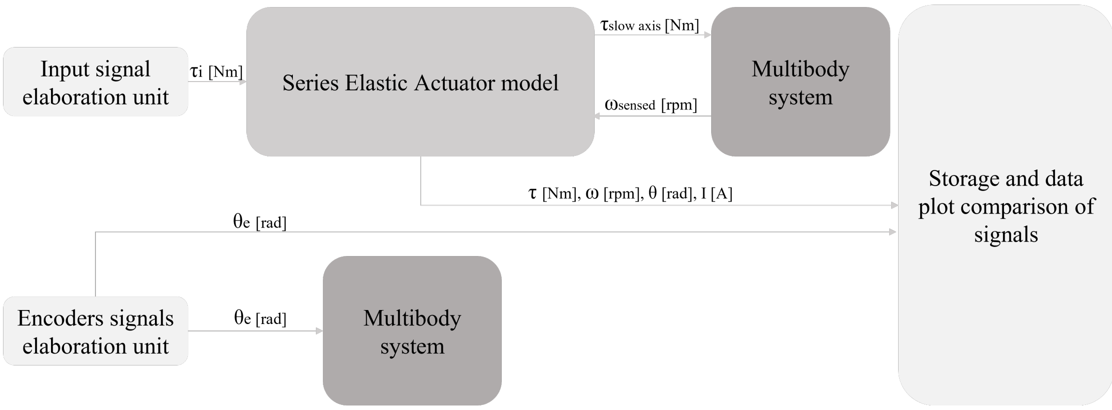

Figure 2.33: Schematic of the Simulink model used to simulate SEA behaviour while to the system is applied a load and it is free to rotates. The input signal is a current, the same signal has previously been used to real time test the SEA at the test bench, the inertial load is simulated by connecting the system to a Multibody assemble that recreates the inertial characteristics of the physical system. The data recorded during the real time measurements are compared with the ones simulated both in quantitative way (data are stored and analyzed) and qualitative way (two identical Multibody system are actuated with the measured and simulated signals and it is observed that the movements are similar).

The SEA model is connected to a Multibody system showed in *Figure 2.34*, the system is composed of three elements identified by different colors since made of different materials and with different inertial characteristics. The Multibody model reproduces the inertial and load conditions of the real actuator. The Multibody model is actuated by the torque sensed after the compliant element. By using a speed sensor block applied on the Multibody rotational joint, the speed is sensed and then provided to the SEA system as a feedback disturbance. Thanks to the computed speed disturbance it is possible to simulate the SEA behaviour in a condition that is as close as possible to the real one where the mass and the inertia of the physical components affect the rotation of the motor. Each component of the Multibody system has been characterized with information about: mass, centre of gravity coordinates and moments of inertia along the x,y,z axes (Table 2.7).

Multibody components data								
MASS [Kg]								
FIRST ELEMENT			SECOND ELEMENT			LOAD		
3,3445368			1,3607781			6,5		
Centre of gravity with respect to fisso coordinate frame [mm]								
FIRST ELEMENT			SECOND ELEMENT			LOAD		
Xg	Yg	Zg	Xg	Yg	Zg	Xg	Yg	Zg
3,37039940+01	-4,0380796e-01	-5,2617922e+01	1,0705110e+02	-1,4305253e+01	4,9312965e-02	1,3056250e+02	-2,6830239e+02	-6,9940210e-02
Principal moments of inertia [kgmm^2]								
FIRST ELEMENT			SECOND ELEMENT			LOAD		
Ix	Iy	Iz	Ix	Iy	Iz	Ix	Iy	Iz
6,8710306e+03	1,4508593e+0	1,5231846e+04	2,1125337e+03	3,8945004e+03	5,2935661e+03	4,1232375e+03	1,5710849e+04	1,8203150e+04

Table 2.7: Multibody model components mechanical characteristics. For the elements that compose the models the mechanical characteristics relative to mass, centre of gravity and moment of inertia have been extracted from CREO Parametric model features.

To estimate the quality of the model the data about motor current, motor speed, and spring displacement have been collected and then compared with the ones obtained during test at the test bench.

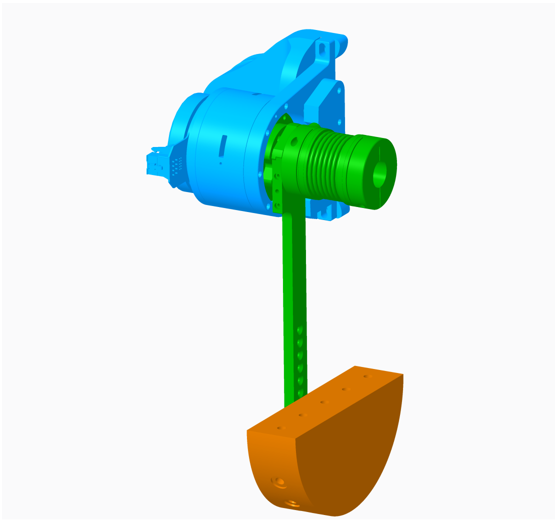

Figure 2.34: CREO model imported inside Simulink Multibody. 1dof system with finite inertial load applied.

2.6 Kinematic study of the 2 dof system

2.6.1 Denavith Hartenberg parameters study

The system is composed of two SEAs mounted together, the DH convection has been used to place the reference frames and to study direct kinematics of the structure. In *Table 2.8* are resumed the DH parameters for the analysed system. The α angle is expressed in degrees while θ_1 and θ_2 are left as general variables because their values change during the different configurations assumed by the robot while moving.

Denavith Hartenberg parameters				
Link	a	α	d	θ
1	0	90	d1	θ1
2	a2	-90	-d2	θ2
Geometrical measurments [mm]				
a2	d1		d2	
326	210,74		106,24	

Table 2.8: Denavith Hartenberg parameters for the 2dof system.

The geometrical features have been measured on the 3D model of the system inside CREO environment as shown in Figure 2.35.

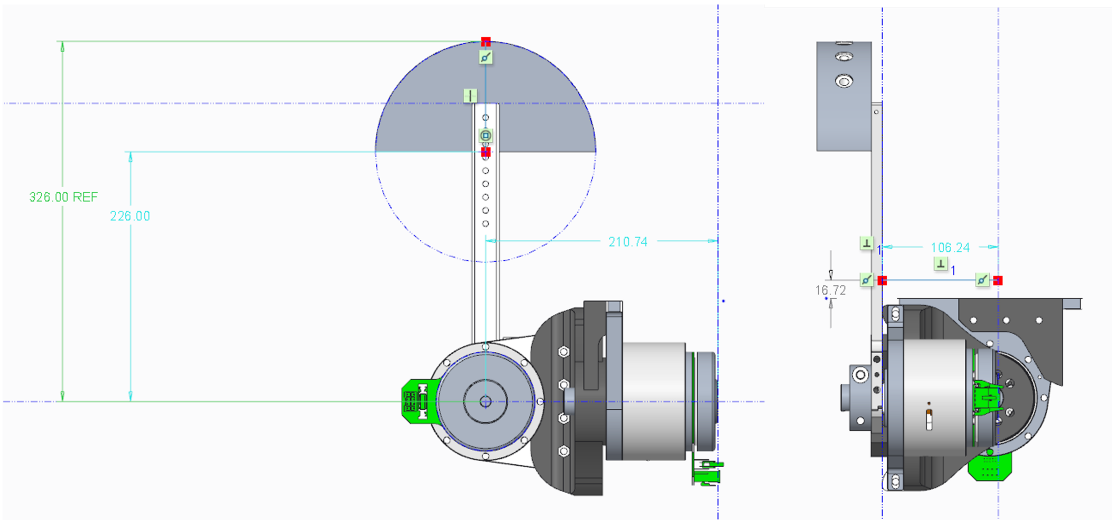

Figure 2.35: Geometrical features measurements of the 2dof system performed on CREO.

Once identified the reference frames and the DH parameters, as described in *Section*

2.1.1, it can be computed the transformation matrix between the base reference frame and the end-effector frame.
Defined:

$$s_{\theta_i} = sin\left(\theta_i\right), c_{\theta_i} = cos\left(\theta_i\right)$$

The transformation matrix between the reference base *Frame0* and *Frame1* is:

$$T_1^0 = \begin{bmatrix} c_{\theta_1} & 0 & s_{\theta_1} & 0 \\ s_{\theta_1} & 0 & -c_{\theta_1} & 0 \\ 0 & 1 & 0 & d_1 \\ 0 & 0 & 0 & 1 \end{bmatrix}$$

The transformation matrix between *Frame1* and *Frame2* is:

$$T_2^1 = \begin{bmatrix} c_{\theta_2} & 0 & -s_{\theta_2} & a_2 c_{\theta_2} \\ s_{\theta_2} & 0 & c_{\theta_2} & a_2 s_{\theta_2} \\ 0 & -1 & 0 & -d_2 \\ 0 & 0 & 0 & 1 \end{bmatrix}$$

Thus, the transformation matrix between the base reference frame and the end-effector frame is given by:

$$T_2^0 = T_1^0 T_2^1 = \begin{bmatrix} c_{\theta_2} c_{\theta_1} & -s_{\theta_1} & -s_{\theta_2} c_{\theta_1} & a_2 c_{\theta_2} c_{\theta_1} - d_2 s_{\theta_1} \\ c_{\theta_2} s_{\theta_1} & c_{\theta_1} & -s_{\theta_2} s_{\theta_1} & a_2 c_{\theta_2} s_{\theta_1} + d_2 c_{\theta_1} \\ s_{\theta_2} & 0 & c_{\theta_2} & a_2 s_{\theta_2} + d_1 \\ 0 & 0 & 0 & 1 \end{bmatrix}$$

The equations of the direct kinematics can be derived by the first three rows of the fourth column of the matrix T_2^0, and can be expressed as:

$$x = a_2 c_{\theta_2} c_{\theta_1} - d_2 s_{\theta_1}$$

$$y = a_2 c_{\theta_2} s_{\theta_1} + d_2 c_{\theta_1}$$

$$z = a_2 s_{\theta_2} + d_1$$

Once the transformation matrix has been computed, it is possible to build a rigid body tree (Figure 2.36) in Matlab environment to verify the rotations around the joint axes and to see the position of the reference frames in the 3D space.

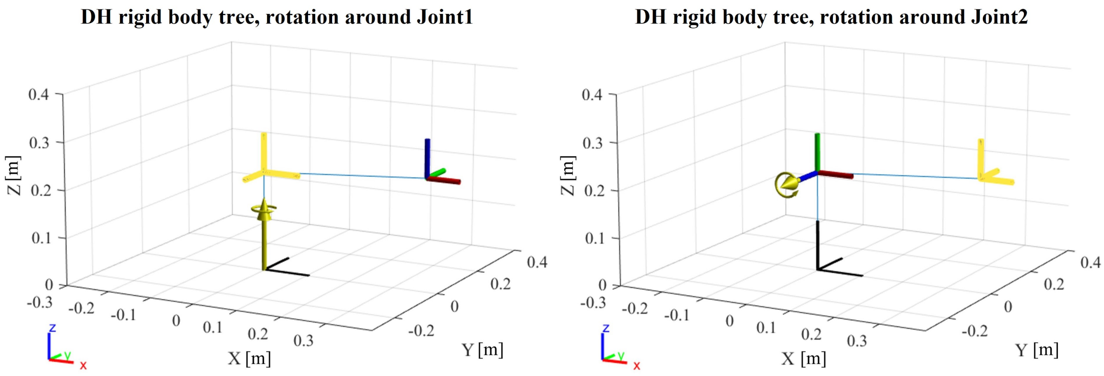

Figure 2.36: Rigid body tree built on Matlab following the Denavith Hartenberg convection.

2.6.2 Modified Denavith Hartenberg parameters study

The modified DH convection has been used to place the reference frames and to study direct kinematics of the structure. In Table 2.9 are resumed the modified DH parameters, computed as described in *Section 2.1.1*, for the analysed system, the α angle is expressed in degrees while θ_1 and θ_2 are left as general variables because their values change during the different configurations assumed by the robot while moving.

Modified Denavith Hartenberg parameters				
Link	a	α	d	θ
1	0	0	d1	θ1
2	0	90	-d2	θ2
3	a2	0	0	0
Geometrical measurments [mm]				
a2	d1		d2	
326	210,74		106,24	

Table 2.9: Modified Denavith Hartenberg parameters for the 2dof system.

Defined:

$$s_{\theta_i} = sin\left(\theta_i\right), c_{\theta_i} = cos\left(\theta_i\right)$$

The transformation matrix between the base frame *Frame0* and *Frame1* can be computed as:

$$T_1^0 = \begin{bmatrix} c_{\theta_1} & -s_{\theta_1} & 0 & 0 \\ s_{\theta_1} & c_{\theta_1} & 0 & 0 \\ 0 & 0 & 1 & d_1 \\ 0 & 0 & 0 & 1 \end{bmatrix}$$

The transformation matrix between the base frame, *Frame1* and *Frame2* can be computed as:

$$T_2^1 = \begin{bmatrix} c_{\theta_2} & -s_{\theta_2} & 0 & 0 \\ 0 & 0 & -1 & d_2 \\ s_{\theta_2} & c_{\theta_2} & 0 & 0 \\ 0 & 0 & 0 & 1 \end{bmatrix}$$

The transformation matrix between the base frame, *Frame2* and *Frame3* is obtained with a pure translation of the frame and can be computed as:

$$T_3^2 = \begin{bmatrix} 1 & 0 & 0 & a_2 \\ 0 & 1 & 0 & 0 \\ 0 & 0 & 1 & 0 \\ 0 & 0 & 0 & 1 \end{bmatrix}$$

Thus, the final transformation matrix between the base frame and the end-effector is obtained as:

$$T_3^0 = T_1^0 T_2^1 T_3^2 = \begin{bmatrix} c_{\theta_2} c_{\theta_1} & -s_{\theta_2} c_{\theta_1} & s_{\theta_1} & a_2 c_{\theta_2} c_{\theta_1} - d_2 s_{\theta_1} \\ c_{\theta_2} s_{\theta_1} & -s_{\theta_2} s_{\theta_1} & -c_{\theta_1} & a_2 c_{\theta_2} s_{\theta_1} + d_2 c_{\theta_1} \\ s_{\theta_2} & c_{\theta_2} & 0 & a_2 s_{\theta_2} + d_1 \\ 0 & 0 & 0 & 1 \end{bmatrix}$$

As for the matrix computed with the DH convention, the equations of the direct kinematics can be derived by the first three rows of the fourth column of the matrix T_3^0, and can be expressed as:

$$x = a_2 c_{\theta_2} c_{\theta_1} - d_2 s_{\theta_1}$$

$$y = a_2 c_{\theta_2} s_{\theta_1} + d_2 c_{\theta_1}$$

$$z = a_2 s_{\theta_2} + d_1$$

The obtained equations for the Cartesian coordinates (x, y, z) correctly corresponds to the ones obtained with the traditional DH convection showing that the two methods bring to the same result.
The rigid body tree built inside Matlab environment is shown in *Figure 2.37*.

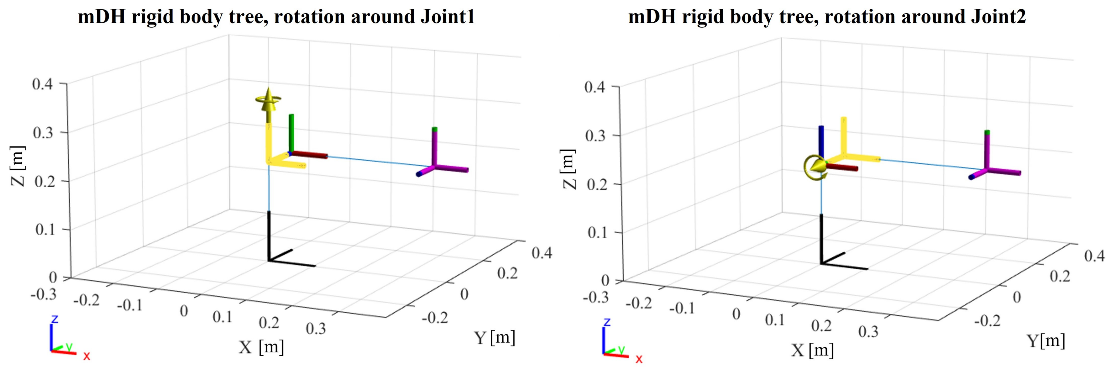

Figure 2.37: Rigid body tree built on Matlab following the modified Denavith Hartenberg convection.

2.6.3 Computation of the working space of the manipulator

It has been developed a Matlab code to compute the set of Cartesian reachable points, the computation has been done considering the angles θ_1 and θ_2 in the ranges reported in *Table 2.10*. The working space, also called cloud point, is computed by considering the geometric parameters of the structure and all the possible combinations of θ_1 and θ_2.

Mechanical stops		
θ	Lower Limit [deg]	Upper limit [deg]
θ1	85	210
θ2	-5	185

Table 2.10: Ranges of the allowed angles for the two joints motion.

The points are obtained thanks to the direct kinematics equations derived with th DH and mDH conventions, since the equations provided by the two methods are the same, also the obtained cloud point coincide.

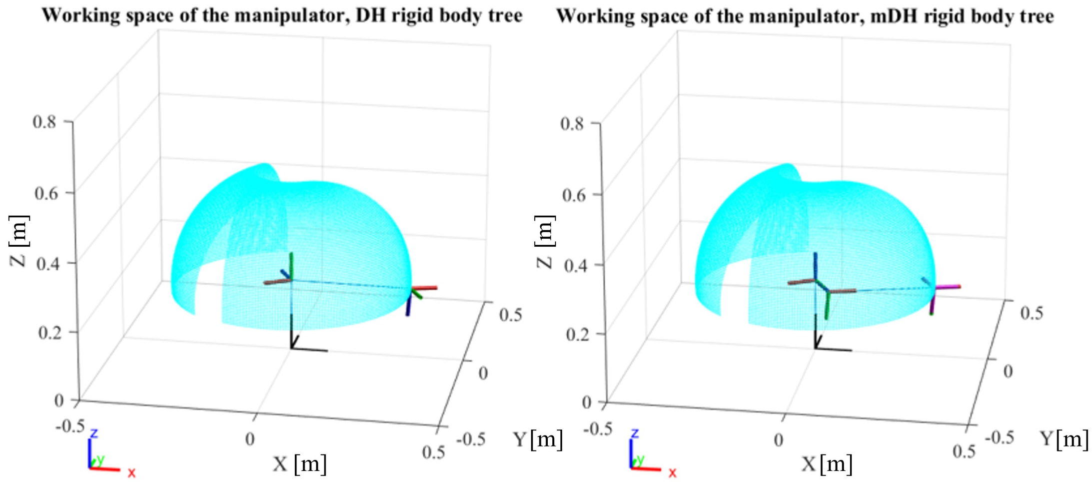

Figure 2.38: Set of reachable points in the Cartesian space, the rigid body trees obtained with the DH and mDH are both represented in a configuration of θ_1 and θ_2 that is inside the cloud point, in particular both the joints are at one of the mechanical stops.

2.6.4 Jacobian matrix computation

A preliminary study for the inverse kinematics analysis is the computation of the Jacobian matrix. Defined:

$$s_{\theta_i} = sin\left(\theta_i\right), c_{\theta_i} = cos\left(\theta_i\right)$$

The Jacobian matrix can be computed following the procedure described in *Section 2.1.2*.

$$p_0 = \begin{bmatrix} 0 \\ 0 \\ 0 \end{bmatrix}, p_1 = \begin{bmatrix} 0 \\ 0 \\ d_1 \end{bmatrix}, z_0 = \begin{bmatrix} 0 \\ 0 \\ 1 \end{bmatrix}, z_1 = \begin{bmatrix} s_{\theta_1} \\ -c_{\theta_1} \\ 0 \end{bmatrix}, p_e = \begin{bmatrix} a_2 c_{\theta_2} c_{\theta_1} - d_2 s_{\theta_1} \\ a_2 c_{\theta_2} s_{\theta_1} + d_2 c_{\theta_1} \\ a_2 s_{\theta_2} + d_1 \end{bmatrix}$$

$$(p_e - p_0) = \begin{bmatrix} a_2 c_{\theta_2} c_{\theta_1} - d_2 s_{\theta_1} \\ a_2 c_{\theta_2} s_{\theta_1} + d_2 c_{\theta_1} \\ a_2 s_{\theta_2} + d_1 \end{bmatrix}, (p_e - p_1) = \begin{bmatrix} a_2 c_{\theta_2} c_{\theta_1} - d_2 s_{\theta_1} \\ a_2 c_{\theta_2} s_{\theta_1} + d_2 c_{\theta_1} \\ a_2 s_{\theta_2} \end{bmatrix}$$

$$z_0 \times (p_e - p_0) = \begin{bmatrix} -a_2 c_{\theta_2} s_{\theta_1} - d_2 c_{\theta_1} \\ a_2 c_{\theta_2} c_{\theta_1} - d_2 s_{\theta_1} \\ 0 \end{bmatrix}, z_1 \times (p_e - p_1) = \begin{bmatrix} -a_2 s_{\theta_2} c_{\theta_1} \\ -a_2 s_{\theta_2} s_{\theta_1} \\ a_2 c_{\theta_2} \end{bmatrix}$$

Finally the geometric Jacobian matrix can be expressed in the form:

$$J = \begin{bmatrix} z_0 \times (p_e - p_0) & z_1 \times (p_e - p_1) \\ z_0 & z_1 \end{bmatrix}$$

The resulting matrix is:

$$J = \begin{bmatrix} -a_2 c_{\theta_2} s_{\theta_1} - d_2 c_{\theta_1} & -a_2 s_{\theta_2} c_{\theta_1} \\ a_2 c_{\theta_2} c_{\theta_1} - d_2 s_{\theta_1} & -a_2 s_{\theta_2} s_{\theta_1} \\ 0 & a_2 c_{\theta_2} \\ 0 & s_{\theta_1} \\ 0 & -c_{\theta_1} \\ 1 & 0 \end{bmatrix}$$

For the purpose of the computation of the inverse kinematic it will be computed the pseudo-inverse of the upper (3×2) matrix of J, so the relevant matrix for the described computation is

$$J = \begin{bmatrix} -a_2 c_{\theta_2} s_{\theta_1} - d_2 c_{\theta_1} & -a_2 s_{\theta_2} c_{\theta_1} \\ a_2 c_{\theta_2} c_{\theta_1} - d_2 s_{\theta_1} & -a_2 s_{\theta_2} s_{\theta_1} \\ 0 & a_2 c_{\theta_2} \end{bmatrix}$$

2.6.5 Inverse kinematics computation

The study of the inverse kinematic has been developed in Matlab environment by writing the code necessary to implement three different approaches:

- Analytic semi-recursive approach: mathematical inversion of the direct kinematics formulas to find the equations for the joints variables θ_1 and θ_2. The obtained inverse kinematic formulas are:

$$c_{\theta_1} = \left(\frac{x a_2 c_{\theta_2} + d_2 y}{a_2^2 c_{\theta_2}^2 + d_2^2} \right), s_{\theta_1} = \left(\frac{y - d_2 c_{\theta_1}}{a_2 c_{\theta_2}} \right)$$

$$c_{\theta_2} = \pm \sqrt{\left(\frac{x^2 + y^2 - d_2^2}{a_2^2} \right)}, s_{\theta_2} = \left(\frac{z - d_1}{a_2} \right)$$

Thus, the joint variables can be expressed as:

$$\theta_1 = \arctan\left(s_{\theta_1}, c_{\theta_1}\right), \theta_1 = \arctan\left(s_{\theta_1}, c_{\theta_1}\right)$$

The arctangent can be computed in Matlab with the command *atan2* that allows to compute the arctangent on four quadrants. Notice that due to the square root there is a sign ambiguity in the definition of the cosine of θ_2 so it is necessary to develop an algorithm able to identify the correct sign for the cosine to avoid to compute wrong θ_1 and θ_2 angles, notice that also θ_1 is dependent on c_{θ_2}. The error can lead to the computation of an algebraically correct solution but this solution can be outside of the allowed range. The problem can be solved by computing θ_1 and θ_2 and checking if they are inside the allowed ranges, if they are not it means that the opposite sign for the c_{θ_2} has to be taken, Another important requirement is that there must be continuity in the solution: two adjacent angles cannot be too far one from the other, this problem can arise when the two angles corresponding to the same cosine are both inside the allowed range so the first control does not affect the decision of the sign. To solve the problem a threshold control is applied: if the difference between the precedent angle and the actually computed one is higher than the threshold, to compute the actual angle it is taken the opposite sign for the cosine. In this way jumps in the computed solution are avoided. Because of the need to apply the two described control before to have the final solution, the method is defined semi-recursive.

- Recursive approach: requires the pseudo-inverse of the Jacobian matrix. A time dependent trajectory is defined to test the approach: the end-effector velocities are obtained by computing the time derivative of the desired trajectory, then with the recursive approach the pseudo-inverse of the Jacobian is used to map these velocities to the joint space. The recursive equation to be implemented is:

  $$q\left(t_{k+1}\right) = q\left(t_k\right) + J^{-1}\left(q\left(t_k\right)\right) v_e\left(t_k\right) \Delta t$$

  The joint variables can so be computed recursively at each sample time, as explained in *Section 2.1.2*.

- ANFIS approach: for each joint is defined an ANFIS characterized with a certain epoch number and membership functions number, then the networks are trained on a data set composed of the pose, and the corresponding joint angle. The pose is provided as the (x, y, z) Cartesian coordinates of the point in the space and the RPY angles that define the orientation of the end-effector. The number of points of the cloud point on which the ANFIS is trained has to be choosen taking into account that the bigger is the data set the lower is the imprecision in predicting an unknown joint variable but the higher is the computational cost and the time required for the training.

The results obtained with the different approaches are reported in *Section 3.2.1*.

2.6.6 Kinematic study of the 2dof test bench system

The 2dof manipulator to be tested at the test bench, described in *Section 2.4.2*, has the same kinematic chain described in *Section 2.6.1* but the geometrical parameters are different because the physical mechanical components has been designed with different sizes with respect to the model described in *Section 2.6.1* that has only been used for an analytic study. The new CREO model that corresponds to the physical test bench and on which the geometrical parameter have been measured is shown in *Figure 2.39* and in *Figure 2.40*, the new parameters are reported in *Table 2.11*. Since, for safety reasons, it has not been mounted the load, the end-effector frame is located at the end of the steel bar and not on the top of the load as in the previous model.

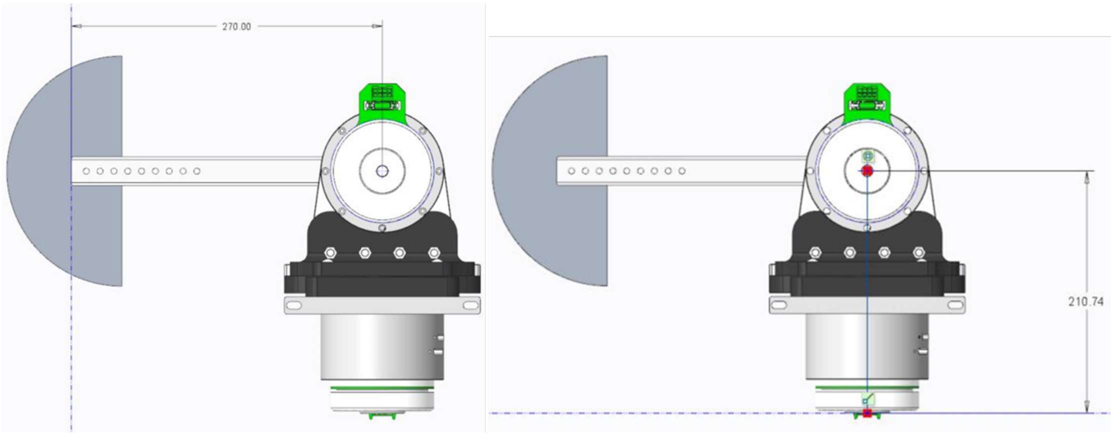

Figure 2.39: Frontal views of CREO CAD model of the 2dof structure: measurements collection to identify the needed geometric parameters for the direct kinematic studio.

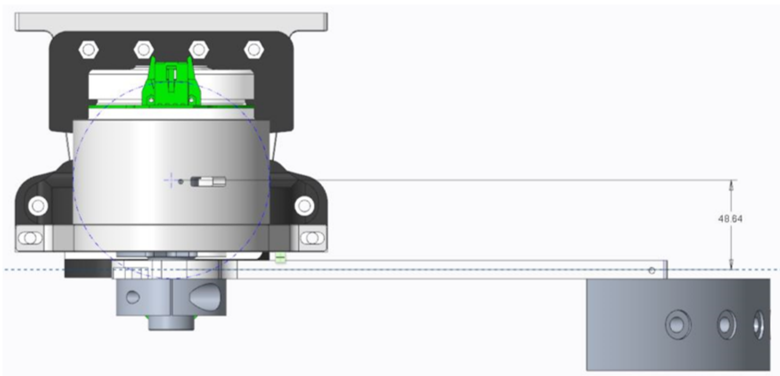

Figure 2.40: Upper view CREO CAD model of the 2dof structure: measurements collection to identify the needed geometric parameters for the direct kinematic studio.

Test bench geometrical measurments [mm]		
a2	d1	d2
270	210,74	48,64

Table 2.11: Collection of the geometrical parameters used for the direct kinematics study. The reported data have been acquired from the CAD model of the 2dof system.

Moreover, the mechanical stops ranges are reduced (Table 2.12), consequently the cloud point is smaller.

Test bench model mechanical stops		
θ	Lower Limit [deg]	Upper limit [deg]
θ1	-15	15
θ2	-30	5

Table 2.12: Mechanical stops that stand the allowed rotation angular ranges for the two joints of the 2dof system.

The rigid body tree and the cloud point have been computed in Matlab environment and are shown in Figure *2.41*.

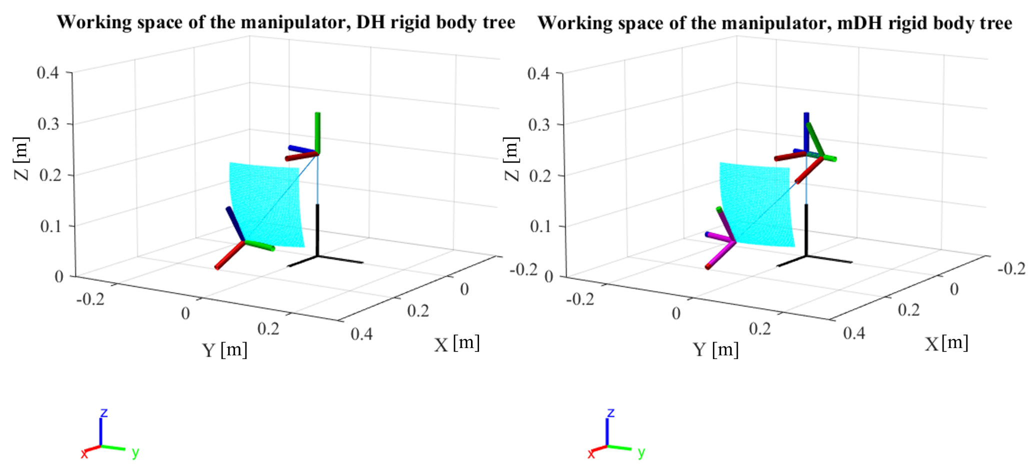

Figure 2.41: Rigid body tree and cloud point plot of the kinematic chain of the 2dof setup used for real time simulations.

Thanks to the study of the working space it is possible to define feasible target trajectories for the end-effector.

2.6.7 Simulink model for real time simulations of 2dof system inverse kinematics implementations

Three different models have been implemented for the inverse kinematic computation. Each model needs different inputs, the analytic semi-recursive approach works on the Cartesian coordinates (x, y, z), the recursive approach wants a velocity profile as input of the system while the ANFIS works on the pose. The results of Matlab simulations for this system are reported in *Section 3.2.2*. After the offline validation of the three proposed methods for the solution of the inverse kinematic, in order to perform real time simulations on the real time target machine, the same functions and algorithms implemented in MATLAB have been reproduced in Simulink, thus, the real time implemented model allows to obtain the same results. The complete model allows to control the physical test bench: the inverse kinematic is computed online and the two actuators move accordingly. From a GUI it is possible to select the inverse kinematic algorithms to be adopted. The movements of the actuators are performed by exploiting the potentialities of the position control implemented by EPOS motor driver. Notice that it is necessary to bring the input data inside the EPOS domain expressed in *Ticks* unit. Thus, it has been chosen as zero reference position, one mechanical stop for each actuator. To bring the computed trajectories inside this domain an offset removal is necessary, then the signal expressed in radiant is converted in ticks unit. The Simulink model up-loadable on Speedgoat (Figure 2.42) is composed of several blocks.

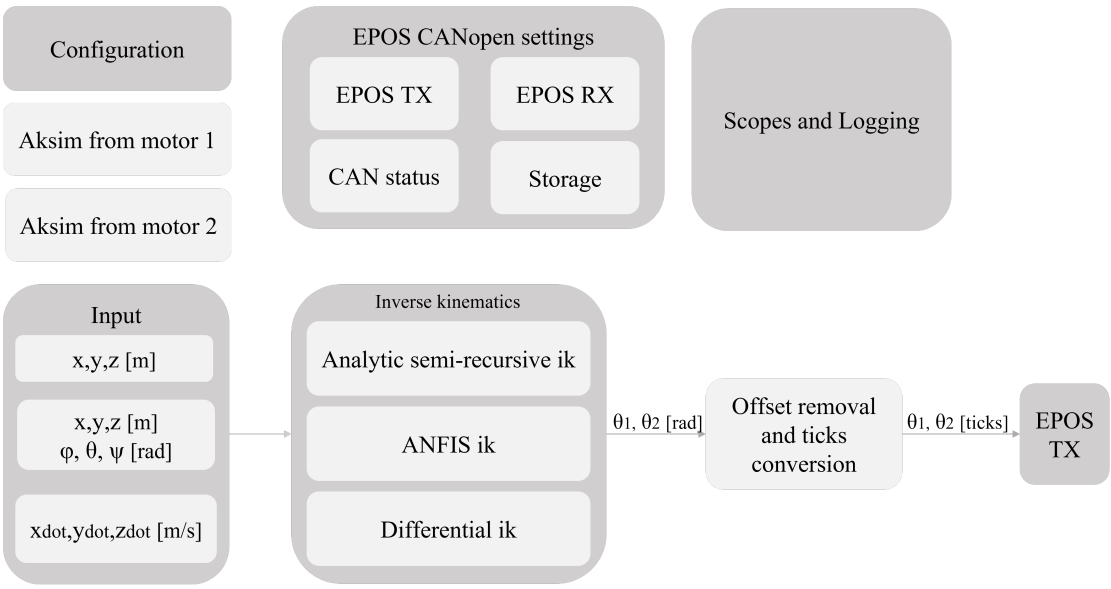

Figure 2.42: Scheme of the Simulink model for the real time simulation of the 2dof test bench system.

The configuration blocks allows to configure the analog input/output ports, the ports are used to read data from the AksIM encoders, these data are both stored and displayed on the Speedgoat monitor. The EPOS CANopen settings block is used to configure the port used to communicate with EPOS devices, moreover the block contains the transmission and the reception settings that allow to communicate to the motor drivers information like the working state, the working mode, the start/stop/reset commands or the trajectory to be performed. The receiving block allows to obtain from the EPOS the required information like the status of the drivers or the actual position reached from the motors. It is possible to store all the information provided by the drivers by reading the correct header on the CAN bus, the results of real-time simulations are shown in *Section 3.2.3*.

2.7 Kinematic study of the 3 dof system

2.7.1 Modified Denavith Hartenberg parameters study

The study of the kinematic chain of the three degrees of freedom system has been done following the modified Denavith Hartenerg convection (Section 2.1.1). The parameters are reported in *Table 2.14*, all the measurements have been taken from a CAD 3D model inside CREO environment (Figure 2.43, Figure 2.44).

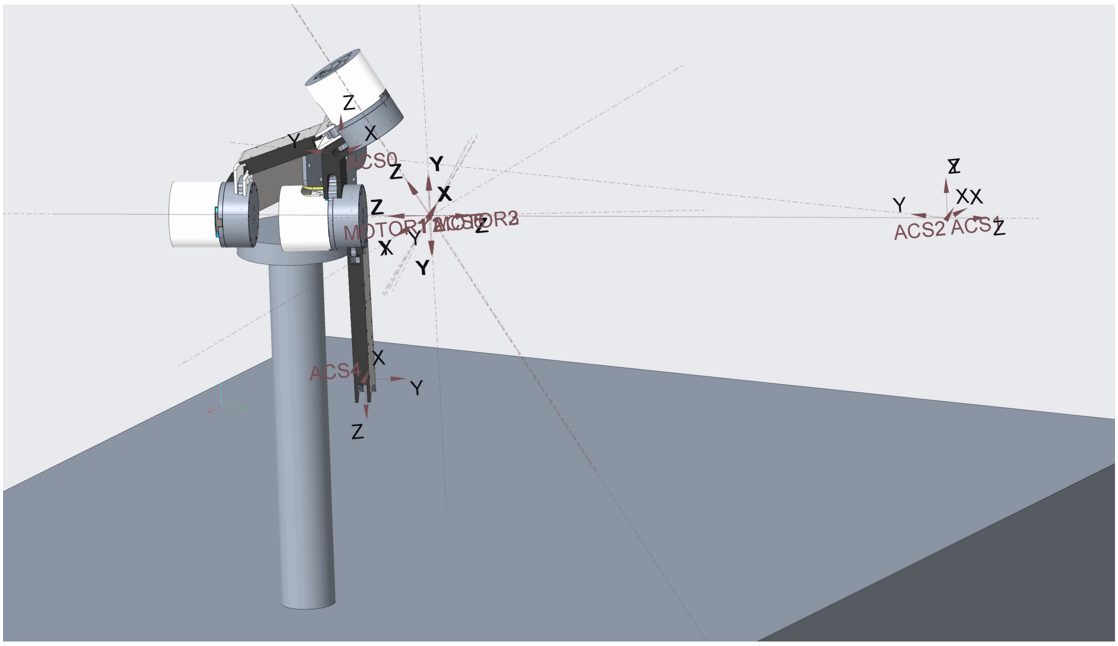

Figure 2.43: CREO model of the 3dof system, the reference frames have been placed according to the modified Denavith Hartenberg convention, thanks to the model it possible to measure the geometric distances needed for the computation of the homogeneous transformation matrices.

Modified Denavith Hartenberg parameters				
Link	a	α [deg]	d [mm]	θ
1	0	0	-721,02	θ1
2	0	-120	0	θ2
3	0	-60	0	θ3
4	0	-90	229,93	0

Table 2.13: Modified Denavith Hartenberg parameters for the 3dof system.

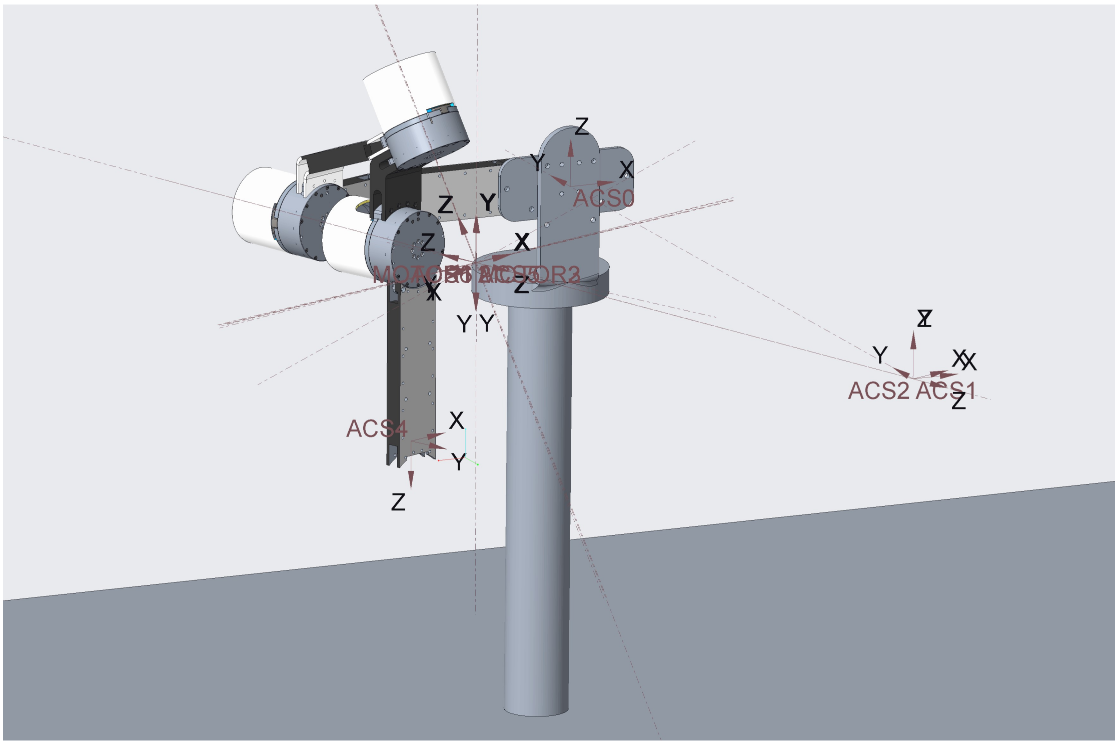

Figure 2.44: CREO model of the 3dof system, view of the references that composes the spherical joint. The base frame is the frame ACS0, the last frame of the chain is the end-effector frame ACS4.

To correlate the base reference frame with the first rotational joint frame, since the frame of the joint has to be placed according to the rules defined by the modified Denavith Hartenber convention, it is necessary to perform three homogeneous transformations:

- A translation along the y *axis* of the quantity $t_{y1} = -950{,}186$ mm

$$T_{y_1} = \begin{bmatrix} 1 & 0 & 0 & 0 \\ 0 & 1 & 0 & t_{y1} \\ 0 & 0 & 1 & 0 \\ 0 & 0 & 0 & 1 \end{bmatrix}$$

- A rotation around z *axis* of $\beta_1 = 20°$

$$R_z = \begin{bmatrix} c_{\beta_1} & -s_{\beta_1} & 0 & 0 \\ s_{\beta_1} & c_{\beta_1} & 0 & 0 \\ 0 & 0 & 1 & 0 \\ 0 & 0 & 0 & 1 \end{bmatrix}$$

- A rotation around *x axis* of $\beta_2 = 90°$

$$R_x = \begin{bmatrix} 1 & 0 & 0 & 0 \\ 0 & c_{\beta_2} & -s_{\beta_2} & 0 \\ 0 & s_{\beta_2} & c_{\beta_2} & 0 \\ 0 & 0 & 0 & 1 \end{bmatrix}$$

Thus, the resulting transformation is

$$T_0^{base} = T_{y_1} R_z R_x$$

$$T_0^{base} = \begin{bmatrix} c_{\beta_1} & -c_{\beta_2} s_{\beta_1} & s_{\beta_2} s_{\beta_1} & 0 \\ s_{\beta_1} & c_{\beta_2} c_{\beta_1} & -s_{\beta_2} c_{\beta_1} & t_{y1} \\ 0 & s_{\beta_2} & c_{\beta_2} & \\ 0 & 0 & 0 & 1 \end{bmatrix}$$

Then the mDH convection can be applied for the following transformations:

- Defined θ_1 the joint variable of *Joint 1*, the transformation between *Frame 0* and the frame of the first joint *Frame 1* is:

$$T_1^0 = \begin{bmatrix} c_{\theta_1} & -s_{\theta_1} & 0 & 0 \\ s_{\theta_1} & c_{\theta_1} & 0 & 0 \\ 0 & 0 & 1 & d_1 \\ 0 & 0 & 0 & 1 \end{bmatrix}$$

- Defined θ_2 the joint variable of *Joint 2* and known the parameter $\alpha_2 = -120°$, the transformation between *Frame 1* and the frame of the second joint *Frame 2* is:

$$T_2^1 = \begin{bmatrix} c_{\theta_2} & -s_{\theta_2} & 0 & 0 \\ s_{\theta_2} c_{\alpha_2} & c_{\theta_2} c_{\alpha_2} & -s_{\alpha_2} & 0 \\ s_{\theta_2} s_{\alpha_2} & c_{\theta_2} s_{\alpha_2} & c_{\alpha_2} & 0 \\ 0 & 0 & 0 & 1 \end{bmatrix}$$

- Defined θ_3 the joint variable of *Joint 3* and known the parameter $\alpha_3 = -60°$, the transformation between *Frame 2* and the frame of the third joint *Frame 3* is:

$$T_3^2 = \begin{bmatrix} c_{\theta_3} & -s_{\theta_3} & 0 & 0 \\ s_{\theta_3} c_{\alpha_3} & c_{\theta_3} c_{\alpha_3} & -s_{\alpha_3} & 0 \\ s_{\theta_3} s_{\alpha_3} & c_{\theta_3} s_{\alpha_3} & c_{\alpha_3} & 0 \\ 0 & 0 & 0 & 1 \end{bmatrix}$$

- Known the parameter $\alpha_4 = -90°$, the transformation between *Frame 3* and *Frame 4* is:

$$T_4^3 = \begin{bmatrix} 1 & 0 & 0 & 0 \\ 0 & c_{\alpha_4} & -s_{\alpha_4} & -d_4 s_{\alpha_4} \\ 0 & s_{\alpha_4} & c_{\alpha_4} & d_4 c_{\alpha_4} \\ 0 & 0 & 0 & 1 \end{bmatrix}$$

Finally to reach the end-effector frame, an additional transformation needs to be performed: a translation along *yaxis* of the quantity $t_{y2} = -107{,}8\ mm$

$$T_{y_2} = \begin{bmatrix} 1 & 0 & 0 & 0 \\ 0 & 1 & 0 & t_{y2} \\ 0 & 0 & 1 & 0 \\ 0 & 0 & 0 & 1 \end{bmatrix}$$

The transformation that allows to correlate the base frame and the end-effector can be obtained as:

$$T_{end-effector}^{base} = T_0^{base} T_1^0 T_2^1 T_3^2 T_4^3 T_{y_2}$$

Analysing the computed transformation matrix it is possible to compute both the *(x,y,z)* Cartesian coordinates and the (ϕ, θ, ψ) orientation angles. A Matlab script has been developed in order to perform the needed computation.

Once the homogeneous transformation matrix has been computed, the rigid body tree can be built in Matlab. The chain is defined with the mDH parameters. The rotations around the three joints of the spherical joint can been highlighted, they are shown in *Figure 2.45*.

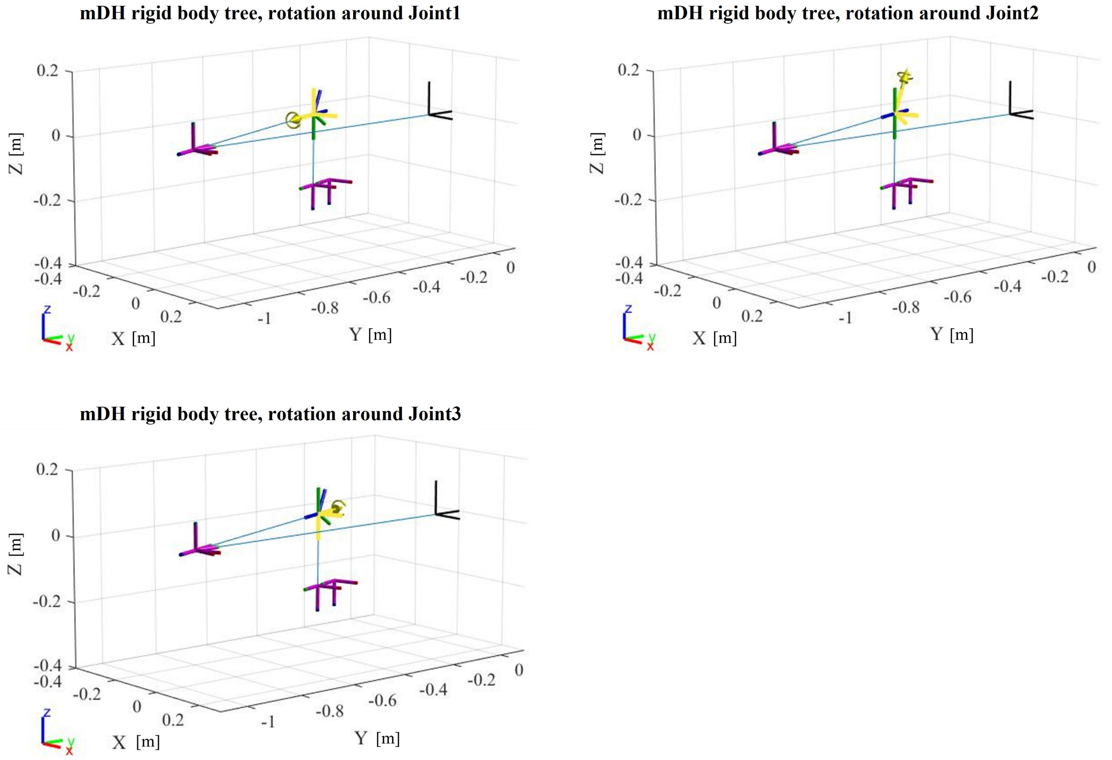

Figure 2.45: Matlab rigid body tree of the three degrees of freedom system, focus on the rotation axes of the three rotational joints.

2.7.2 Computation of the working space of the manipulator

Test bench model mechanical stops		
θ	Lower Limit [deg]	Upper limit [deg]
θ1	-64	46
θ2	3	173
θ3	-50	130

Table 2.14: Modified Denavith Hartenberg parameters for the 3dof system.

The set of reachable points inside the Cartesian space has been computed by combining the formulas of the (x, y, z) coordinates with the known ranges of allowed angles for the three joints. The ranges of θ_1, θ_2 and θ_3 are defined by the mechanical stops that limit the rotation of the actuator. The necessary data have been acquired from the CREO model of the manipulator.

The resulting cloud point (Figure 2.46) is a portion of a sphere, as expected since the glenohumeral joint is a spherical joint.

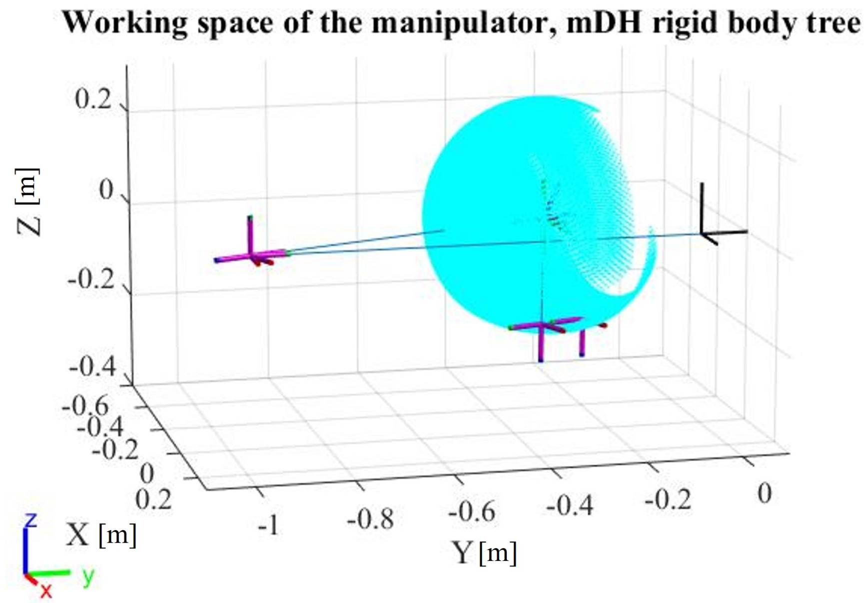

Figure 2.46: Working space of the three degrees of freedom test bench.

The cloud point computation is based on the equations of the Cartesian coordinates, thus to verify the correctness of the study of the direct kinematics the computed homogeneous transformation matrices have been compared with the ones automatically provided by CREO software. Inside CREO it is possible to define the reference frames of the chain by orienting the axes basing on the geometrical features of the model components, then it is possible to obtain the transformation matrix between one frame and another. This validation method was used to verify the computed transformations.

Vicon acquisitions to verify the working space

The analysed system has been tested real time, to ensure that the computed cloud point was correct the Vicon motion capture system has been used to acquire the end-effector positions in the Cartesian space while the manipulator was moving. Different markers have been applied on the structure to reconstruct the chain, the most important markers were the base and the end-effector one, since the movement of the second is referred to the position of the first (Section 2.4.3). From the obtained results (Section 3.3.1) it is possible to notice that the theoretically computed trajectory corresponds to the one acquired with the Vicon system. The test also shown that, since the theoretically computed cloud point fits the test bench one, it is theoretically possible to acquire the data relative to the target trajectory with the Vicon motion capture system and then provide these data to the inverse kinematic to reproduce the desired movement. The necessary markers have to be placed carefully to reduce the errors on the measurements, moreover additional markers have to be used to geometrically compute the orientation of the end-effector, three markers should be an adequate number.

2.7.3 Inverse kinematic computation

The inverse kinematics of the three degrees of freedom system has been computed tanks to the training of ANFIS networks. The ANFIS approach as been implemented both inside a Matlab code and inside two Simulink models, one used to evaluate offline the performances of the ANFIS, the other used to perform real time testing on the real time target machine.
ANFIS approach is a valid method to compute the joints variables, the input provided to the networks is the pose of the end-effector at each sample time. One ANFIS has been trained for each joint, thus three data set have been defined to train the networks.
The ANFIS prediction based on unknown variables is based on the knowledge of the training data sets: $(x, y, z, \phi, \theta, \psi, \Theta_i)$, i = 1,2,3. The results of the inverse kinematic computed with the described approach are reported in *Section 3.3.2*.
The purpose of the manipulator is the rehabilitation of the shoulder, so possible rehabilitative trajectories have been analyzed. To test the system the data relative to flexion and abduction movements were collected, the manipulator was connected to the real time target machine, with the support of a physiotherapist the exoskeleton was moved to perform the desired path, the AksIM data were recorded during all the test, then the data have been elaborated and used to compute the pose of the end-effector. The pose is then given as input to the inverse kinematic computational ANFIS block, exploiting the EPOS position control the robot performs the desired movement, it is a first implementation of a record-and-reply algorithm.

2.7.4 Simulink model for real time simulations of the 3dof test bench system inverse kinematics implementations

The model has been developed to be uploaded on the real time target machine Speedgoat. The model (Figure 2.47) is composed of different blocks. The configuration block allows to set the communication between Speedgoat and the external devices, for this test bench the communication protocols used are CAN and CANopen protocols. CAN communication is used between Speedgoat and AksIM encoders, CANopen protocol is used for the communication with the EPOS motor drivers.

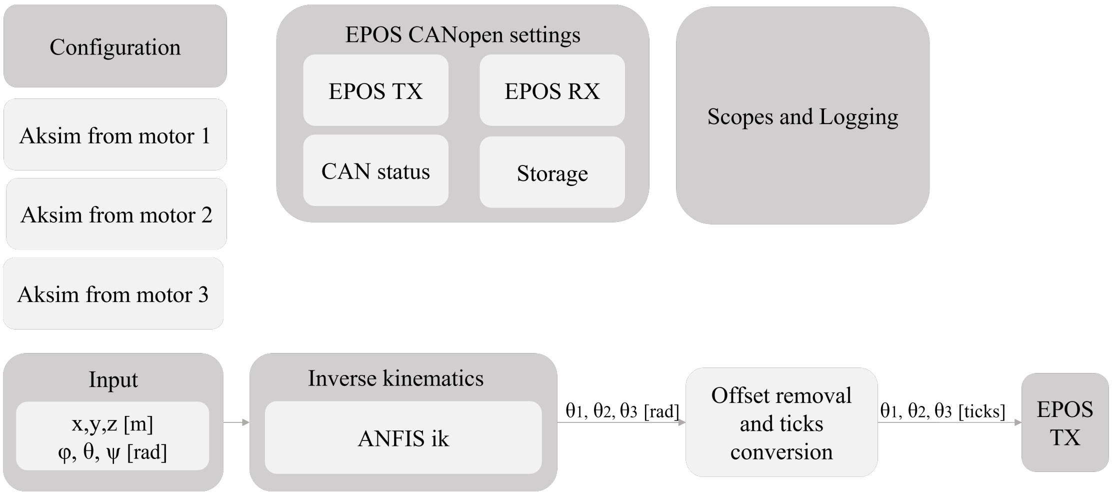

Figure 2.47: Scheme of the Simulink model for real time testing of the 3dof manipulator.

From AskIm are received the data relative to the encoders positions for the three actuators, these data are stored and made available offline. The inverse kinematics is computed online by evaluating real-time the ANFIS networks previously trained, the input to the system is the pose of the end-effector inside the Cartesian space, to test the system, two physiological trajectories have been defined: abduction trajectory and flexion trajectory. From a developed GUI it is possible to select the desired path, the corresponding input set is then provided to the system. After the computation of the joints variables, the data are elaborated and converted in Ticks unit. Saturation blocks have been used for safety reasons to guarantee that the system does not bring the motors outside the range defined by the mechanical stops. The elaborated signals are provided to EPOS position control to move the actuators. The settings of EPOS working mode occurs via GUI, the test are done in CSP mode.

2.7.5 Simulink model for real time simulations of the 3dof test bench system, admittance control

During the rehabilitation therapy, one of the requirements for the exoskeleton used to treat the impaired limb, is that the mechatronic structure can behave in a compliant way. To obtain the desired behaviour it is possible to implement an admittance control able to exploit the torque sensitive capability of the SEA. A Simulink model (Figure 2.48) has been designed to be uploaded on Speedgoat real-time target machine to control the 3dof manipulator.

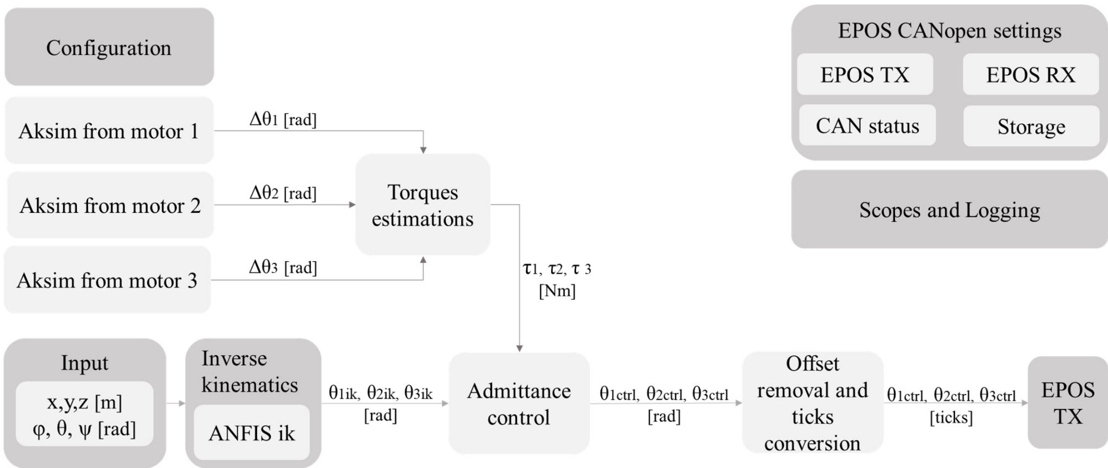

Figure 2.48: Scheme of the Simulink model for real time testing of the 3dof manipulator controlled with an admittance control to make the system behaviour compliant.

The model is a modified version of the model descried in *Section 2.7.4*. Inside the inverse kinematics computational block, three moving average filters (one for each ANFIS joint computed signal) have been implemented. The aim of the moving average filters is to assure that the ANFIS computed signals are not affected by discontinuities, once the filter window length has been chosen, the output of the filter is the average of the samples collected inside the filter window. Discontinuities, also of reduced entities, must be avoided because their presence leads the actuators to instantaneously change the rotation direction, a resulting sudden movement of the joints results, this condition has to be avoided in order to guarantee a smooth movement and a not dangerous condition for the patient. With respect to the previous model, two additional blocks have been designed, one is dedicated to the elaboration of the AksIM data: known the torsional stiffness of the spring K, the difference between the encoders positions $\Delta\theta$ and the offset of the encoders it is possible to compute an estimation of the torques τ, externally exerted to the motors. By applying the Hooke's law the motor torque $\tau_m = K\Delta\theta$ can be computed, this measure includes both the contribute of the externally applied torque and a contribute due to the structure weight. By subtracting the constant torque contribute due to the weight of the structure (experimentally estimated) the torque τ applied to the joint from the user can be computed. The torques computed are given, together with the joint angles computed by the inverse kinematic, as input to the admittance control block. Two different admittance controllers have been designed, the first (Figure 2.49) allows to assign to the actuators a damper like behaviour in response to external torques. The second model (Figure 2.50) has been used to attribute to the system both a damping and a stiffens characteristics, thus to make the actuators behave in response to external applied torques in a viscous-elastic way.

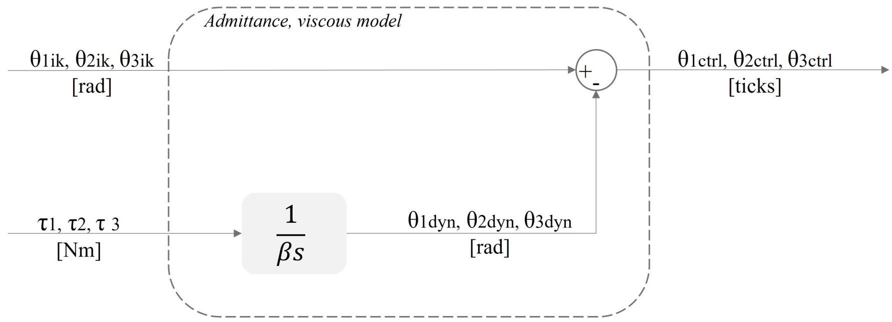

Figure 2.49: Admittance control scheme: viscous behaviour, implementation of the transfer function that describes the dynamic of the system, three displacement variables are of interest: θ_{ik} is the position computed by the inverse kinematic, θ_{dyn} is the dynamic contribute due to the application of an external torque, from the comparison of the two measures the control position to be given to the position control, θ_{ctrl}, is computed.

The viscous model allows to compute a dynamic displacement contribute signal that is proportional to the externally applied torque, the torque signal is elaborated by the transfer function that describes the dynamic of the system and, since the damping coefficient β is expressed in $\frac{Nm}{rad}$, the obtained signal is a displacement measure. The dynamic computed contribute is compared with the target one (imposed by the inverse kinematic computation) and from the comparison is obtained the control displacement signal that, once converted in ticks unit, can be given as input to the EPOS position control (Figure 2.49). The resulting behaviour, verified with experiments at the test bench, is that the system can be manually moved away from the target position (inside predefined ranges, it has been set that the dynamic contribute can affect the position of ±20°). The user will experience a certain resistance while moving the manipulator, the viscous characteristic can

be adjusted to obtain a desired interaction.
The pure position control does not allow any kind of modulation of the control signal in response to externally applied forces, the viscous behaviour admittance control make it possible to interact with the structure allowing to move the manipulator joints in the neighborhood of the target positions.

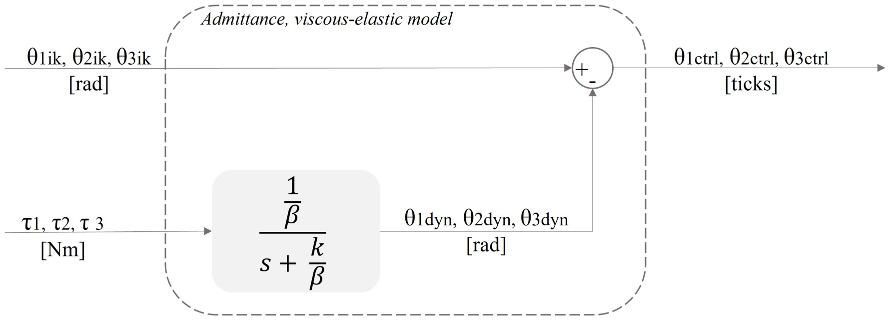

Figure 2.50: Admittance control scheme: viscous-elastic behaviour, implementation of the transfer function that describes the dynamic of the system, three displacement variables are of interest: θ_{ik} is the position computed by the inverse kinematic, θ_{dyn} is the dynamic contribute due to the application of an external torque, from the comparison of the two measures the control position to be given to the position control, θ_{ctrl}, is computed.

The drawback of a pure viscous model is that after the system has been moved away from the target position there is no effect that brings the system back to the original position. For this purpose an elastic characteristic (Figure 2.50) can be implemented inside the transfer function, the dynamics of the system becomes viscous-elastic and thanks to the elastic element the system is able, after the perturbation, to return to the original position. The characteristics of the spring and of the damper, thus K and β factors can be adjusted to obtain a desired interaction. For the analyzing application an interesting development can be the modulation of those parameters according to the phase of the performed movement. During a flexion movement, for example, it is desired to guide the arm movement during the descending phase, so an higher damping coefficient can be set, otherwise during the ascending phase a lower damping coefficient is preferable to provide only support. The modulation of the spring stiffness allows to obtain a faster or slower movement to return to the target position. The combination of both the parameters allow to make the exoskeleton compliant to the patient movements.

Chapter 3

Results

3.1 SEA modelling

3.1.1 Functioning of the implemented SEA Simulink model

The Simulink model of the SEA, described in *Section 2.5.2*, has been tested under different load conditions, the torque exerted by the motor and the resistive torque applied by the load for the different tests are resumed in table 3.1.

	Free run system	**No movement system**	**Motor drags load**	**Load drags motor**
Motor torque [Nm]	0.25	0.25	0.25	0.25
Load torque [Nm]	0	25	15	35

Table 3.1: The torques applied by the motor and by the load are reported. Different torques values have been tested to simulate several working conditions: free run system, no movement system, system where the motor drags the load and where the load drags the motor have been analyzed.

Free run system

Free run system: any load is applied, the motor has not resistance and can freely rotate.

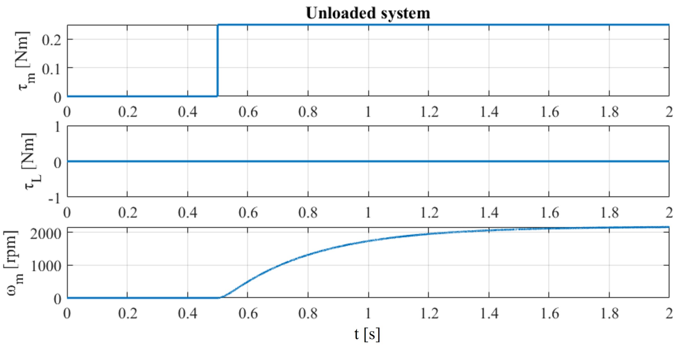

Figure 3.1: Free run system results: when the motor starts to apply a torque it can freely rotates without encountering resistance, thus the rotational speed continuously increases.

No movement system

No movement system: the combination of motor torque and resisting torque applied to the system results in a null rotational speed, thus in a blocked system without motion.

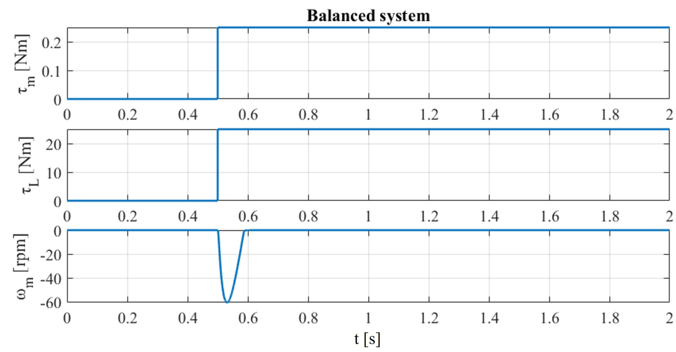

Figure 3.2: No movement system results: blocked system with null speed and motion. The combination of the torque exerted by the motor and the resisting torque brings the velocity of the motor to drop to a null value.

Motor drags load

Motor drags load: the power is transmitted from the motor to the load, the motor torque can overcome the resistive torque. The motor can drag the load during its motion, thus the resulting motor speed is positive.

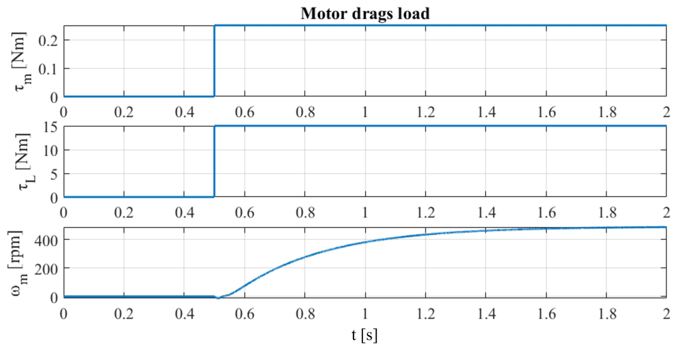

Figure 3.3: Motor drags load results: the motor torque is able to overcome the resisting torque, thus the motor is able to rotates, the velocity can increase but it is limited by the application of the load.

Load drags motor

Load drags motor: the power is transmitted from the load to the motor, the resisting torque overcomes the motor torque, thus, the motor cannot drag the load during its motion, the resulting motor speed is negative.

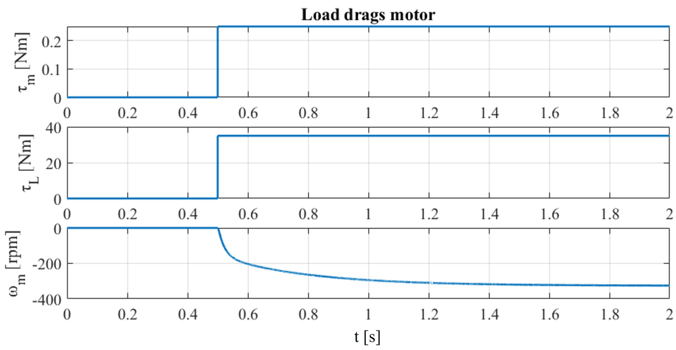

Figure 3.4: Load drags motor results: the resisting torque overcomes the one exerted by the motor, thus the motor is not able to rotates following the direction provided by the input driving signal. The rotation motion of the motor is driven by the load that drags the actuators, thus the motor velocity decreases.

3.1.2 Frequency analysis of real time collected data: infinite inertial load

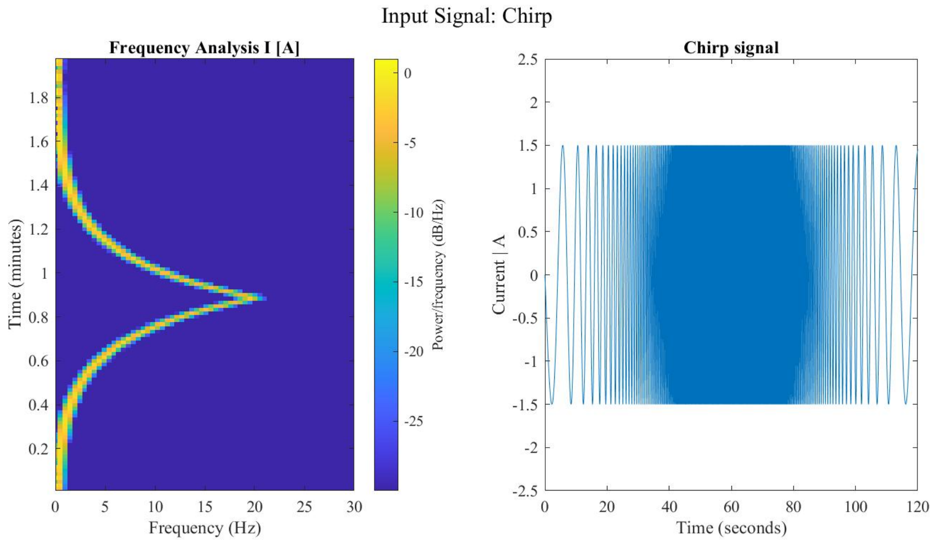

Figure 3.5: Input current chirp signal and its frequency analysis. The signal is a logarithmic bidirectional chirp with a maximum reachable frequency of *20 Hz*. The spectrogram plot is used to highlight the different frequencies assumed by the chirp signal.

The frequency analysis of the compliant element mounted inside the SEA has been done by testing the system with a chirp current signal.
A chirp is a signal with constant amplitude and variable frequency. The chirp signal is obtained from a cosine function that is elaborated by setting the amplitude and by modulating the output frequency sweep. The Simulink block generates a swept-frequency cosine. It has been chosen to adopt a bidirectional sweep mode and a logarithmic type of frequency sweep. Bidirectional sweep analyses two consecutive sample times and provides a signal that for the first half corresponds to the unidirectional counter part while for the second half provides the mirrored image of the first part of the signal. The desired target frequency for the chirp is $f = 20Hz$, the obtained signal and the frequency spectrum are shown in *Figure 3.5*.

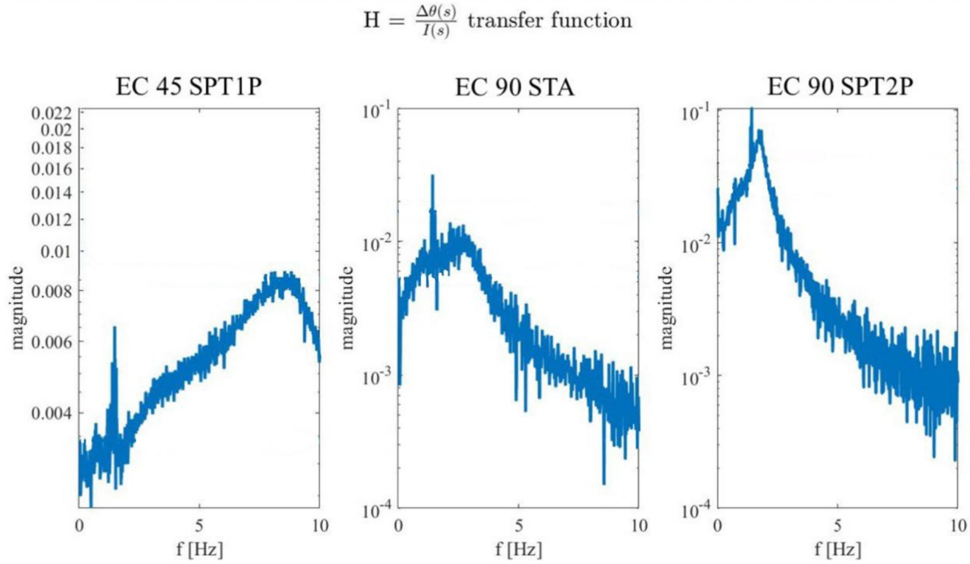

Figure 3.6: Magnitude Bode diagram of the behaviour of the three analyzed actuators. It has been analyzed the transfer function that relates the encoders measured displacement with the input provided current. The diagrams have been used to compute the resonant peak and the corresponding resonant frequency, these data represents an indication of the optimal working condition for the usage of the analyzed compliant element.

For the analyzed compliant elements the Bode diagrams of the magnitude have been studied. The modulation of the displacement $\Delta\theta$ has been analyzed to understand the best frequency for the correct working of the compliant element. The optimal frequency is the resonant one that can be measured from the Bode diagrams shown in *Figure 3.6*, the resonant frequencies for the three systems under test are reported:

- EC45 with SPT1P compliant element: $f_{res} = 7.93\ Hz$
- EC90 with STA compliant element: $f_{res} = 2.53\ Hz$
- EC90 with SPT2P compliant element: $f_{res} = 1.64\ Hz$

From the analysis of the Bode diagram of the displacement data provided by the encoders and of the torque measurements of the torsiometer, it has been verified that the two quantities can be correlated by the multiplication for a constant (Figure 3.7). The constant that relates one quantity to the other is the torsional stiffness of the compliant element under test, thus the linear relation $\tau = k\Delta\theta$ results satisfied.

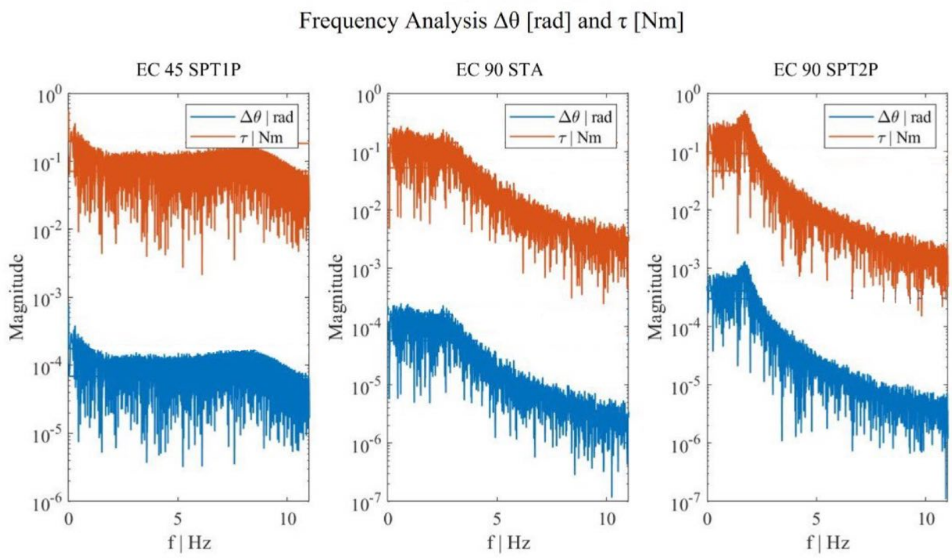

Figure 3.7: Frequency torque analysis, the diagram shows the behavior of the torque at the frequency variation. The results have also been compared with the frequency analysis of the displacement to verify the linear relation between the two quantities.

The torque frequency analysis, done for the three compliant elements, shows that the higher intensity of the torque measurements occurs at the same resonant frequencies evaluated in *Figure 3.6*. The torque intensity decreases at the increasing of the frequencies as shown in *Figure 3.8*.

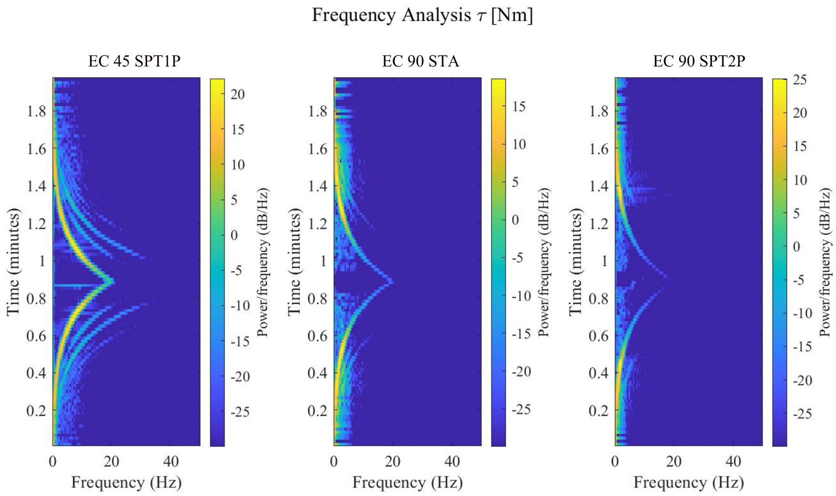

Figure 3.8: Spectrogram plot used to analyse the torque-frequency relation. The intensity of the torque grows in the neighborhood of the resonant frequency that, as expected, represents the best working condition.

The accuracy of the sensor (SEA) can be analyzed by evaluating the linear model of the acquired data. A regression line can be estimated and the residuals between the desired data and the experimental ones. Thanks to this analysis (Figure 3.9) an estimation of the error affecting the torque measurements can be obtained.

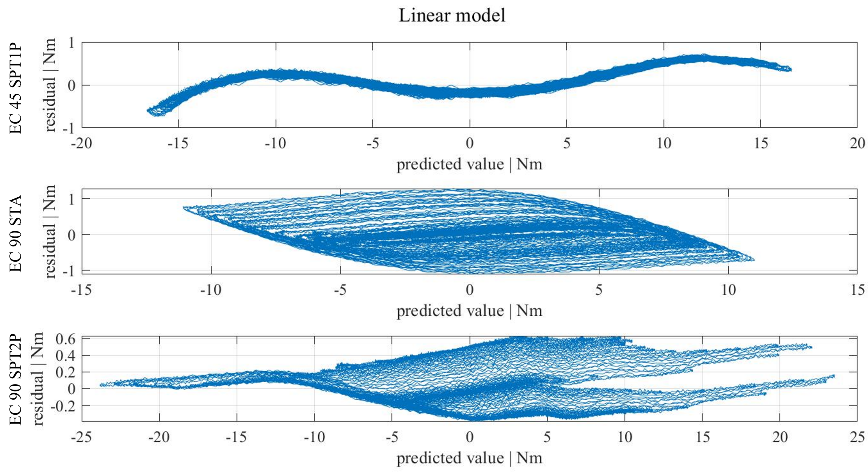

Figure 3.9: Linear model for the torques analysis, mapping between the measured torque and the error, expressed in terms of residuals, that affect the measure.

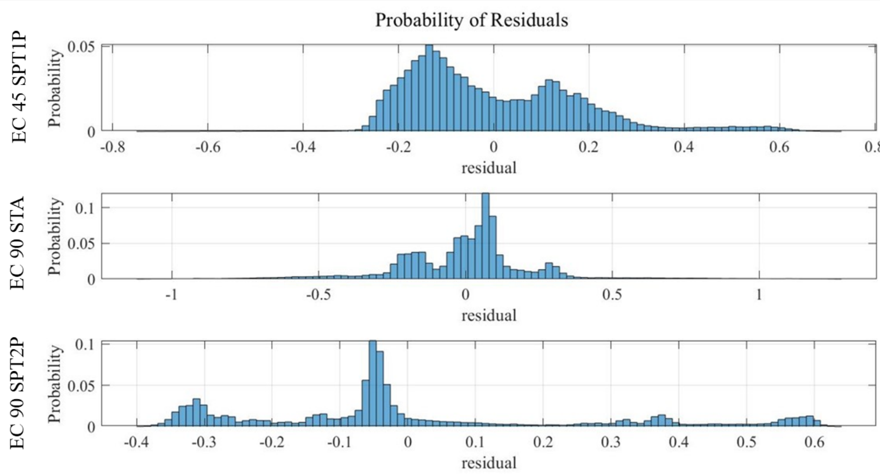

Figure 3.10: Probability distribution of the residuals error that affects the torques measurements.

From the linear models of the three compliant elements (Table 3.2, Table 3.3, Table 3.4) can be also evaluated the torsional stiffness of the compliant element, that results to be:

- $K_{sta} = 1072.6\ \frac{Nm}{rad}$
- $K_{spt1p} = 961.47\ \frac{Nm}{rad}$
- $K_{spt2p} = 384.88\ \frac{Nm}{rad}$

The probability related to the residual errors occurrence is shown in *Figure 3.10.*

EC45 SPT1P Linear regression model: T ~ 1+Δθ Encoder					
Estimated coefficients					
		Estimate	SE	tStat	pValue
Intercept		0,18318	0,0005368	341,25	0
Δθ Encoder		-961,47	0,094135	-10214	0
Observations and errors data					
Number of observations	Error degrees of freedom	RMSE	R-Sqared	Adjusted R-Sqared	F-statistics vs. constant model
120000	119998	0,184	0,999	0,999	104000000

Table 3.2: Linear regression model for a system composed by EC45 motor and SPT1P compliant element: model data and focus on the estimated compliant element stiffness, obtained as the slope of the $\frac{\Delta\theta}{\tau}$ line.

EC90 STA Linear regression model: T ~ 1+Δθ Encoder					
Estimated coefficients					
		Estimate	SE	tStat	pValue
Intercept		-0,064286	0,00070213	-91,559	0
Δθ Encoder		-1072,6	0,19636	-5462,2	0
Observations and errors data					
Number of observations	Error degrees of freedom	RMSE	R-Sqared	Adjusted R-Sqared	F-statistics vs. constant model
120000	119998	0,243	0,996	0,996	29800000

Table 3.3: Linear regression model for a system composed by EC90 motor and STA compliant element: model data and focus on the estimated compliant element stiffness, obtained as the slope of the $\frac{\Delta\theta}{\tau}$ line.

EC90 SPT2P Linear regression model: T ~ 1+Δθ Encoder					
Estimated coefficients					
		Estimate	SE	tStat	pValue
Intercept		0,049504	0,00075675	65,417	0
Δθ Encoder		-384,88	0,054574	-7052,4	0
Observations and errors data					
Number of observations	Error degrees of freedom	RMSE	R-Sqared	Adjusted R-Sqared	F-statistics vs. constant model
120000	119998	0,262	0,998	0,998	49700000

Table 3.4: Linear regression model for a system composed by EC90 motor and SPT2P compliant element: model data and focus on the estimated compliant element stiffness, obtained as the slope of the $\frac{\Delta\theta}{\tau}$ line.

The hysteresis of the sensors have been evaluated to have an estimation of the quality of the measurements provided by the compliant element. Due to the presence of hysteresis, when considering an input it results that different corresponding values of output can be obtained.

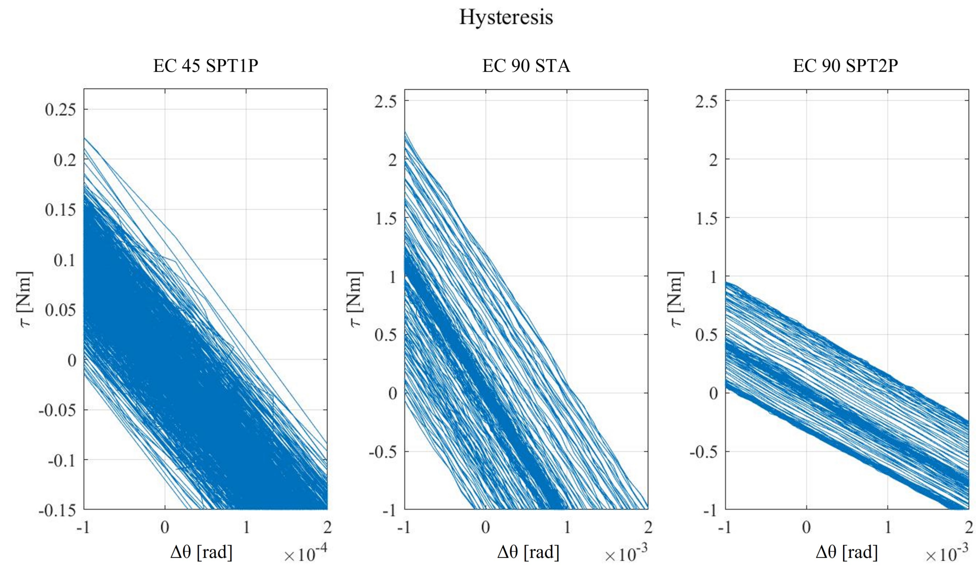

Figure 3.11: Hysteresis evaluation for the analyzed sensors: the results shows that the SEA with EC90 motor, tested with the same chirp input current, have an higher hysteresis with the star geometry, this may be due to the higher number of pins on the design. An higher number of pins means higher losses of energy due to the friction and gliding between components. Also the forces applied in the contact point between the spring and the external component affect the hysteresis, also in this case, more pins means more forces applied and so an higher hysteresis.

The lower is the hysteresis the more precise the measurement. By varying the maximum and minimum torque ranges also the hysteresis varies, the larger the range, the higher the hysteresis. The choice of the compliant element material does not relevantly affect the hysteresis while the geometry is determinant. One possible hypothesis is that the energy losses occurs in the contact point between the springs and the external components. For the star geometry the number of pins is higher, all the pins have to rotates. Thus, the energy lost in the star geometry is higher than the one measured with the spiral geometry where there are less pins.

Torsional stiffness evaluation of the compliant element for different EC45-SPT1P SEAs (FSJ45A joints)

Four actuators, each composed of an EC45 motor, an Harmonic Drive and a SPT1P custom made compliant element, have been tested to evaluate the effective torsional stiffness of the springs (Figure 3.12).

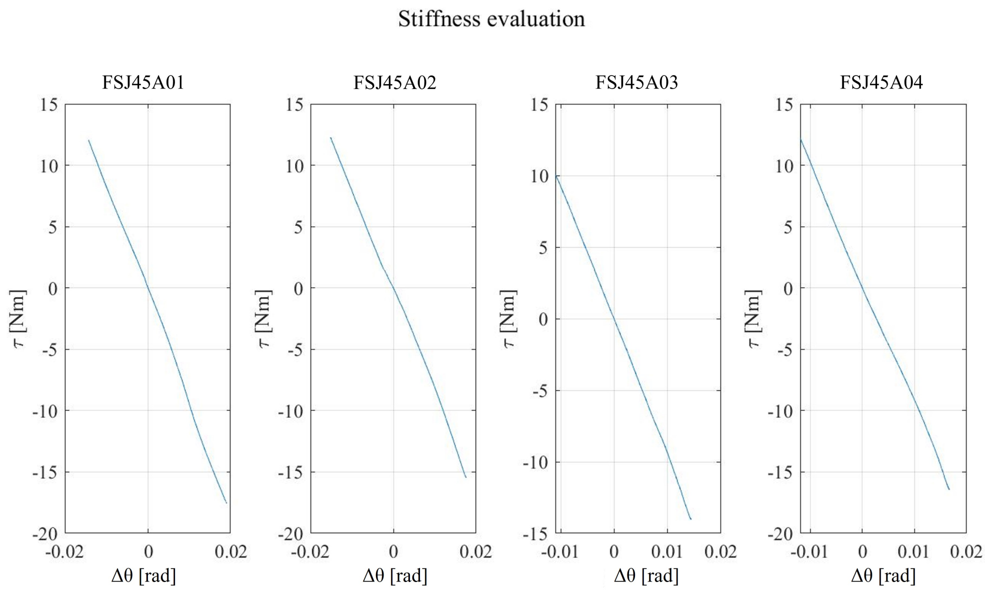

Figure 3.12: Comparison between torque-displacement relations for different SEA joints, EC45 motor with SPT1P compliant element have been tested.

Since the spiral geometry resulted to be subject to different material strain in different points of the components and it resulted to be difficult to be replicated during the production, in order to obtain an accurate evaluation of the stiffness for each torsional element, it has been chosen to test each systems with a variable ramp input current signal (increasing current amplitude from -4A to 4A).

FSJ45A01 - Linear regression model: T ~ 1+Δθ Encoder					
Estimated coefficients					
		Estimate	SE	tStat	pValue
Intercept		-0,40625	0,0017993	-225,79	0
Δθ Encoder		-901,52	0,16749	-5382,4	0
Observations and errors data					
Number of observations	Error degrees of freedom	RMSE	R-Sqared	Adjusted R-Sqared	F-statistics vs. constant model
44001	43999	0,361	0,998	0,998	2,9e+07

Table 3.5: Linear regression model for the FSJ45A01 joint. Data of the model and focus on the compliant element stiffness estimation.

FSJ45A02 - Linear regression model: T ~ 1+Δθ Encoder					
Estimated coefficients					
		Estimate	SE	tStat	pValue
Intercept		-0,2449	0,0019412	-126,16	0
Δθ Encoder		-838,02	0,17256	-4856,4	0
Observations and errors data					
Number of observations	Error degrees of freedom	RMSE	R-Sqared	Adjusted R-Sqared	F-statistics vs. constant model
44001	43999	0,383	0,998	0,998	2,36e+07

Table 3.6: Linear regression model for the FSJ45A02 joint. Data of the model and focus on the compliant element stiffness estimation.

FSJ45A03 - Linear regression model: T ~ 1+Δθ Encoder					
Estimated coefficients					
		Estimate	SE	tStat	pValue
Intercept		-0,13787	0,00078613	-175,38	0
Δθ Encoder		-950,05	0,087895	-10809	0
Observations and errors data					
Number of observations	Error degrees of freedom	RMSE	R-Sqared	Adjusted R-Sqared	F-statistics vs. constant model
44001	43999	0,16	1	1	1,17e+08

Table 3.7: Linear regression model for the FSJ45A03 joint. Data of the model and focus on the compliant element stiffness estimation.

FSJ45A04 - Linear regression model: T ~ 1+Δθ Encoder					
Estimated coefficients					
		Estimate	SE	tStat	pValue
Intercept		0,241	0,0013324	180,88	0
Δθ Encoder		-987,14	0,12905	-7649,2	0
Observations and errors data					
Number of observations	Error degrees of freedom	RMSE	R-Sqared	Adjusted R-Sqared	F-statistics vs. constant model
44001	43999	0,261	0,999	0,999	5,85e+07

Table 3.8: Linear regression model for the FSJ45A04 joint. Data of the model and focus on the compliant element stiffness estimation.

The obtained data have been elaborated by computing a linear model from which the torsional stiffness can be acquired (Table 3.5, Table 3.6, Table 3.7, Table 3.8). The resulting torsional stiffnesses are:

- $K_{FSJ45A01} = 901.52\ \frac{Nm}{rad}$
- $K_{FSJ45A02} = 838.02\ \frac{Nm}{rad}$
- $K_{FSJ45A03} = 950.05\ \frac{Nm}{rad}$
- $K_{FSJ45A04} = 987.14\ \frac{Nm}{rad}$

Speedgoat and Simulink, torque and displacement data comparison

In *Section 2.5.3* has been described the Simulink model used to reproduce the behaviour of the SEA when to the system is applied an infinite inertial load. The results obtained from Simulink simulations and the data acquired at the test bench have been compared in terms of displacements and torques (Figure 3.13). The developed model resulted able to reproduce the behaviour of the real actuators.

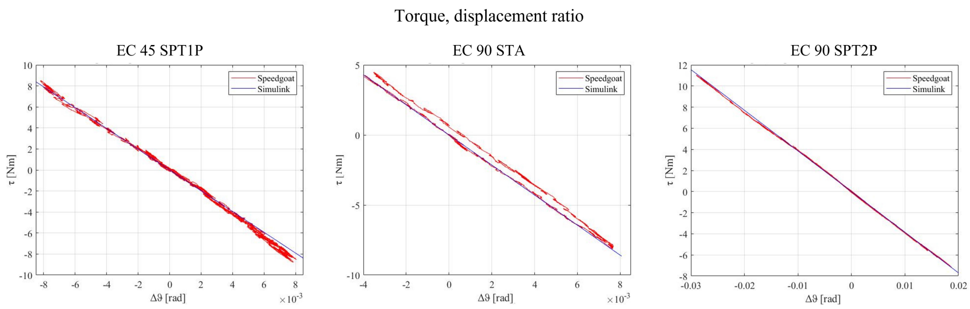

Figure 3.13: Torque and displacement data comparison between measurements real-time acquired and simulated data. The system was subject to an infinite inertial load.

3.1.3 Speedgoat and Simulink data comparison: finite inertial load

EC45 motor with SPT1P compliant element

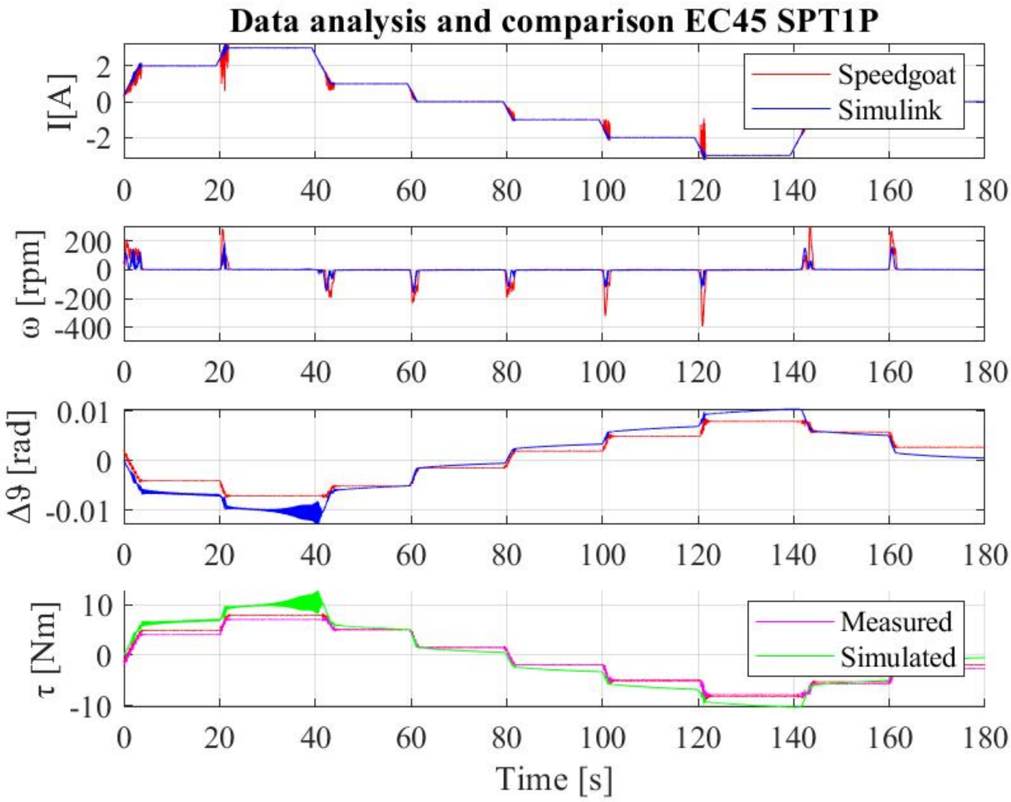

Figure 3.14: Current, speed, displacement and torque data comparison between measurements real-time acquired at test bench connected to Speedgoat (red) and the simulated Simulink (blue) results. To the system is applied a finite inertial load. The torque subplot shows also the measurement done with the industrial torsiometer (pink) that overlaps with the Speedgoat measurements (red) obtained as $\tau = K_t \Delta\theta$, and the measure done with the Simscape torsiometer (green) that overlaps with the Simulink measurements (blue) obtained as $\tau_{sim} = K_t \Delta\theta_{sim}$

The actuators EC45-SPT1P, EC90-STA and EC90-SPT2P have been real time tested with a finite inertial load applied. The results obtained have been compared with the ones provided by the Simulink simulation of the model described in *Section 2.5.4*. The correct behaviour of the designed model has been verified by evaluating the errors between the expected values of current, speed, displacement and torques with the ones obtained from the simulation. In *Figure 3.14*, it is reported, as example, a qualitative comparison between Simulink and Speedgoat data. All the actuators have been tested and simulated, the results in terms of absolute errors distributions are shown in *Figure 3.15*, *Figure 3.16* and *Figure 3.17*. The error distributions have been analysed for measurements of current, speed, displacement and torque. The considered reference value is the one acquired during test bench real time testing on Speedgoat, the errors are measured between the simulated Simulink data and the reference ones. The analysis have been done for EC45-SPT1P, EC90-STA and EC90-SPT2P joints. To better interpret the reported results, a further analysis could be done by referring the obtained errors to the full scale, from a preliminary analysis it results that the models can be refined to improve the simulation precision, a future development can be the introduction of the non-ideality factors inside the model.

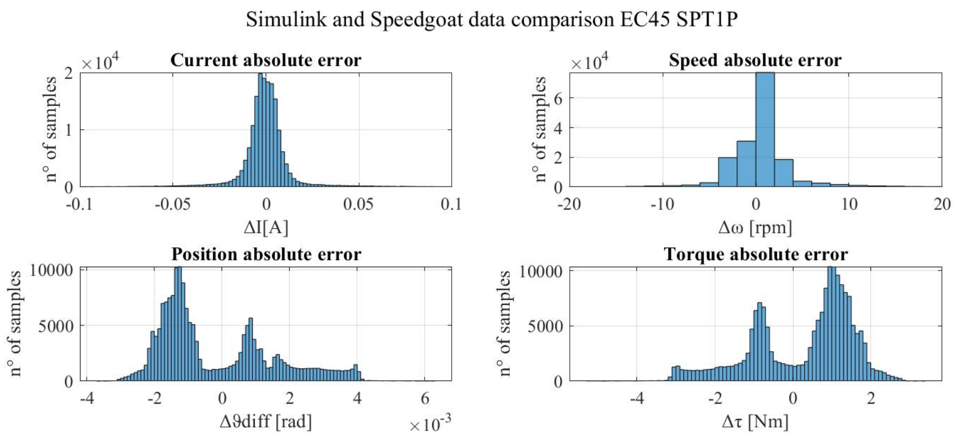

Figure 3.15: Absolute errors distributions for current, speed, displacement and torque measurements. The reference value is the one acquired with Speedgoat test bench real time testing, the error is measured between the simulated Simulink data and the reference ones. The system under test is EC45-SPT1P.

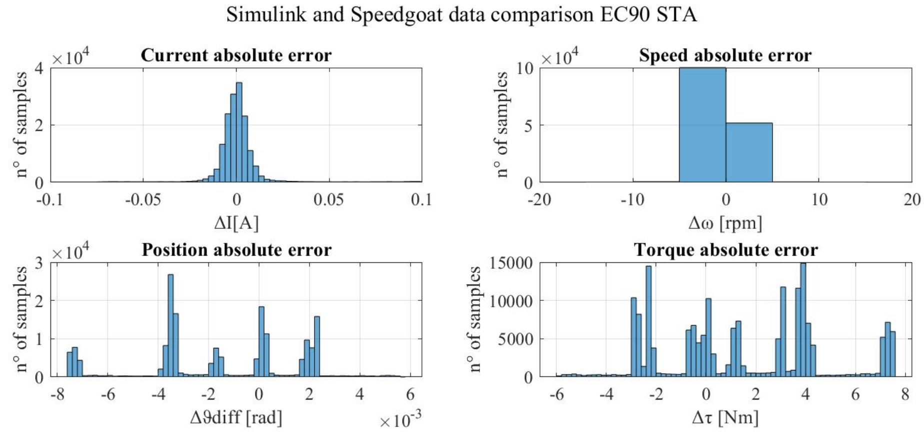

Figure 3.16: Absolute errors distributions for current, speed, displacement and torque measurements. The reference value is the one acquired with Speedgoat test bench real time testing, the error is measured between the simulated Simulink data and the reference ones. The system under test is EC90-STA.

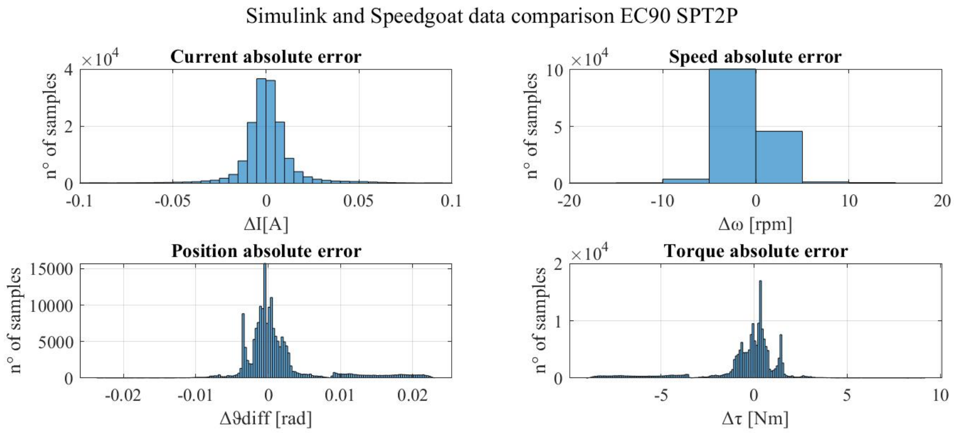

Figure 3.17: Absolute errors distributions for current, speed, displacement and torque measurements. The reference value is the one acquired with Speedgoat test bench real time testing, the error is measured between the simulated Simulink data and the reference ones. The system under test is EC90-SPT2P.

3.2 Two degrees of freedom systems study

3.2.1 Analysis of the inverse kinematics results for the case study 2dof system configuration

To identify the parameters for the settings of the ANFIS training, different combinations of number of membership functions (Mf) and epoch number (En) have been tested, the ANFIS was trained and then the performances over the prediction of the angles needed to perform a desired trajectory were evaluated. Since the set of training data, composed by the cloud point and the orientations, contains a high number of data, a computational limit has been encountered that did not allow Matlab to train the ANFIS with a membership function number greater than two, in these cases a warning regarding the possibility of run out of memory, during the computation, was provided by Matlab, thus the required training cannot be completed, and in some cases it caused the stuck of Matlab application. The trainings have been performed on a Dell Precision 5820 Tower X-Series device, with a Intel(R) Core(TM) i9-10940X CPU at 3.30GHz 3.31GHz processor, 32.0 GB RAM, 64-bit operating system. By varying the epoch number it results that, for the case under analysis, the higher is the parameter the better is the prediction (Figure 3.18, Figure 3.19).

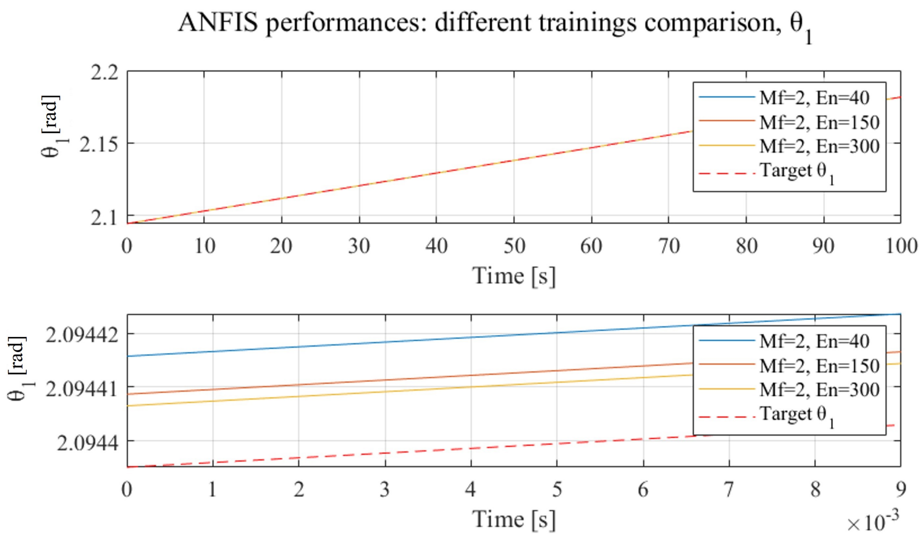

Figure 3.18: Comparison between the θ_1 angles predicted by three different ANFIS and the theoretically computed one. On top it is shown the full signal, on the bottom a zoom in on the first 9 ms of the same signal. 2dof system.

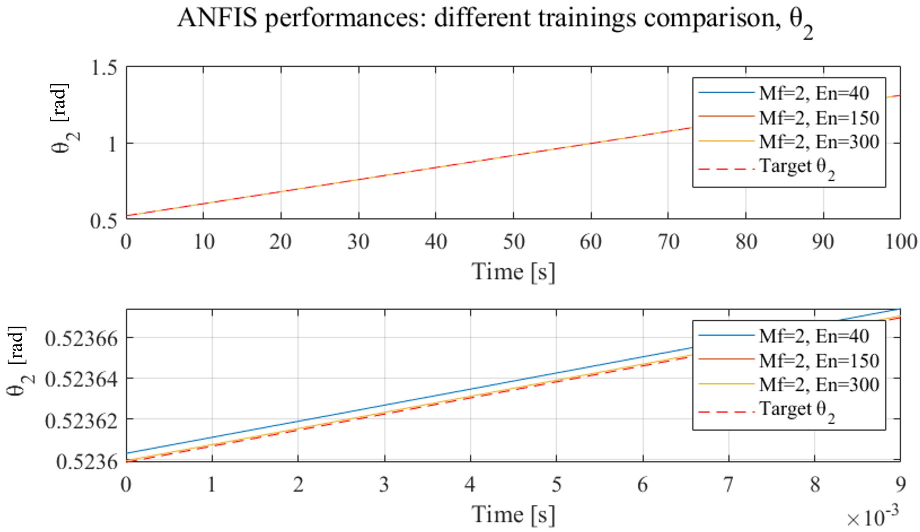

Figure 3.19: Comparison between the θ_2 angles predicted by three different ANFIS and the theoretically computed one. On top it is shown the full signal, on the bottom a zoom in on the first 9 ms of the same signal. 2dof system.

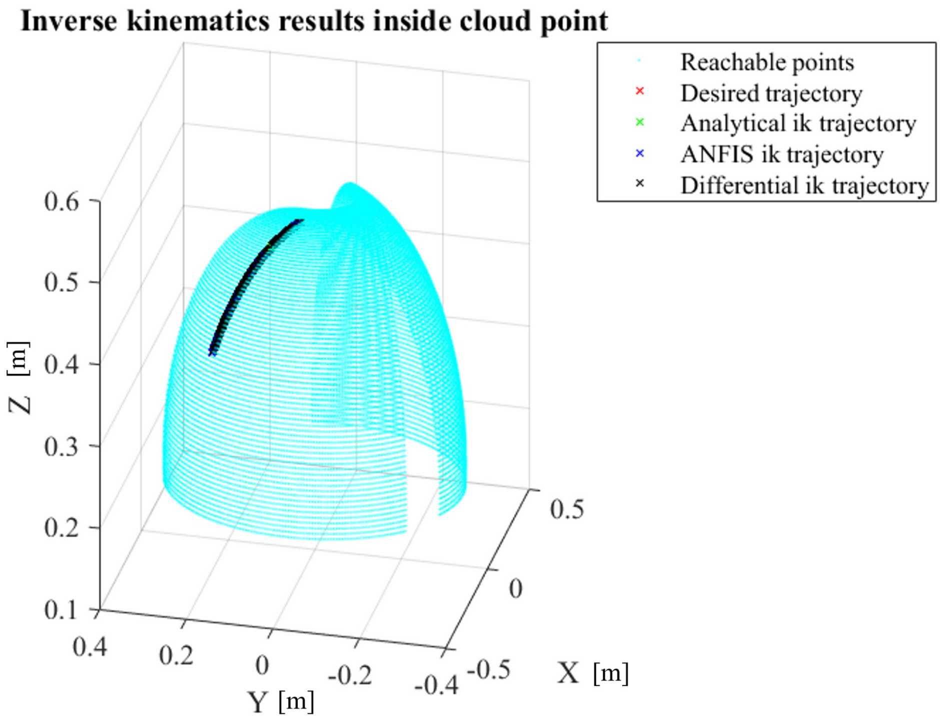

Figure 3.20: Comparison between the trajectories obtained with the inverse kinematics computed angles and the target one, 2dof system.

The angles obtained with the three inverse kinematics approaches have been used to compute, using the direct kinematics formulas, the trajectory of the end-effector inside the cloud point. All the computed trajectories well follow the desired one (Figure 3.20). For the ANFIS method the networks adopted were the most performing shown in *Figure 3.18* and in *Figure 3.19* so with $Mf = 2$ and $En = 300$. To evaluate the performances of the three methods, the absolute errors between the angles computed with the inverse kinematics and the reference ones (the reference angles are the ones used to compute the trajectory that is then given as input to the inverse kinematic algorithms) have been computed. The absolute errors distributions (Figure 3.21, Figure 3.22) have been analysed over a test made of 100000 samples in order to understand the entity of the error and the frequency, in terms of number of samples, of its occurrence.

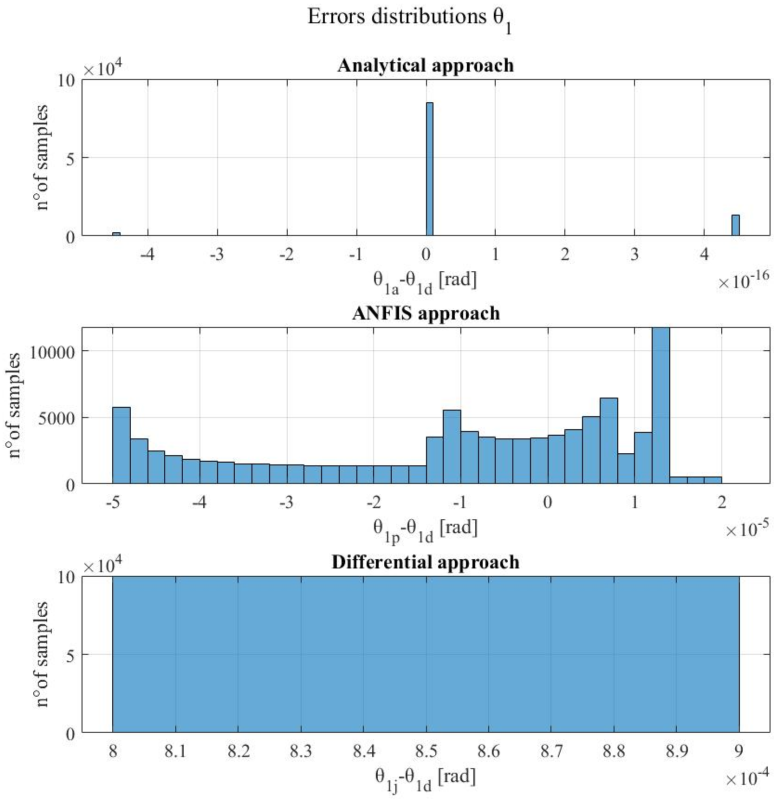

Figure 3.21: Absolute errors distributions for the computation of θ_1 through the analytical, the ANFIS and the differential approaches. 2dof system.

For the standard methods the error is essentially constant, all the samples of the differential methods are affected by the same error, also the error for the analytic approach is mostly concentrated on one value. The errors that affect the ANFIS prediction are more variable, this is coherent with the predictive and uncertain nature of the method.

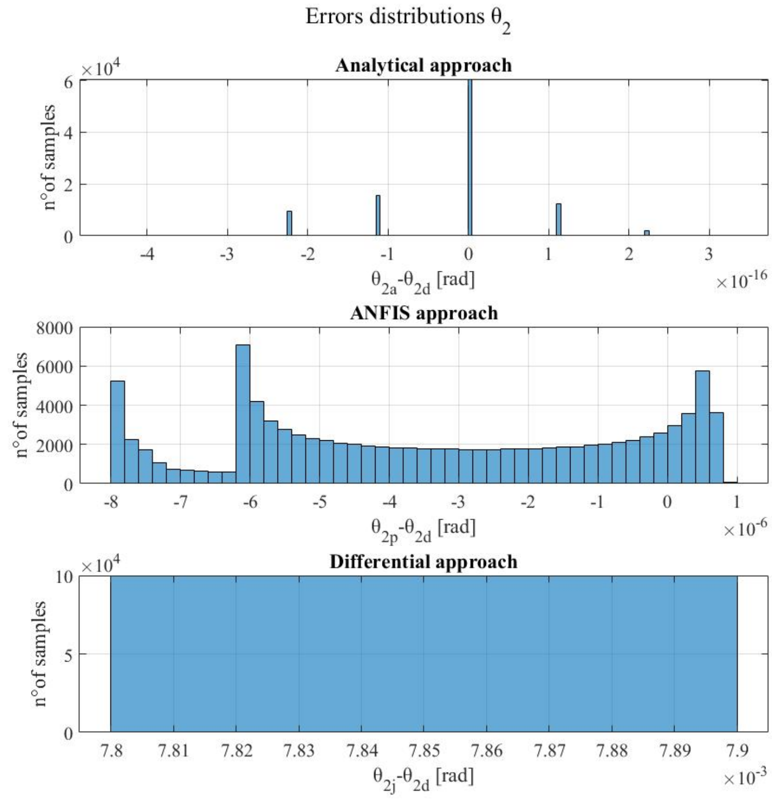

Figure 3.22: Absolute errors distributions for the computation of θ_2 through the analytical, the ANFIS and the differential approaches. 2dof system.

The results show that the ANFIS approach is an effective method for the inverse kinematic resolution, in fact the errors over the prediction of the joint variables are not significantly higher than the ones obtained with the standard methods. Also the resulting errors on the computed positions in the Cartesian space have been evaluated (Figure 3.23).

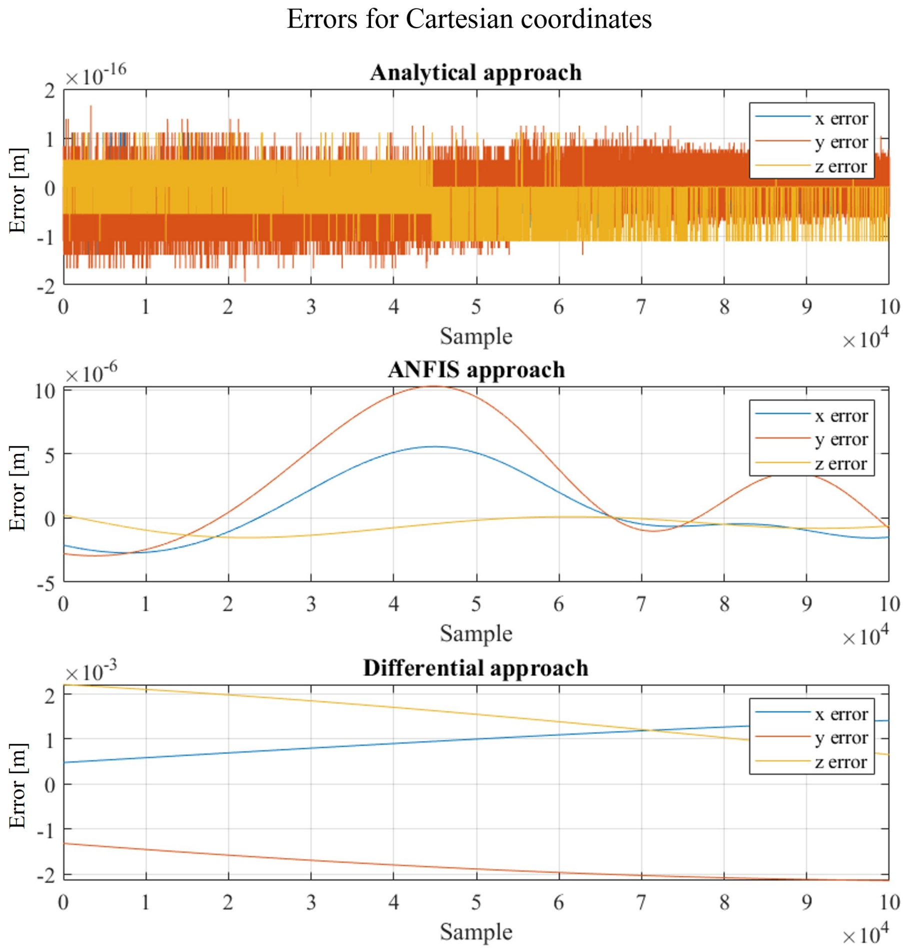

Figure 3.23: Absolute errors distributions over the Cartesian coordinates computed with angles obtained through the analytical, the ANFIS and the differential approaches. 2dof system.

3.2.2 Analysis of the inverse kinematics results for the testing of the test bench 2dof system configuration

To analyse the variability of ANFIS performances, different networks have been trained exploring different combinations of numbers of membership functions and the epoch numbers. After training, the ANFIS have been tested on the same data, then the RMSE have been computed for each predicted angle.
The results show that the lowest error is obtained for the networks trained with $Mf = 4$ and $En = 300$. The results are shown both with a surface representation and a 2D map, in both the cases the lighter is the color the worse is the prediction (Figure 3.24, Figure 3.25).
It is possible to notice that the increasing of the membership function number it is not sufficient to guarantee a better prediction, it is necessary also to correctly choose the epochs number.
Thus, the selection of the two parameters cannot be done independently, the prediction output is dependent on the combination of both the parameters. The predictor capability of the different trained ANFISs resulted to be very accurate, in the worse scenario the RMSE is in the order of 10^{-5} radians.

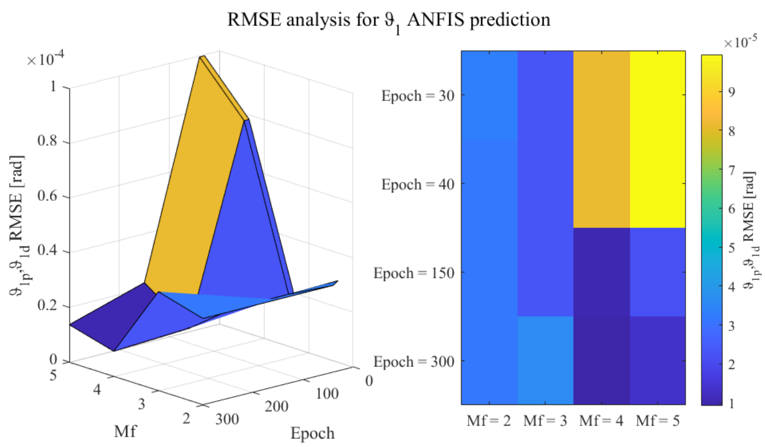

Figure 3.24: Analysis of the performances of the ANFIS in predicting θ_1 angle, different combinations of the number of membership functions (Mf) and epochs have been tested. The metric used for the evaluation is the RMSE between the predicted result and the expected one.

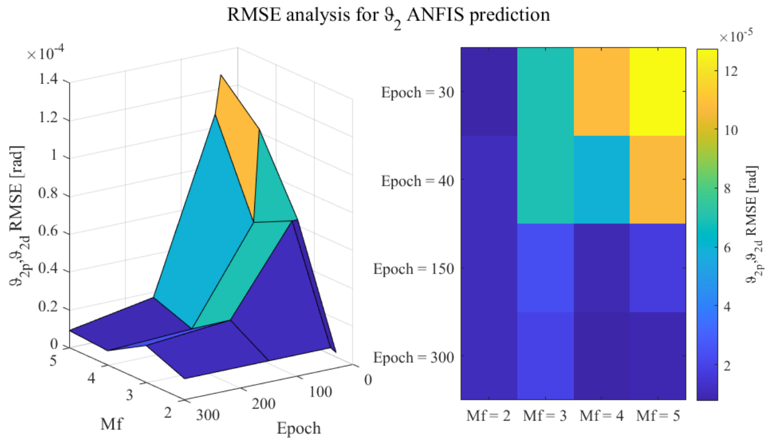

Figure 3.25: Analysis of the performances of the ANFIS in predicting θ_2 angle, different combinations of the number of membership functions (Mf) and epochs have been tested. The metric used for the evaluation is the RMSE between the predicted result and the expected one.

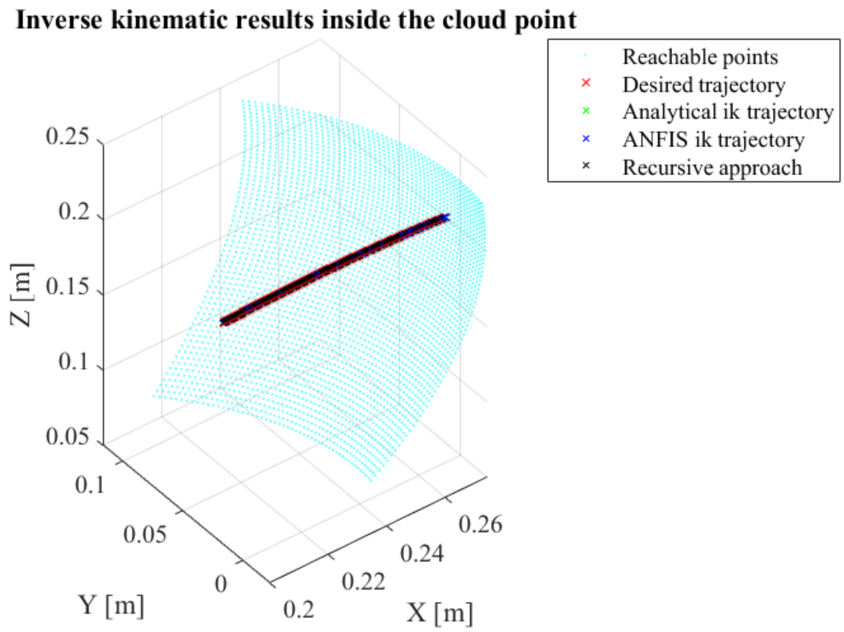

Figure 3.26: Comparison between the trajectories obtained with the inverse kinematics computed angles and the target one for the 2dof test bench system.

The trajectories computed with the angles provided by the inverse kinematics

algorithm have been compared with the target one an plotted on the working space (Figure 3.26). Each method is able to correctly predict the joint variables to obtain the desired movement of the end-effector inside the Cartesian space. For the ANFIS inverse kinematics the network used where trained with $Mf = 4$ and $En = 300$ that resulted to be the most performing (Figure 3.24, Figure 3.25).
The absolute errors distributions have been analysed over a test of 100000 samples for the computation of θ_1 and θ_2, moreover in *Figure 3.27* are shown the obtained errors on the Cartesian coordinates of the resulting trajectories.

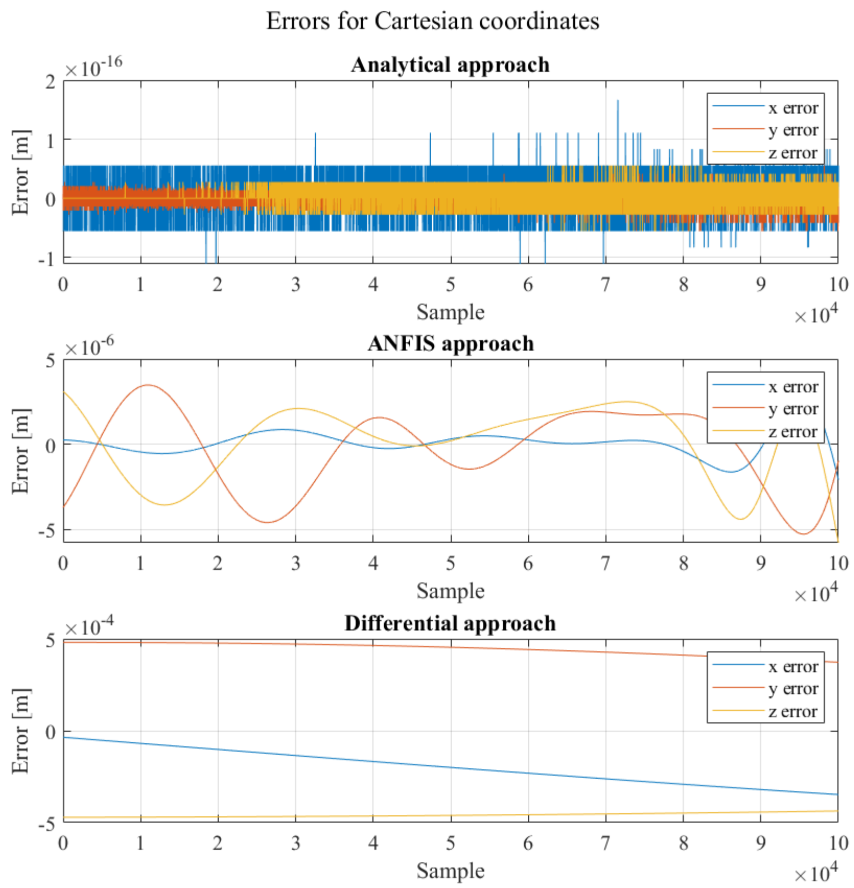

Figure 3.27: Absolute errors distributions, for the 2dof test bench system, over the Cartesian coordinates computed with angles obtained through the analytical, the ANFIS and the differential approaches.

The errors distributions have been analysed like for the previous configuration, ANFIS method resulted to be effective and with an higher variability of the errors that affects the computations with respect to the traditional methods (Figure 3.28,Figure 3.29).Even if the ANFIS error is larger than the ones of the analytic and differential approaches, its entity is sufficiently small to make the performances of this method comparable and competitive with the other methods.

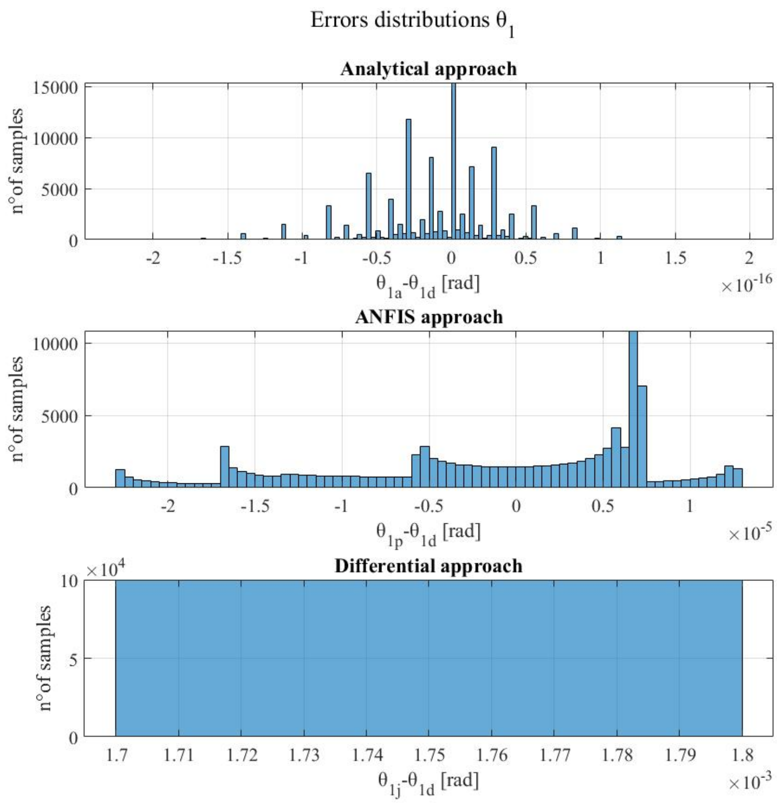

Figure 3.28: Absolute errors distributions, for the 2dof test bench system, for the computation of θ_1 through the analytical, the ANFIS and the differential approaches.

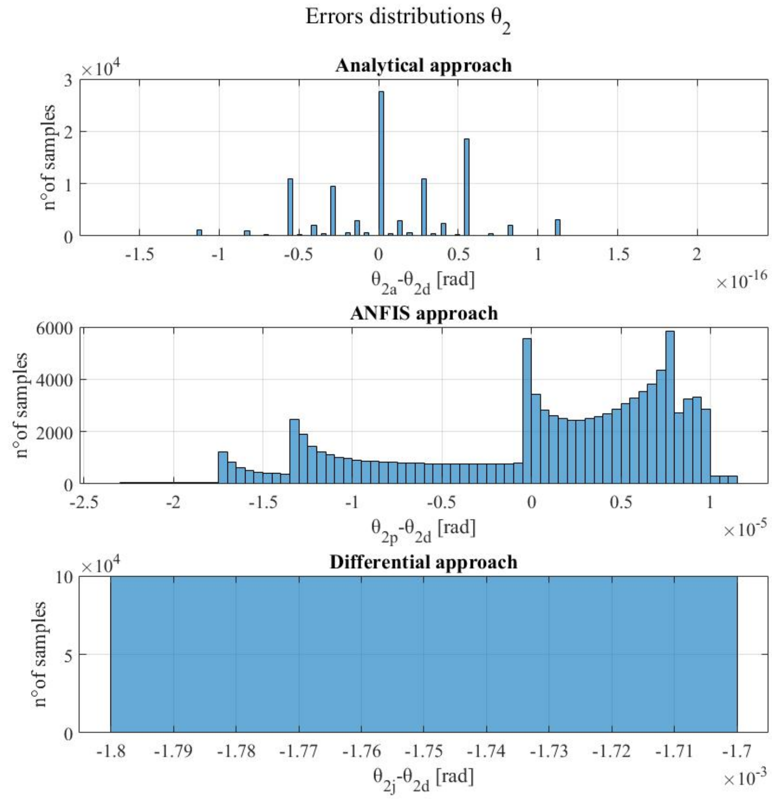

Figure 3.29: Absolute errors distributions, for the 2dof test bench system, for the computation of θ_2 through the analytical, the ANFIS and the differential approaches.

Even if the ANFIS error is larger than the ones of the analytic and differential approaches, its entity is sufficiently small to make the performances of this method comparable and competitive with the other methods.

3.2.3 Results of the real time test at the 2dof test bench

The actuators mounted at the test bench and controlled by EPOS motor drivers have been tested real-time tanks to Speedgoat real time target machine. Offline it has been defined a desired trajectory to be performed by the end-effector inside the cartesian space (Figure 3.30) The Simulink model described in Section 2.38, has as input the pose of the end-effector. The model is uploaded on the real time target machine, then once the EPOS have been enabled and set, the test can be started.

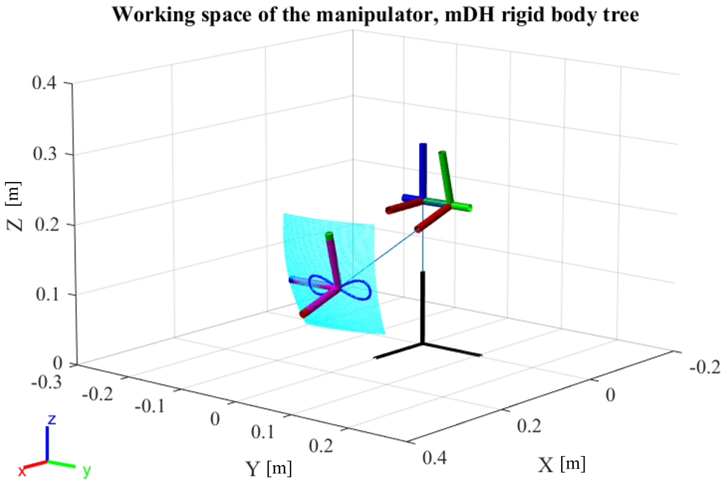

Figure 3.30: Three-dimensional representation of the target trajectory inside the cloud point. The 2dof manipulator starts to perform the trajectory from the configuration shown by the rigid body tree scheme.

The inverse kinematic is computed online with one of the possible methods, the angles computed are elaborated to fit the EPOS range (from one mechanical stop that is the zero reference to the other mechanical stop) and converted in Ticks unit.

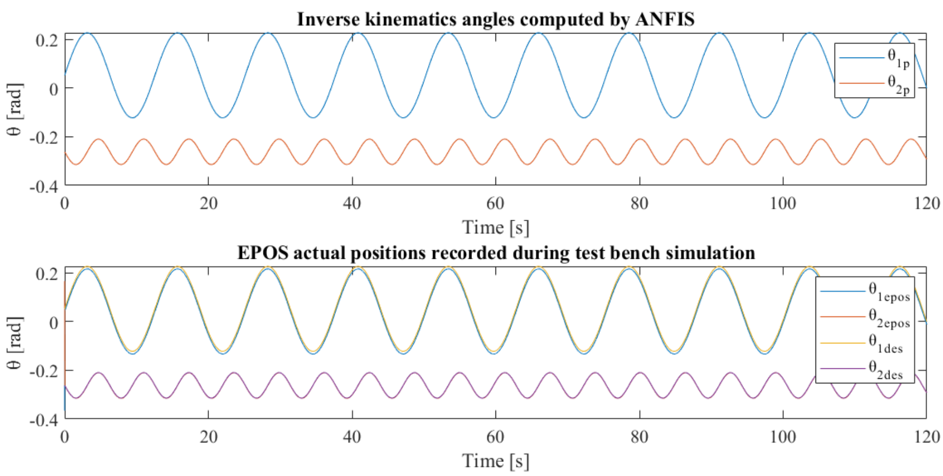

Figure 3.31: Real-time simulations results comparison, θ_1 and θ_2 computed by ANFIS ik, EPOS elaborated signals and target angles.

From the EPOS are recorded the information in Ticks about the actual position of the actuators, these measures can be transformed again to be compatible with the ranges defined with the DH convection. After the elaboration of the data read by the EPOS it is possible to verify that the position control is effectively reproducing the angles computed by the inverse kinematics, ANFIS method was adopted. In *Figure 3.31* are shown the ANFIS on-line computed angles, the angles registered by the EPOS and the target angles. The target angles are defined a priory and inside the allowed ranges, then with their values the desired trajectory is computed, thus by comparing these reference angles with the ones read by the EPOS it can be proved that the ANFIS online inverse kinematic is working in the proper way.

3.3 Three degrees of freedom systems study

3.3.1 Validation of the cloud point through Vicon motion capture acquisitions

The Vicon motion capture system has been used to acquire the spatial position of the end-effector while performing a certain movement. The data has been collected and then elaborated and imported inside Matlab. Since all the measurements acquired are referred to a reference frame defined by the calibration instrument, the data needs to be elaborated and then referred to the desired reference base frame. During the movement of the robot, while acquiring the end-effector motion via Vicon, also the AksIm data have been recorded. The encoders data have been filtered and imported inside Matlab, then with the direct kinematics formulas the Cartesian coordinates and orientations have been computed to obtain the pose inside the manipulator working space. The data computed with the direct kinematics that belongs to the theoretically computed cloud point, have been compared with the position acquired with Vicon system.

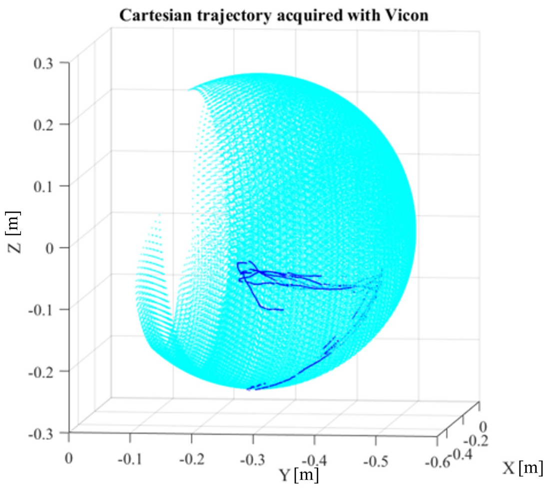

Figure 3.32: Comparison between data acquired with Vicon motion capture system and data computed with the direct kinematics from the displacement measurements provided by encoders. Test used to validate the working space of the 3dof manipulator. The data acquired with Vicon fit the theoretically computed cloud point.

The results show that the data acquired with Vicon system fit the theoretically computed cloud point. The errors that affects the results are due to imprecision during the markers placement, due to the fact that markers have a physical dimension that affect the position of the reference that results shifted with respect to the position of the theoretically defined ones. Moreover, while moving the manipulator it happened that some markers were not continuously recognized so this is another source of error. Even if experimental errors, mainly due to missing data points, affect the measurements, the Vicon acquisition system resulted a good validation instrument.

3.3.2 Study of the inverse kinematic with ANFIS joint variables evaluation

The study of the inverse kinematics for the 3dof system has been done by exploiting ANFIS prediction capabilities. The objective of the study was to make the manipulator reproduce two physiological rehabilitative movements: abduction and flexion (Figure 3.33).

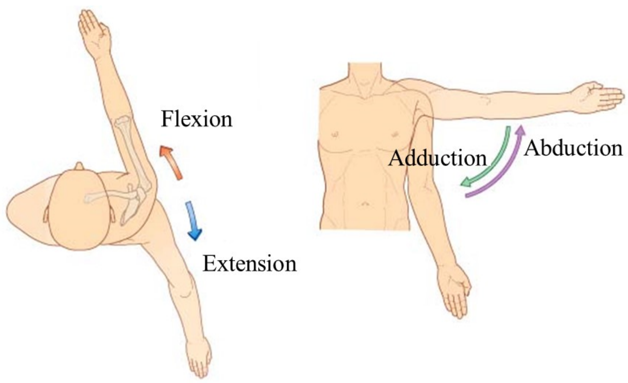

Figure 3.33: Movements of the shoulder joint: flexion and abduction.

The study of the desired trajectory has been done thanks to the support of a physiotherapist. During a passive mode the exoskeleton has been moved to perform the desired rehabilitative exercises, the data provided by the AksIM encoders have been recorded. The obtained data have been translated exploiting the direct kinematics formulas into a Cartesian pose. Thanks to the validation done with the Vicon system, a possible development is the acquisition of the pose during a Vicon motion capture section and the usage of these data as input to the inverse kinematic.
ANFIS networks have been trained on a data-set composed of the Cartesian coordinates, the three spatial orientations and the corresponding joint variable. Two different joint set variable have been used to train the different networks, one set made of more points nearest one with respect to the other (bds=bigger data set), the other set with less, more spaced data (sds=smaller data set).

Abduction trajectory

Once the abduction trajectory has been defined inside the Cartesian space, four different ANFIS networks have been trained and tested for the prediction of the necessary joints variables. ANFIS were trained on the smaller and on the larger data set and with two membership functions and the epoch number set to 250 or 350. The predicted resulting angles are shown in *Figure 3.34* where it is possible to qualitative analyze the behaviour of the predicted data with respect to the target trajectory (that is available since acquired from encoders).

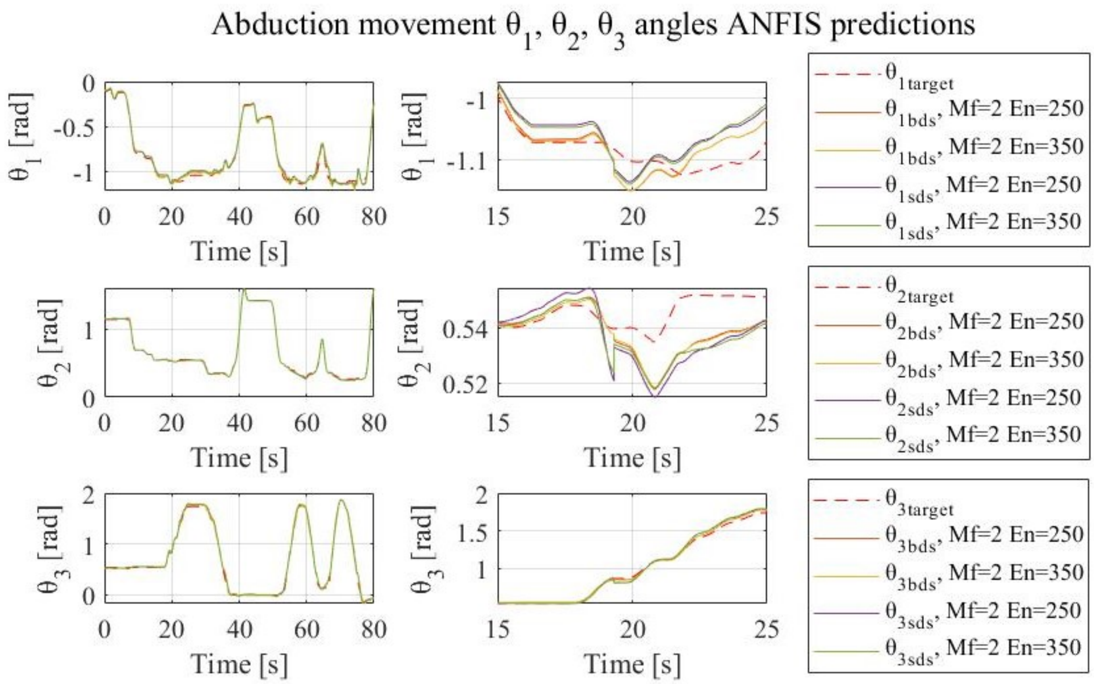

Figure 3.34: ANFIS evaluation: qualitative comparison for the ANFIS prediction of the joints variables to perform the abduction movement. Four ANFIS are compared for the prediction of each joint variable, ANFIS trained on a bigger data set (bds) and on a smaller one (sds), the training is done with 2 membership functions and the epoch number set to 250 or 350.

The absolute errors that affect the ANFIS prediction of the three joints variables have been analyzed. The errors distributions are reported in *Figure 3.35*. It is possible to notice that the ANFISs trained on the larger cloud point allow to map with an higher precision the input to the output, thus the errors are lower. Anyway the errors of the prediction made with the ANFIS trained on the smaller cloud point are not significantly worse than the others, moreover the ANFIS prediction power in this case is better utilized because ANFIS can correctly predict the values without having a wider data set that risks to make the computation based more a on a decision-tree approach than on a predictive one, also the computational cost is significantly reduced. For these reasons, it has been decided to use the ANFIS trained on the smaller cloud point (Mf=2, En=350) for the online computation of the joints variables.

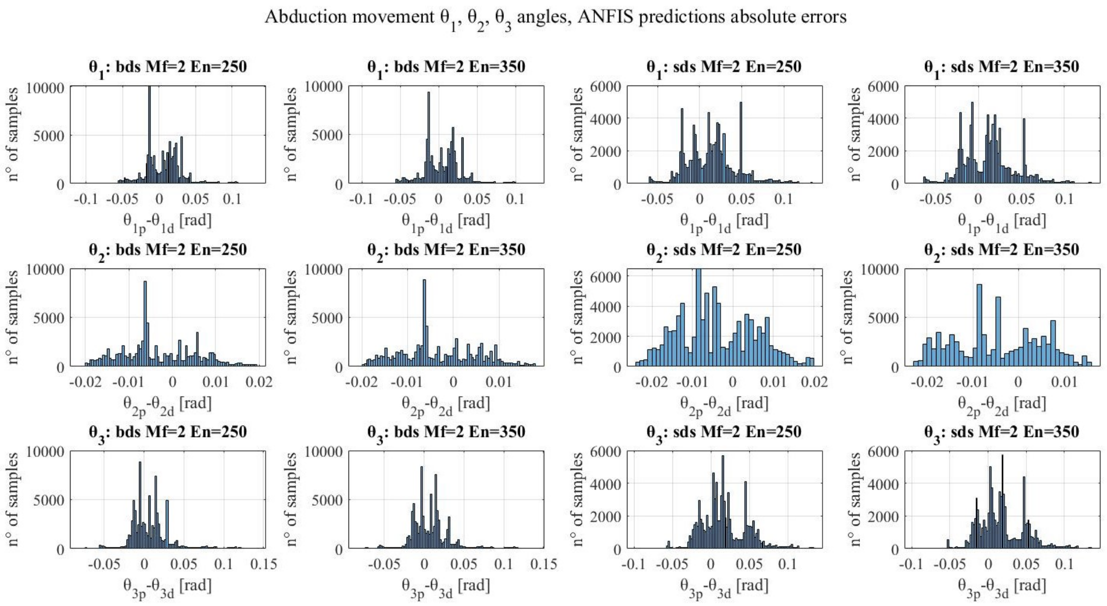

Figure 3.35: Errors distribution for the prediction of the joints variables for the abduction trajectory. Comparison between the different ANFIS.

An evaluation of the RMSEs for the Cartesian coordinates of the end-effector, is reported in *Figure 3.36*, the coordinates are computed starting from the ANFIS predicted joints variables by exploiting the direct kinematics formulas. The obtained trajectory is also qualitatively compared with the target one and showed in *Figure 3.37*, the set of reachable points is plotted and the rigid-body-tree represented in the configuration that corresponds to the starting position to perform the trajectory.

Abduction trajectory test: ANFIS errors on Cartesian coordinates evaluation				
	Smaller training data set		Larger training data set	
	Mf=2 En=250	Mf=2 En=350	Mf=2 En=250	Mf=2 En=350
x RMSE [m]	0.0022	0.0022	0.0019	0.0018
y RMSE [m]	0.0029	0.0031	0.0026	0.0025
z RMSE [m]	0.0039	0.0036	0.0026	0.0028

Figure 3.36: RMSEs for the computation of the Cartesian coordinates, for the abduction trajectory, computed with the direct kinematics formulas with the ANFIS predicted angles. ANFIS resulted to be a valid method to compute the inverse kinematics, the errors done for the end-effector position are acceptable for the wanted application.

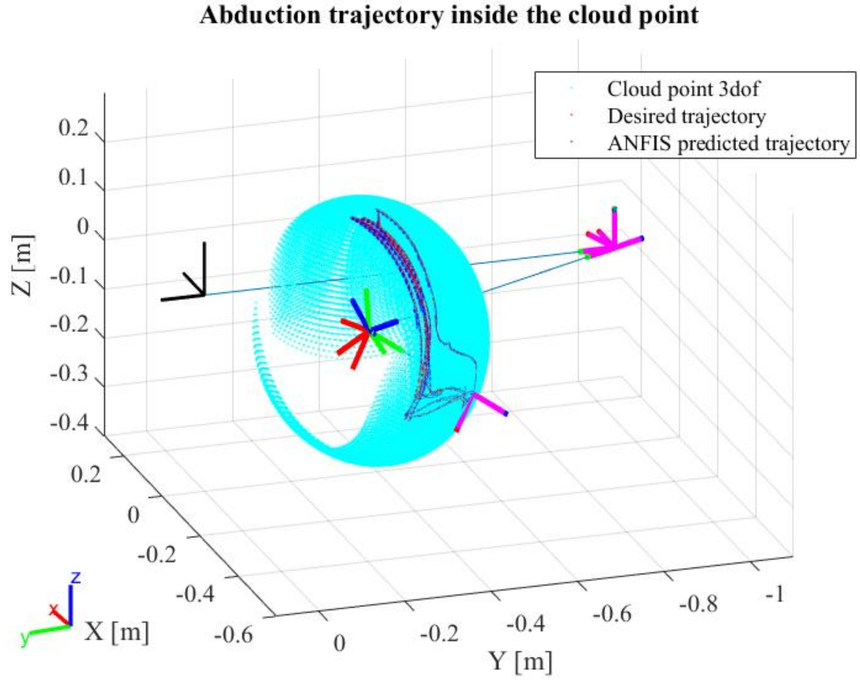

Figure 3.37: Target trajectory and ANFIS predicted abduction trajectory comparison. Set of reachable points and rigid-body-tree representation in the starting position to perform the trajectory. ANFIS training data: sds, Mf=2, En=350

It has been noticed that the values predicted by the ANFIS sometimes present discontinuities which can cause an instant changing of actuator rotation direction. This condition results in sudden fast movements of the actuators, such a behaviour is not acceptable during rehabilitative exercises. In order to avoid that dangerous behaviour it has been implemented a moving average filter that is able, by mediating the signals collected in a predefined window, to delete the presence of discontinuities. A trade off must be reached between the window length of the filter, the allowed delay and the modulation of the signal to obtain a delayed signal that maintains the same amplitude and that does not result to be excessively modified in the shape. It has been chosen a window length of 900 samples (0.9 seconds) to obtain the described features. The filter is applied to the output of the inverse kinematics block. The filtered signals, compared with the original ones, for the abduction are reported in *Figure 3.38*.

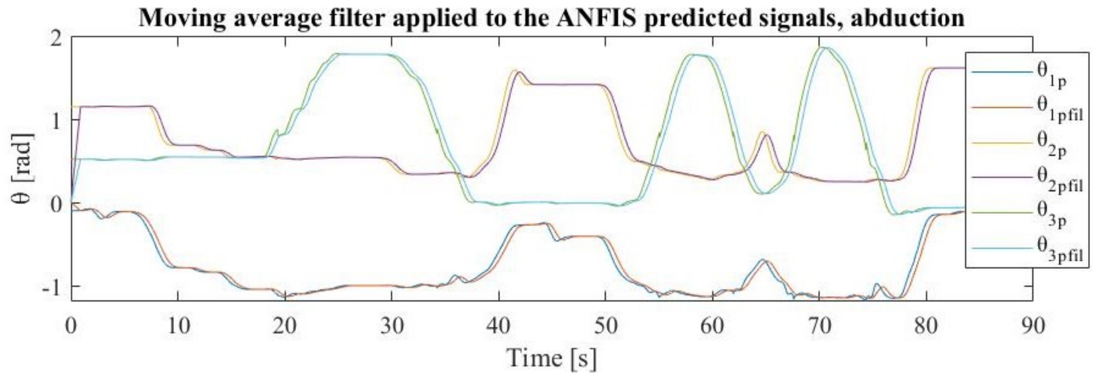

Figure 3.38: Abduction trajectory: comparison between the joint variables signals predicted by ANFIS and the same signals filtered with a moving average filter (window length of the filter set to 900 samples), the discontinuities of the signals can be deleted by the filter, the effect is a smoothing of the signal and the introduction of a delay.

Flexion trajectory

Once the flexion trajectory has been defined inside the Cartesian space, four different ANFIS networks have been trained and tested for the prediction of the necessary joints variables. As for the abduction the training of the networks has been done on a sds or on a bds an with Mf=2 and En=250 or En=350. The qualitative evaluations of the resulting predicted angles are shown in *Figure 3.39*.

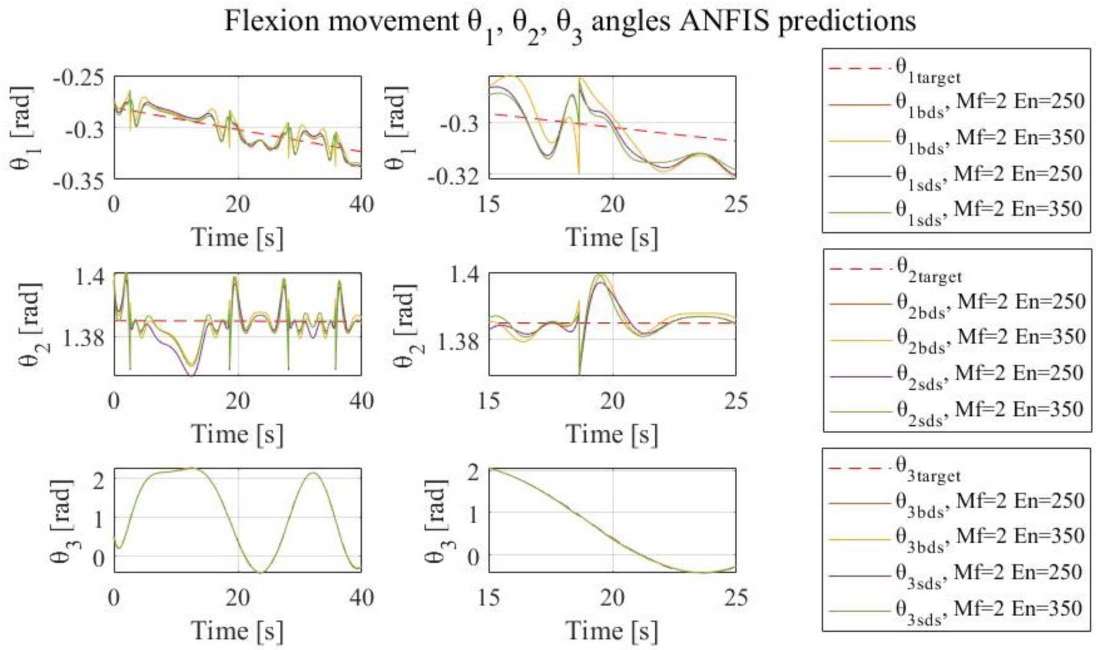

Figure 3.39: ANFIS evaluation: qualitative comparison for the ANFIS prediction of the joints variables to perform the flexion movement. Four ANFIS are compared for the prediction of each joint variable, ANFIS trained on a bigger data set (bds) and on a smaller one (sds), the training is done with 2 membership functions and the epoch number set to 250 or 350.

The absolute errors distributions in predicting the joints variables are reported in *Figure 3.40*.

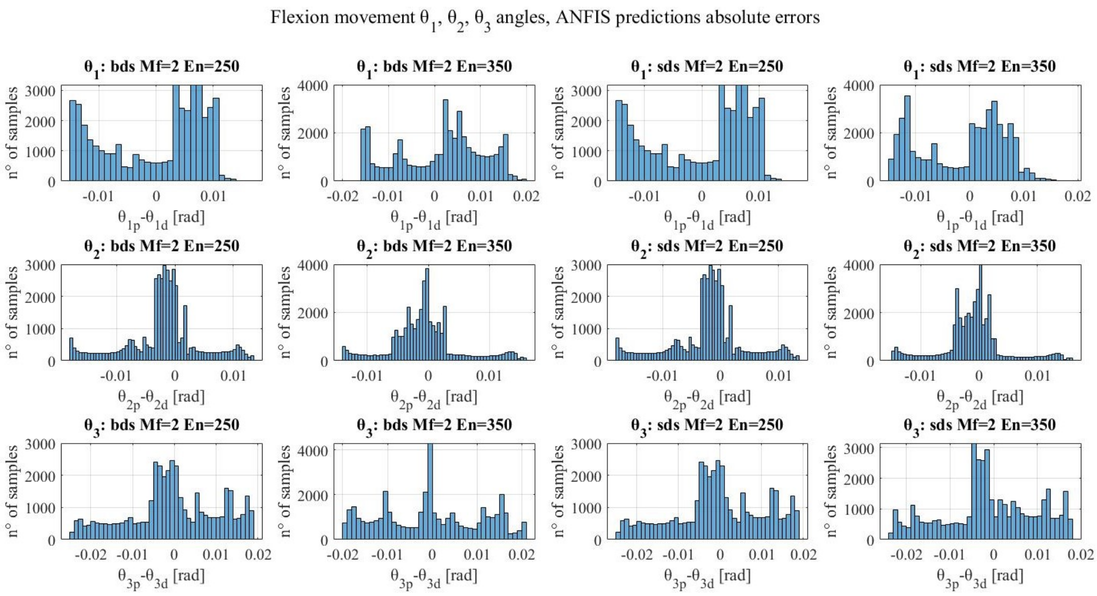

Figure 3.40: Errors distribution for the prediction of the joints variables for the flexion trajectory. Comparison between the different ANFIS.

The evaluation of the RMSEs (Figure 3.41) for the Cartesian coordinates of the end-effector is reported. The obtained trajectory is qualitatively compared with the target one in *Figure 3.42*, moreover it is shown the set of reachable points and the rigid-body-tree represented in the configuration that corresponds to the starting position to perform the flexion trajectory.

Flexion trajectory test: ANFIS errors on Cartesian coordinates evaluation				
	Smaller training data set		Larger training data set	
	Mf=2 En=250	Mf=2 En=350	Mf=2 En=250	Mf=2 En=350
x RMSE [m]	0.0020	0.0015	0.0020	0.0019
y RMSE [m]	0.0017	0.0017	0.0017	0.0020
z RMSE [m]	0.0024	0.0022	0.0024	0.0024

Figure 3.41: RMSEs for the computation of the Cartesian coordinates, for the flexion trajectory. The errors done for the end-effector position are acceptable for the wanted application.

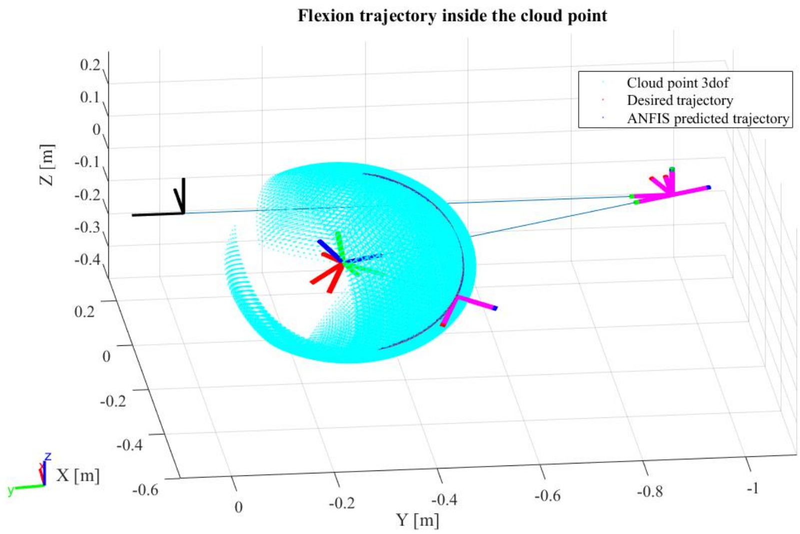

Figure 3.42: Target trajectory and ANFIS predicted flexion trajectory comparison. Set of reachable points and rigid-body-tree representation in the starting position to perform the trajectory. ANFIS training data: sds, Mf=2, En=350

In order to avoid the discontinuity problem, described in *Section 3.3.2*, the output of the inverse kinematics computed with ANFIS is fileterd with a moving average filter (window length of 900 samples (0.9 seconds)). The filtered signals, compared with the original ones, for the flexion are reported in *Figure 3.43*.

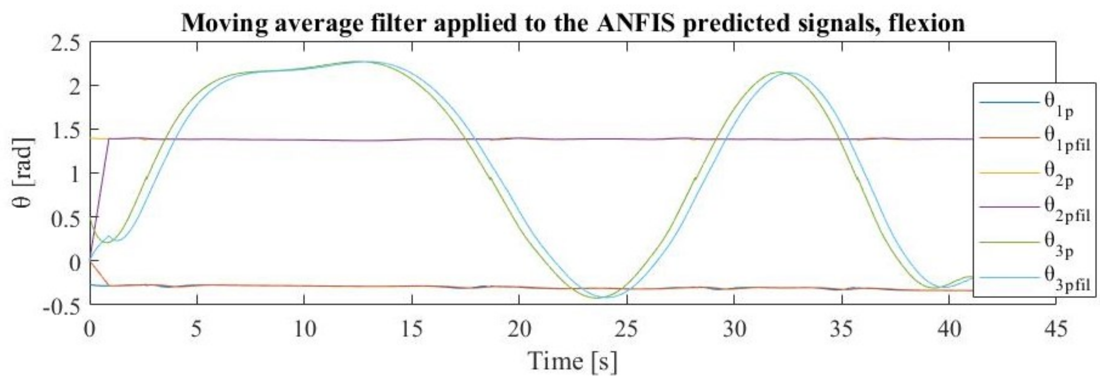

Figure 3.43: Flexion trajectory: comparison between the joint variables signals predicted by ANFIS and the same signals filtered with a moving average filter (window length of the filter set to 900 samples), the discontinuities of the signals can be deleted by the filter, the effect is a smoothing of the signal and the introduction of a delay.

3.4 Three degrees of freedom system admittance control, real time simulations results

The implemented admittance controls have been real time tested on the 3dof structure connected to Speedgoat real time target machine. The presented results have been recorded during a real time test while a human-machine interaction was performed. The manipulator was manually moved, so an external torque applied to the manipulator, this torque was provided as input to the admittance control and elaborated by the transfer function (it describes the dynamic of the model, viscous for the first implementation and viscous-elastic for the second developed controller) to obtain the dynamic position contribute (Section 2.1.4). The performed test have been done by settings the desired end-effector pose fixed to one point inside the space, thus the joint variables computed with the inverse kinematics are constant.

Admittance control: pure viscous behaviour

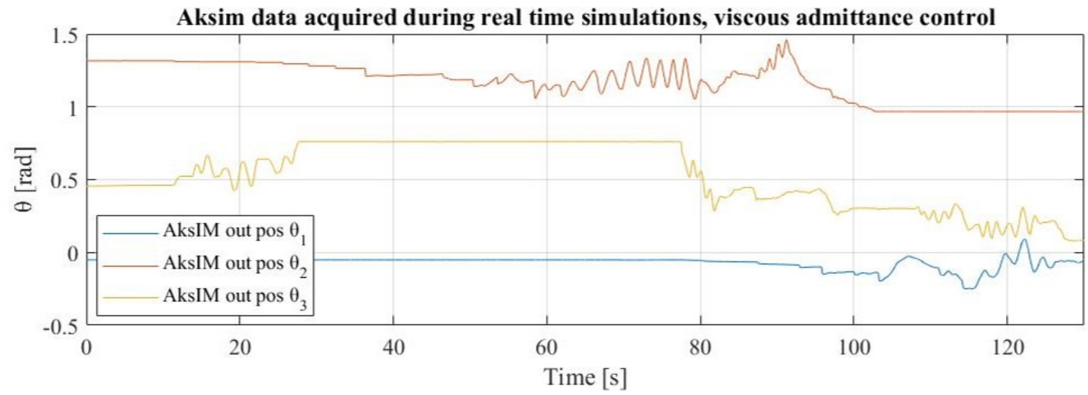

Figure 3.44: Viscous admittance control: AksIM data recorded during a human-robot interaction. Thanks to the admittance the system can be moved away from the target position, the user experiences a compliant behaviour of the manipulator. Since there is no component that brings the system back to the original target position, when the interaction is ended the system maintains its actual position.

The admittance control has been implemented to make the system behaves like a damper, it is possible to see in *Figure 3.44* that even if the target position was set to a fixed point, there are oscillations of the encoders readings, around the target positions, due to the interaction with the user. The user was manually moving the manipulator, in fact the admittance control allows to move away from the target position the manipulator. When the interaction stops the manipulator remains in the last position since there is any component that brings the system back to the original target position. The value of the damping coefficients for the three admittance controllers (one for each actuator) have been experimentally decided by varying from the GUI the values and testing the system response during a user-machine interaction. For the showed results $\beta_1 = \beta_2 = \beta_3 = 20\frac{Nm*s}{rad}$.

Admittance control: viscous-elastic behaviour

The dynamic of the system is modeled as a damper-spring system. The implementation of an elastic element allows to obtain the coming back to the target position of the manipulator after the human-robot interaction is ended. The torques estimated from the SEAs compliant elements are composed of two contributes, the fixed torque due to the structural construction and weight of the mechatronic structure and the contribute applied by the user during the interaction with the manipulator, the latter is used by the admittance control to compute the dynamic position contribute. The system has been tested with an applied load of mass $m = 3kg$ to simulate the upper limb weight and see the system response in a condition close to the real application where the impaired limb of the patient is inside the structure. The AksIM recorded data are reported (Figure 3.45), the reference signal is the one computed by the inverse kinematic, from the recorded AksIM data it is possible to notice that every time the system sense an external torque contribute, the system is moved away from the target position and then brought back to the desired position thanks to the behaviour assigned by the presence of the elastic element in the dynamic model. The value of the damping coefficients and of the springs stiffness for the three admittance controllers (one for each actuator) have been experimentally decided by real time varying, from the GUI, the values and testing the system response during a user-machine interaction.
For the showed results the parameters:

$$\beta_1 = \beta_2 = 15\frac{Nm*s}{rad}, \beta_3 = 10\frac{Nm*s}{rad}, k_1 = 10\frac{Nm}{rad}, k_2 = 15\frac{Nm}{rad}, k_3 = 16\frac{Nm}{rad}$$

has been chosen as value to obtain the desired compliant behaviour of the manipulator.

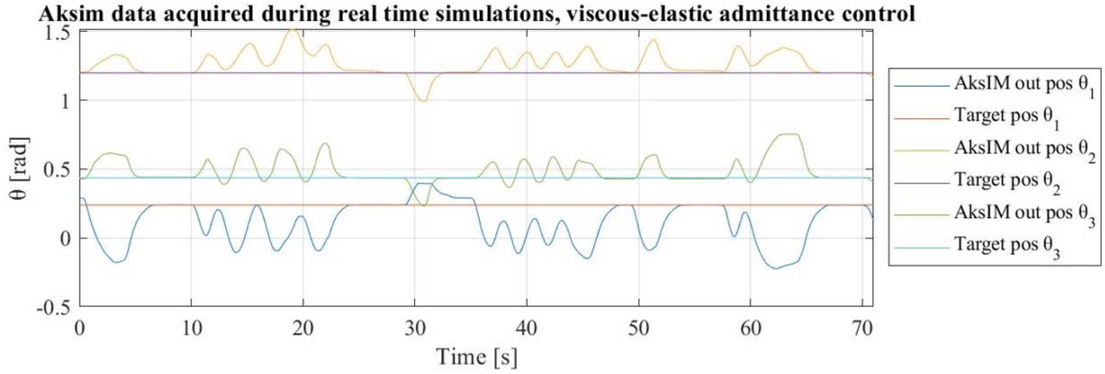

Figure 3.45: Viscous-elastic admittance control: AksIM data recorded during a human-robot interaction, comparison with the constant reference positions computed by the inverse kinematics. Thanks to the admittance the system can be moved away from the target position, the user experiences a compliant behaviour of the manipulator and then he/she can be driven back to the target position thanks to the elastic behaviour.

The implemented admittance control allows to make the robot behaves in a compliant way when the user applies an external torque to the structure. The potentiality of the sensorized joints are exploited and it was confirmed that their implementation for rehabilitative applications is ideal to guarantee an appropriate patient-robot interface interaction.

Chapter 4

Discussion and conclusion

The aim of the presented thesis was the analysis of the main mechatronic aspects of an exoskeleton design: the study of the actuation system, of the kinematic chain and the design of the control strategy.

4.1 Actuation system analysis

During the first study phase, the electromechanic actuation system has been studied (Section 2.3.2), the SEAs system components have been analyzed and a Simulink-Simscape model of the joint has been developed (Section 2.5.2). The purpose of the design of a simulation environment is dual, it allows to save time in testing the device and it makes it possible to avoid a damage to the mechanical components. The model resulted to be efficient in reproducing the SEA behaviour under different working condition, the validation of the model has been done thanks to a comparison between the data obtained from real-time testing of the actuators and data obtained by the simulation of the developed model (Section 3.1.3). To configure the connection and the communication between the actuator servomotor controllers, the encoders and Speedgoat real time target machine both a Simulink model and a graphic user interface have been developed (Section 2.5.1).
The SEAs have been tested and analyzed in order to study the characteristics of the elastic elements (custom torsional springs) the analysis purpose was both the study of the frequency behaviour of the components and of the element mechanical characteristics. Data relative to the sensor hysteresis (Section 3.1.2) and relative to the compliant element stiffness evaluation (Section 3.1.2) have been collected.

4.2 Kinematic analysis of 2dof and 3dof structures

The characterized joints were assembled to obtain two systems, the first was a two degrees on freedom structure while the other a three degrees of freedom kinematic chain. The systems direct and inverse kinematics have been studied. The 2dof structure corresponds to the human body scapular joint, it will be part of the FloatEVO exoskeleton and mimics the human scapulohumeral rhythm which is the kinematic interaction between the scapula and the humerus. The inverse kinematic of the system has been studied with three different methods: analytical, differential and ANFIS based approaches (Section 2.6). The 3dof structure joints are dedicated to perform movements for the rehabilitation of the glenohumeral joint, the inverse kinematic has been computed with the ANFIS based approach (Section 2.7). Both the structures have been studied both offline by implementing MATLAB codes and Simulink models. Then, online testing has been done by developing Simulink models deployed on Speedgoat real time target machine, controlled with a dedicated GUI, that communicates with the motor drivers and collect the desired data (Section 2.6.7, Section 2.7.4). By exploiting the position control of the motor drivers it was possible to make the robotic structure perform a desired trajectory, a pose reference was provided to the system, an online inverse kinematics computation allowed to estimate the necessary joints configurations to obtain the desired end-effector position inside the Cartesian space (Section 3.2.1, Section 3.2.2, Section 3.3.2). From the analysis results, the unconventional ANFIS based inverse kinematics solution resulted to be competitive with the traditional ones, with the advantage that it does not need the analytical computation of the inverse kinematics equations that is one of the limits of the analytical approach that can be used only if the problem has a precise solution. The study of different training data sets and training options has shown that the precision of the predictor capability of ANFIS can be modulated to find a tradeoff between an accurate enough solution and a not excessively heavy computational cost (Section 3.2.1, Section 3.2.2, Section 3.3.2). Further studies can be done to explore the potentiality of the neural networks in inverse kinematics applications, different training options or the definition of networks based on different decisions algorithms could be tested to understand the limits and the advantages of this unconventional approach. The analysis of the 3dof structure with Vicon motion capture systems (Section 3.3.1) has been used as validation method to confirm the correctness of the analytically computed manipulator working space.

4.3 Admittance control

Exoskeletons used for rehabilitation purposes must be able to guarantee a safe human-robot interaction. The implementation of SEAs makes available measurements that can be used to quantitatively estimate the interface forces and torques. By evaluating the torques sensed by the sensorized elements, thanks to the implementation of a control, it is possible to make the system behave in a desired way when an external torque is applied from the patient to the structure. By doing so, it becomes possible to treat situations like spastic movements or the occurrence of limb resistance while performing a task and to make the system able to adequately response to these situations, avoiding to hurt the patient and making the user experience a compliant response of the exoskeletons. An admittance control has been developed to accomplish the desired requirements. The dynamic of the system has been modeled in the first admittance filter implementation, as a damper, thus a pure viscous behaviour was obtained. The model of the admittance controller has been developed in Simulink and then implemented inside the model uploadable on Speedgoat (Section 2.7.5 and Figure 2.49). The experimental tests (performed in real-time connecting the 3dof structure to Speedgoat) have shown that during a human-robot interaction, when an external torque is sensed, the system can be moved away from the target position following the patient movement (Section 3.4), viscous behaviour can be modulated by changing the viscosity coefficient of the virtual damper.
Another admittance control has been implemented, making the dynamic of the system equal to the one of a spring-damper system (Section 2.7.5 and Figure 2.50). By introducing an elastic component, once the system is moved away from the target position, it is also possible to modulate the return movement to the desired reference by changing the virtual spring stiffness characteristic (Section 3.4).

4.4 Conclusion

Exoskeleton mediated rehabilitation can become a powerful instrument to improve the rehabilitation therapy outcome, the focus point of all the performed studies and analysis is the interaction of the structure with the patient. The aim of the presented thesis was the analysis of the main mechatronic aspects of an exoskeleton design: the study of the actuation system, the analysis of the kinematic chain and the implementation of a control strategy. During the first part of the project the actuation system of the exoskeleton has been analyzed, both testing and modelling aspects have been considered. The SEAs compliant elements characteristics have been analyzed by real-time testing the joints under different load conditions, then, the acquired data have been elaborated to obtain the frequency analysis

and to compute the elastic characteristics of the tested compliant elements. A Simulink model of the SEA has been implemented in Simulink and Simscape, after the components characterization, the model resulted able to reproduce the SEA attitude. The second part of the thesis focused on the kinematic study of 2dof and 3dof manipulators, the analysis of an unconventional Fuzzy-Logic based method, used to solve the inverse kinematics problems, resulted to be a useful and effective tool comparable with the traditional methods. The kinematic chains have been studied inside Matlab and Simulink. After the inverse kinematics computation, by deploying a Simulink developed model on Speedgoat real time target machine, it was possible to made the test benches follow desired trajectories exploiting the position control performed by the servo motor controllers.
Exoskeletons used for rehabilitation purposes must be able to guarantee a safe human-robot interaction. The implementation of SEAs allows to access interesting measurements that can be used to quantitatively estimate the forces and torques at the interface. The design of an admittance control allowed to make the 3dof system to behave in a desired way when an external torque is applied from the patient to the structure, two dynamics models have been implemented: pure viscous and viscous-elastic. The control strategies have been real time tested on Speedgoat, the resulting behaviours during the interaction with a user were: the possibility to move the robot away from the target position following the patient movements and the capability of the system to return back to the reference position.
Considering the conducted analysis it is possible to conclude that the presented sensorized actuation system (SEA), resulted to be able to provide an effective torque measurement that allows to take into account the presence of a human inside the structure, resulting a valid design choice considering the rehabilitative purpose of the analysed exoskeleton. The performed kinematic analysis, could be useful in further studies in order to understand if the mechatronic structure well adapts to the human body, allowing a correct alignment between the physiological joints, and the exoskeleton ones. Moreover, the study of the working space of the manipulator can be of interest to understand which are the possible configurations that causes a collision between the patient and the machine. Once the critical configurations have been identified different strategies can be adopted to avoid these conditions. The control strategy makes it possible to obtain a safer interaction for the patient and an adequate support during the exercises. By implementing the described admittance control it becomes possible to treat situations like spastic movements or the occurrence of limb resistance while performing a task and to make the system able to response to these situations avoiding hurting the patient. A further study can be done to implement a variable admittance control where the viscous and elastic characteristics can assume different values depending on the ongoing exercise. This development could be useful to realize an optimal support to the patient, that depending on the exercise and on the phase of the movement must

be helped and supported in different ways. The implementation of a "record and reply" strategies in combination with a variable admittance control can allow to acquire the joints angles data to be reproduced and then reproduce the trajectory with a compliant reply. All the reported design aspects, studies and the proposed developments aim to obtain an improved outcome of the rehabilitation session.

Bibliography

[1] World Health Organization Website. URL: https://www.who.int (cit. on p. 1).

[2] Minitero della Salute. URL: https://www.salute.gov.it/portale/salute/p1_5.jsp?id=28&area=Malattie_cardiovascolari (cit. on p. 1).

[3] American Stroke Association. URL: https://www.stroke.org/en (cit. on p. 1).

[4] Sveen U., Bautz-Holter E., Sodring K.M., Wyller T.G., and Laake K. «Association between impairments, self-care ability and social activities 1 year after stroke.» In: *Disability and Rehabilitation* 21(8) (1999), pp. 372–377 (cit. on p. 1).

[5] Pollock A., Farmer S.E., Brady M.C., Langhorne P., Mead G.E., Mehrholz J., and van Wijck F. «Interventions for improving upper limb function after stroke». In: *Cochrane Database of Systematic Reviews* 11 (2014) (cit. on pp. 1, 2).

[6] Maciejasz P., Eschweiler J., Gerlach-Hahn K., Jansen-Troy A., and Leonhardt S. «A survey on robotic devices for upper limb rehabilitation». In: *Journal of NeuroEngineering and Rehabilitation* 11(3) (2014) (cit. on pp. 2–4, 6).

[7] Brokaw E.B., Murray T., Nef T., and Lum P.S. «Retraining of interjoint arm coordination after stroke using robot-assisted time-independent functional training.» In: *J Rehabil Res Dev.* 48(4) (Nov. 2011), pp. 299–316 (cit. on p. 2).

[8] Bosch J., O'Donnell M.J., Barreca S., Thabane L, and Wishart L. «Does Task-Oriented Practice Improve Upper Extremity Motor Recovery after Stroke? A Systematic Review». In: *International Scholarly Research Notices* (2014) (cit. on p. 2).

[9] Bobath B. *Adult Hemiplegia: Evaluation and Treatment. 2nd Edition.* London: Butterworth-Heinemann, 1990 (cit. on p. 2).

[10] Niyetkaliyev A. S., Hussain S., Ghayesh M.H., and Alici Gursel. «Review on Design and Control Aspects of Robotic Shoulder Rehabilitation Orthoses». In: *IEEE TRANSACTIONS ON HUMAN-MACHINE SYSTEMS* 47(6) (Dec. 2017), pp. 1134–1145 (cit. on pp. 2, 3, 6).

[11] Proietti T., Crocher V., Roby-Brami A., and Jarrasse N. «Upper-Limb Robotic Exoskeletons for Neurorehabilitation: A Review on Control Strategies.» In: *IEEE Rev Biomed Eng.* 9 (Apr. 2016), pp. 4–14 (cit. on pp. 2, 4–8).

[12] Hongjun H., Deyu Y., Fuqiang L., Iei W., and Jinhao S. «A Review of the Control Solution for Rehabilitation Robot». In: *Proceedings of the 12th International Convention on Rehabilitation Engineering and Assistive Technology* (2018), pp. 259–262 (cit. on p. 2).

[13] Islam Md R., Spiewak C., Rahman M., and Fareh R. «A Brief Review on Robotic Exoskeletons for Upper Extremity Rehabilitation to Find the Gap between Research Prototype and Commercial Type.» In: *Advances in Robotics and Automation* 6 (Jan. 2017) (cit. on pp. 3, 4).

[14] Piggott L. and Ziat M. «Haptic Neurorehabilitation and Virtual Reality for Upper Limb Paralysis: A Review». In: *Critical Reviews in Biomedical Engineering* 44(1-2) (Jan. 2016), pp. 1–32 (cit. on p. 3).

[15] Gopura R.A.R.C. and Kiguchi K. «Mechanical designs of active upper-limb exoskeleton robots: State-of-the-art and design difficulties». In: *IEEE 11th International Conference on Rehabilitation Robotics Kyoto International Conference Center* (July 2009), pp. 178–187 (cit. on p. 3).

[16] Otten A., Voort C., Stienen A., Aarts R., van Asseldonk E., and van der Kooij H. «LIMPACT:A Hydraulically Powered Self-Aligning Upper Limb Exoskeleton». In: *IEEE/ASME transactions on mechatronics* 20(5) (2015), pp. 2285–2298 (cit. on p. 3).

[17] Rehmat N., Zuo J., Meng W., Liu Q., Xie S., and Liang H. «Upper limb rehabilitation using robotic exoskeleton systems: a systematic review». In: *International Journal of Intelligent Robotics and Applications* 2(3) (Sept. 2018), pp. 283–295 (cit. on p. 3).

[18] Gopura R.A.R.C. and Bandara D.S.V. «A brief review on upper extremity robotic exoskeleton systems». In: *6th International Conference on Industrial and Information Systems* (Aug. 2011) (cit. on p. 3).

[19] Varghese R.J., Freer D., Deligianni F., Liu J., and Yang G-Z. «Wearable Robotics for Upper-Limb Rehabilitation and Assistance: A Review of the State-of-the-Art, Challenges, and Future Research». In: *Wearable Technology in Medicine and Health Care.* (Jan. 2018), pp. 23–69 (cit. on pp. 3, 6).

[20] Shen Y., Ferguson W. P., and Rosen J. «UPPER LIMB EXOSKELETON SYSTEMS—OVERVIEW». In: *Wearable Robotics* (2020) (cit. on p. 3).

[21] Gull M. A., Bai S., and Bak T. «A Review on Design of Upper Limb Exoskeletons». In: *Robotics* 9(1) (2020) (cit. on pp. 5, 6).

[22] Ren Y., Kang S.H., Park H.S., Wu Y.N., and Zhang L. «Developing a Multi-Joint Upper Limb Exoskeleton Robot for Diagnosis, Therapy, and Outcome Evaluation in Neurorehabilitation». In: *IEEE Transactions on Neural Systems and Rehabilitation Engineering* 21 (May 2013), pp. 490–499 (cit. on p. 6).

[23] Molteni F., Gasperini G., Cannaviello G., and Guanziroli E. «Exoskeleton and End-Effector Robots for Upper and Lower Limbs Rehabilitation: Narrative Review». In: *PMandR* 10 (Sept. 2018), S174–S188 (cit. on p. 6).

[24] Kim H., Miller L.M., Fedulow I., Simkins M., Abrams G.M., Byl N., and Rosen J. «Kinematic data analysis for post-stroke patients following bilateral versus unilateral rehabilitation with an upper limb wearable robotic system.» In: *IEEE Trans Neural Syst Rehabil Eng.* 21(2) (Mar. 2013), pp. 153–164 (cit. on p. 7).

[25] Guidali M., Duschau-Wicke A., Broggi S., Klamroth-Marganska V., Nef T., and Riener R. «A robotic system to train activities of daily living in a virtual environment». In: *Medical and biological engineering and computing* 49(10) (July 2011), pp. 1213–1223 (cit. on p. 7).

[26] Kinetec. URL: `http://www.wearable-robotics.com/kinetek/products/alex/` (cit. on p. 9).

[27] Hocoma. URL: `https://www.hocoma.com/solutions/armeo-power/` (cit. on p. 9).

[28] Harmonicbionics. URL: `https://www.harmonicbionics.com/about` (cit. on p. 9).

[29] Pirondini E. and al. «Evaluation of a New Exoskeleton for Upper Limb Post-stroke Neuro-rehabilitation: Preliminary Results.» In: *Jensen W., Andersen O., Akay M. (eds) Replace, Repair, Restore, Relieve – Bridging Clinical and Engineering Solutions in Neurorehabilitation. Biosystems and Biorobotics.* 7 (2014), pp. 637–645 (cit. on p. 9).

[30] Sicuri C., Porcellini G., and Merolla G. «Robotics in shoulder rehabilitation.» In: *Muscles, ligaments and tendons journal* 4 (Apr. 2014), pp. 207–213 (cit. on p. 9).

[31] Armeo®Power. URL: `https://www.hocoma.com/solutions/armeo-power/technical-data-sheet/` (cit. on p. 9).

[32] Siciliano B., Sciavicco L., Villani L., and Oriolo G. *Robotics modelling planning and control.* Springer London Ltd, 2010 (cit. on pp. 12–21).

[33] Chennakesava Reddy A. «DIFFERENCE BETWEEN DENAVIT - HARTENBERG (D-H) CLASSICAL AND MODIFIED CONVENTIONS FOR FORWARD KINEMATICS OF ROBOTS WITH CASE STUDY». In: *International Conference on Advanced Materials and manufacturing Technologies (AMMT)* (Dec. 2014), pp. 267–286 (cit. on pp. 18, 19).

[34] Tokarz K. and Kieltyka S. «Geometric approach to inverse kinematics for arm manipulator». In: *Proceedings of the 2003 International Conference on Machine Learning and Cybernetics* 1 (July 2010) (cit. on p. 19).

[35] Sariyildiz E., Ucak K., Ohnishi K., Oke G., and Temeltas H. «Intelligent systems based solutions for the kinematics problem of the industrial robot arms». In: *2013 9th Asian Control Conference (ASCC)* (June 2013), pp. 1–6 (cit. on pp. 19, 21).

[36] Dongare A., Kharde R. R., and Kachare A. D. «Introduction to Artificial Neural Networks». In: (2012) (cit. on p. 22).

[37] Armaghani D.J. and Asteris P.G. «A comparative study of ANN and ANFIS models for the prediction of cement-based mortar materials compressive strength». In: *Neural Comput and Applic.* 33 (2021), pp. 4501–4532 (cit. on pp. 22, 24).

[38] Jang J.-S. R. «ANFIS: adaptive-network-based fuzzy inference system». In: *IEEE Transactions on Systems, Man, and Cybernetics* 23(3) (1993), pp. 665–685 (cit. on pp. 22–26).

[39] Chen D.W. and Zhang J.P. «Time series prediction based on ensemble ANFIS.» In: *2005 International Conference on Machine Learning and Cybernetics* (2005), pp. 3552–3556 (cit. on p. 24).

[40] Kamel T.S., Moustafa Hassan M.A., and El-Morshedy A. *Using a Combined Artificial Intelligent Approach In Distance Relay For Transmission Line Protection In EPS.* Sept. 2009, pp. 1–6 (cit. on p. 24).

[41] Rajabi Kuyakhi H. and Tahmasebi-Boldaji R. «A novel ANFIS model to prediction of the density of n-alkane in different operational condition». In: *Petroleum Science and Technology* 37 (Oct. 2019), pp. 1–6 (cit. on p. 24).

[42] Turki M., Bouzaida S., Sakly A., and Faouzi M.S. *Adaptive Control of Nonlinear System Using Neuro-Fuzzy Learning by PSO Algorithm.* Mar. 2012 (cit. on p. 24).

[43] Tarno A. et al. «Adaptive Neuro Fuzzy Inference System (ANFIS) approach for modeling paddy production data in Central Java». In: *Journal of Physics: Conference Series* 1217 (2019) (cit. on p. 25).

[44] Ankarali A. and Cilli M. «ANFIS Inverse Kinematics and Hybrid Control of a Human Leg Gait Model». In: *Academic Platform Journal of Engineering and Science* 1 (Jan. 2013), pp. 34–49 (cit. on p. 26).

[45] Wei L.X., Wang H.R., and Li Y. «A new solution for inverse kinematics of manipulator based on neural network». In: *International Journal of Computers, Communications and Control* 2 (2003), pp. 1201–1203 (cit. on p. 26).

[46] Dembys J., Gao Y., and Desouza G.N. «A Study on Solving the Inverse Kinematics of Serial Robots using Artificial Neural Network and Fuzzy Neural Network». In: *International Journal of Computers, Communications and Control* (June 2019), pp. 1–6 (cit. on p. 26).

[47] Howard D.W. and Zilouchian A. «Application of Fuzzy Logic for the Solution of Inverse Kinematics and Hierarchical Controls of Robotic Manipulators». In: *Journal of Intelligent and Robotic Systems* 23 (Oct. 1998), pp. 217–247 (cit. on p. 26).

[48] Mariotti E., Magrini E., and De Luca A. «Admittance Control for Human-Robot Interaction Using an Industrial Robot Equipped with a F/T Sensor». In: *2019 International Conference on Robotics and Automation (ICRA)* (2019), pp. 6130–6136 (cit. on p. 27).

[49] Keemink A.Q., van der Kooij H., and Stienen A.H. «Admittance control for physical human–robot interaction». In: *The International Journal of Robotics Research* 37(11) (2018), pp. 1421–1444 (cit. on p. 27).

[50] Ott C., Mukherjee R., and Nakamura Y. «Unified Impedance and Admittance Control». In: *2010 IEEE International Conference on Robotics and Automation* (2010), pp. 554–561 (cit. on p. 27).

[51] Anam K. and Al-Jumaily A.A. «Active Exoskeleton Control Systems: State of the Art». In: *Procedia Engineering, International Symposium on Robotics and Intelligent Sensors 2012 (IRIS 2012)* 41 (2012), pp. 988–994 (cit. on p. 27).

[52] Li Z., Huang B., Ye Z., Deng M., and Yang C. «Physical Human–Robot Interaction of a Robotic Exoskeleton By Admittance Control». In: *IEEE Transactions on Industrial Electronics* 65(12) (Dec. 2018), pp. 9614–9624 (cit. on p. 27).

[53] Seraji H. «Adaptive admittance control: an approach to explicit force control in compliant motion». In: *Proceedings of the 1994 IEEE International Conference on Robotics and Automation* 4 (1994), pp. 2705–2712 (cit. on p. 28).

[54] Vicon. «Vicon Nexus User Guide». In: (June 2020) (cit. on pp. 29, 30).

[55] Vicon. URL: `https://www.vicon.com/` (cit. on p. 30).

[56] MatWorks®. URL: `https://it.mathworks.com/products/matlab.html` (cit. on p. 31).

[57] MatWorks®. URL: https://it.mathworks.com/products/simulink.html (cit. on p. 31).

[58] MatWorks®. URL: https://it.mathworks.com/products/simscape.html (cit. on p. 31).

[59] MatWorks®. URL: https://it.mathworks.com/products/simscape-multibody.html (cit. on p. 32).

[60] MatWorks®. URL: https://it.mathworks.com/products/matlab/app-designer.html (cit. on p. 32).

[61] ptc®. URL: https://www.ptc.com/it/products/creo (cit. on p. 32).

[62] Frisoli A. «Exoskeletons for upper limb rehabilitation». In: *Rehabilitation Robotics* (Jan. 2018), pp. 75–87 (cit. on p. 33).

[63] Yu H., Huang S., Chen G., Pan Y., and Guo Z. «Human–Robot Interaction Control of Rehabilitation Robots With Series Elastic Actuators». In: *IEEE Transactions on Robotics* 31(5) (2015), pp. 1089–1100 (cit. on p. 33).

[64] Calanca A. and Fiorini P. «Human-Adaptive Control of Series Elastic Actuators». In: *Robotica* (Dec. 2014) (cit. on p. 33).

[65] Li X., Pan Y., Chen G., and Yu H. «Adaptive Human–Robot Interaction Control for Robots Driven by Series Elastic Actuators». In: *IEEE Transactions on Robotics* 33(1) (Feb. 2017), pp. 169–182 (cit. on p. 33).

[66] Cempini M. et al. «Relevance of Series-Elastic actuation in rehabilitation and assistance robotic: Two cases of study». In: *2015 IEEE 1st International Forum on Research and Technologies for Society and Industry Leveraging a better tomorrow (RTSI)* (2015), pp. 76–81 (cit. on p. 33).

[67] Zhao W., Wang J., Qian W., Xiao X., and Guo Z. «Design of a Compliant Upper-Limb Rehabilitation Exoskeleton based on Novel Series Elastic Actuators». In: *2021 IEEE/ASME International Conference on Advanced Intelligent Mechatronics (AIM)* (2021), pp. 566–571 (cit. on p. 33).

[68] Crea S. et al. «A novel shoulder-elbow exoskeleton with series elastic actuators». In: *2016 6th IEEE International Conference on Biomedical Robotics and Biomechatronics (BioRob)* (2016), pp. 1248–1253 (cit. on p. 33).

[69] Harmonic Drive®. URL: https://harmonicdrive.de/en/technology/harmonic-drive-strain-wave-gears (cit. on p. 36).